

# Numerical simulation of the influence of nutrients upon water quality in Manukau Harbour

Implementation and calibration of a DelWAQ water-  
quality model

*Prepared for Watercare Services Ltd*

*September 2023*

Prepared by:  
Niall Broekhuizen  
Glen Reeve

For any information regarding this report please contact:




Niall Broekhuizen  
Ecological modeller  
Coastal & Estuarine Processes  
856 1798

National Institute of Water & Atmospheric Research Ltd  
PO Box 11115  
Hamilton 3251

Phone +64 7 856 7026

NIWA CLIENT REPORT No: 2022269HN (version 1.1)  
Report date: September 2022  
NIWA Project: WSL16205

Revision	Description	Date
Version 1.0	Final version sent to client	16 September 2022
Version 1.1	Minor amendments in response to comments from external reviewer	8 September 2023

Quality Assurance Statement		
	Reviewed by:	David Plew
	Formatting checked by:	Carole Evans
	Approved for release by:	Neale Hudson

---

© All rights reserved. This publication may not be reproduced or copied in any form without the permission of the copyright owner(s). Such permission is only to be given in accordance with the terms of the client's contract with NIWA. This copyright extends to all forms of copying and any storage of material in any kind of information retrieval system.

Whilst NIWA has used all reasonable endeavours to ensure that the information contained in this document is accurate, NIWA does not give any express or implied warranty as to the completeness of the information contained herein, or that it will be suitable for any purpose(s) other than those specifically contemplated during the Project or agreed by NIWA and the Client.

## Contents

<b>Executive summary.....</b>	<b>7</b>
<b>1 Introduction.....</b>	<b>10</b>
1.1 In this report .....	13
<b>2 The DelWAQ model .....</b>	<b>14</b>
2.1 Introduction to DelWAQ.....	14
2.2 Phytoplankton dynamics.....	15
2.3 The operational components of DelWAQ.....	16
2.4 Viewing DelWAQ model results .....	17
2.5 Operational application of DelWAQ and DeltaFM in this project.....	18
2.6 Numerical integration.....	18
<b>3 DelWAQ model setup .....</b>	<b>19</b>
3.1 Spatial domain.....	19
3.2 Catchment boundary conditions (excluding WWTPs) .....	20
3.3 Atmospheric nutrient loading .....	22
3.4 Māngere WWTP effluent boundary conditions .....	25
3.5 Clarks Beach and Waiuku WWTP effluent boundary conditions.....	26
3.6 Kingseat WWTP effluent boundary conditions .....	26
3.7 Oceanic boundary conditions.....	27
3.8 Initial conditions .....	30
3.9 Other aspects of parameterisation .....	33
3.10 Wetting and drying.....	33
<b>4 Calibration of DelWAQ .....</b>	<b>36</b>
4.1 Background .....	36
4.2 Methods.....	38
4.3 Model performance measures.....	42
4.4 Model calibration .....	44
4.5 Results .....	45
<b>5 Discussion.....</b>	<b>73</b>
5.1 Overall performance of the model .....	73
5.2 Performance expectations .....	74

5.3	Model simplifications.....	75
5.4	Model utility.....	78
<b>6</b>	<b>Conclusions and recommendations .....</b>	<b>80</b>
<b>7</b>	<b>Acknowledgements .....</b>	<b>81</b>
<b>8</b>	<b>Glossary of abbreviations and terms.....</b>	<b>82</b>
	<b>References.....</b>	<b>83</b>
<b>9</b>	<b>83</b>	
<b>Appendix A</b>	<b>Time series boxplots.....</b>	<b>85</b>
<b>Appendix B</b>	<b>Target Diagrams.....</b>	<b>100</b>
<b>Appendix C</b>	<b>Box and whisker plot description .....</b>	<b>104</b>
<b>Appendix D</b>	<b>DYNAMO best-fit parameters .....</b>	<b>105</b>
<b>Appendix E</b>	<b>Phytoplankton dynamics – BLOOM, DYNAMO and MICROPHYT .....</b>	<b>109</b>
<b>Appendix F</b>	<b>Numerical integration of model governing equations .....</b>	<b>113</b>

## Tables

Table 3-1:	Summary of manners in which model state-variables were derived from field measurements.	29
Table 3-2:	Derivation of benthic state-variables.	32
Table 4-1:	Summary of model performance measures.	49

## Figures

Figure 1-1:	Manukau Harbour location map, with catchment.	11
Figure 2-1:	Schematic illustration of the state-variables and relationships available within the DelWAQ suite.	14
Figure 3-1:	Illustration of the spatial domain of the DelWAQ model.	20
Figure 3-2:	Manukau harbour location map, with TOPNET model output (i.e., catchment derived river flow) locations showing the 217 freshwater sources.	21
Figure 3-3:	Long-term average flows and nitrogen concentrations, loads and relative contributions to Manukau Harbour.	24
Figure 3-4:	Long-term average flows and phosphorus concentrations, loads and relative contributions to Manukau Harbour.	25
Figure 4-1:	HEMP water quality sampling sites used by Watercare and Auckland Regional Council.	37
Figure 4-2:	Total nitrogen measured at Manukau Harbour (HEMP) sampling locations.	38



Figure 4-3:	Boxplots of phytoplankton carbon:Chla ratios measured at seven sites in Pelorus Sound.	41
Figure 4-4:	Example target diagram: y-axis is normalised bias ( $B^*$ ) and x-axis is normalised RMSD ( $RMSD'^*$ ).	43
Figure 4-5:	Graphical representation of the performance of DelWAQ water-quality simulations undertaken using DYNAMO.	46
Figure 4-6:	Target diagram for dissolved oxygen at all sample sites.	50
Figure 4-7:	Target diagram for total phosphorus at all sample sites.	50
Figure 4-8:	Measured and hindcast dissolved oxygen and total phosphorus: station Weymouth.	51
Figure 4-9:	Measured and hindcast dissolved oxygen and total phosphorus: station HQW 10.	51
Figure 4-10:	Hindcast and observed surface-layer and seasonal-average salinity.	55
Figure 4-11:	Hindcast and observed surface-layer and seasonal-average dissolved oxygen (Oxy).	56
Figure 4-12:	Hindcast and observed surface-layer and seasonal-average total nitrogen (TotN).	57
Figure 4-13:	Hindcast and observed surface-layer and seasonal-average total phosphorus (TotP).	58
Figure 4-14:	Hindcast and observed surface-layer and seasonal-average ammonium ( $NH_4$ ).	59
Figure 4-15:	Hindcast and observed surface-layer and seasonal-average nitrate ( $NO_3$ ).	60
Figure 4-16:	Hindcast and observed surface-layer and seasonal-average phosphorus ( $PO_4$ ).	61
Figure 4-17:	Hindcast and observed surface-layer and seasonal-average chlorophyll-a (Chla).	62
Figure 4-18:	Drop in salinity and increase in total nitrogen associated with the passage of ex-tropical cyclone Wilma.	64
<b>Figure 4-19:</b>	<b>False colour maps illustrating model performance for salinity at each monitoring station.</b>	66
<b>Figure 4-20:</b>	<b>False colour maps illustrating model performance for dissolved oxygen at each monitoring station.</b>	66
Figure 4-21:	False colour maps illustrating model performance for total nitrogen at each monitoring station.	67
Figure 4-22:	False colour maps illustrating model performance for total phosphorus at each monitoring station.	68
Figure 4-23:	False colour maps illustrating model performance for ammonium at each monitoring station.	69
Figure 4-24:	False colour maps illustrating model performance for nitrate at each monitoring station.	70
Figure 4-25:	False colour maps illustrating model performance for dissolved reactive phosphorus at each monitoring station.	71
Figure 4-26:	False colour maps illustrating model performance for chlorophyll-a at each monitoring station.	72
Figure A-1:	Measured and modelled data from Weymouth. The boxplots show all the measured data.	85

Figure A-2:	Measured and modelled data from Waiuku Town Basin. The boxplots show all the measured data.	86
Figure A-3:	Measured and modelled data from Wairopa. The boxplots show all the measured data.	87
Figure A-4:	Measured and modelled data from Titiranga. The boxplots show all the measured data.	88
Figure A-5:	Measured and modelled data from Puketutu. The boxplots show all the measured data.	89
Figure A-6:	Measured and modelled data from HWQ Nga Kuia. The boxplots show all the measured data.	90
Figure A-7:	Measured and modelled data from HWQ 80. The boxplots show all the measured data.	91
Figure A-8:	Measured and modelled data from HWQ 70. The boxplots show all the measured data.	92
Figure A-9:	Measured and modelled data from HWQ 60. The boxplots show all the measured data.	93
Figure A-10:	Measured and modelled data from HWQ 40. The boxplots show all the measured data.	94
Figure A-11:	Measured and modelled data from HWQ 30. The boxplots show all the measured data.	95
Figure A-12:	Measured and modelled data from HWQ 10. The boxplots show all the measured data.	96
Figure A-13:	Measured and modelled data from Harbour Mouth. The boxplots show all the measured data.	97
Figure A-14:	Measured and modelled data from Grahams. The boxplots show all the measured data.	98
Figure A-15:	Measured and modelled data from Weymouth. The boxplots show all the measured data.	99
Figure B-1:	Target diagram for salinity at all the sample sites.	100
Figure B-2:	Target diagram for total nitrogen at all the sample sites.	100
Figure B-3:	Target diagram for total phosphorus at all the sample sites.	101
Figure B-4:	Target diagram for ammonia at all the sample sites.	101
Figure B-5:	Target diagram for chlorophyll-a at all the sample sites.	102
Figure B-6:	Target diagram for soluble phosphorus at all the sample sites.	102
Figure B-7:	Target diagram for nitrate at all the sample sites.	103
Figure B-8:	Target diagram for oxygen at all the sample sites.	103
Figure E-1:	Example of a “strobe effect” in surface chlorophyll concentrations in northern Manukau Harbour as predicted by the BLOOM model.	110
Figure E-2:	Panel A. Predicted DYNAMO benthic diatoms ( $\text{g C m}^{-2}$ ) on the bed at Nga Kuia HEMP monitoring station. Panel B. Dissolved silica ( $\text{g m}^{-3}$ ) in the water column.	111

## Executive summary

We report on a programme of work coupling a whole-of-harbour water-quality model (DelWAQ) to an existing hydrodynamic model (DeltaFM) of Manukau Harbour. This report focusses on the implementation and calibration of a DelWAQ model and the utility of the calibrated model vis-à-vis Watercare's aims to better understand the impact on harbour water quality of the discharge from the Māngere wastewater treatment plant (WWTP). Simulations to understand the impact of alternative scenarios (catchment or waste-water plant inputs into the harbour etc.) in order to better understand how harbour water-quality may respond to future catchment land use change etc., lie outside the scope of this report.

The implemented DelWAQ model incorporates discharges of water and nutrients from tidal creeks and rivers that drain into the harbour, wastewater discharges into the harbour (Waiuku, Clarks Beach, Kingseat and Māngere), and stormwater inflows. The model simulates the effect of nutrients on harbour water quality.

The model implementation consisted of:

- defining the model spatial domain,
- generating catchment boundary conditions and point sources (inflows of water, nutrients – including from the WWTPs – and momentum), atmospheric nutrient loadings, and oceanic boundary conditions (which include inflows of water, salt, nutrients and momentum), and
- developing numerical schemes for integrating the model governing equations and handling wetting and drying of intertidal flats.

We simulated phytoplankton and seabed nutrient dynamics, which are critical to water quality, with an enhanced benthic algal module (MICROPHYT) and the DYNAMO phytoplankton-dynamics module in DelWAQ.

We calibrated the model against one year (2010–2011) of data from the Harbour Environment Monitoring Programme measurements of oxygen, nitrate, ammoniacal nitrogen, total phosphorus, dissolved reactive phosphorus, total nitrogen, chlorophyll-*a* and salinity at 15 monitoring stations across the harbour. The 2010–2011 period was chosen for use in the calibration as it represents 'typical' conditions.

The model performance is shown quantitatively by two performance metrics: normalised bias ( $B^*$ ) and normalised root-mean-squared difference ( $RMSD^*$ ) between model hindcasts and observations. The bias provides a measure deviation between observed and hindcasted temporal-means. The root mean square difference provides a measure of the time-sum of instantaneous differences between observation and simulation. We also calculated an 'error radius' that is a combination of the individual bias and RMSD scores, which provided a convenient visual indication of model performance.

We chose to define the 'best fit' model parameterisation as that one which yielded the lowest overall 'error radius' of the numerous model configurations that we tested. This implies that we gave all water-quality properties and all stations equal weight when determining overall best-fit. The best-fit model hindcasts and observations are in agreement to better than an order of magnitude; only in rare instances do the hindcasts and observations persistently disagree by more than a factor of two.

The best-fit model:

- reproduces **salinity** very well throughout the harbour. Whilst universally small, the biases are largest at stations HWQ60, HWQ80, Weymouth and HWQ40. At the former three, the model under-predicts the long-term average salinity a little. At the latter, it over-predicts the long-term average,
- over-predicts **oxygen** in the NE of the harbour and under-predicts it in the vicinity of the harbour mouth,
- over-predicts **total nitrogen** around the harbour mouth, in the immediate vicinity of the Māngere WWTP outfall, and in Waiuku inlet,
- under-predicts **total phosphorus** at most sites,
- over-predicts **ammonium** close to the open ocean, but under-predicts it elsewhere, especially in the NE of the harbour and in Waiuku inlet,
- under-predicts **nitrogen in the form of nitrate** close to the Māngere WWTP and at Waiuku, but over-predicts it elsewhere,
- under-predicts **dissolved reactive phosphorus** close to the Māngere WWTP, but over-predicts it elsewhere in the NE of the harbour, and
- over-predicts **chlorophyll-*a*** at most stations in the NE of the harbour but under-predicts it elsewhere.

Relative to the scales of short-term and seasonal variability, the over/under -predictions for salinity, nitrate and oxygen tend to be smaller than those for other variables.

We conclude that:

- the model reproduces the qualitative characteristics (seasonal cycles and spatial trends) of all the calibration data adequately,
- the model reproduces the quantitative dynamics of salinity, nitrate and dissolved oxygen well, and
- the model is less successful at reproducing the quantitative dynamics of particulate and non-nitrate solute nutrient components (particularly phosphorus).

Whilst the calibrated model has not been validated against independent data, we believe that the DelWAQ water-quality model described herein is fit for:

- scenario modelling at seasonal temporal scales and large-scale sub-regions of the harbour (e.g., quadrants or octants), with a focus on qualitative and relative changes in water quality,
- exploring the consequences of moderately large-scale change in nutrient loading from the catchment and/or wastewater treatment plants, and
- exploring responses to one-off, large-scale changes in individual point sources.

Whilst this report focusses upon reporting the development and calibration of the model, rather than reporting scenario investigations, a key inference from the simulations that we have undertaken is that nutrient loads from Māngere WWTP are having a readily discernible (in the simulation results) influence throughout much of the NE of the harbour (Māngere inlet and the waters of the open harbour around Puketutu Island). Sometimes, its influence is evident in the upper parts of the central, open harbour and eastern flanks of the harbour as far as the seaward end of the Pahurehure inlet. We believe that changes of a few tens of percent to nutrient inflows from Māngere WWTP, when entered into the model, will yield changes in simulated water quality in the harbour that will be readily discernible at the scenario time (seasonal) and space (harbour octant) scales<sup>1</sup>.

---

<sup>1</sup> We have not yet undertaken any suitable numerical trials to verify this belief.

# 1 Introduction

Watercare Services Limited (Watercare) is a wholly-owned business unit of Auckland Council. Watercare is responsible for the treatment and supply of potable water, and for the treatment and disposal of wastewater across most of the Auckland region. Wastewater discharge occurs at several wastewater treatment plants (WWTPs) across the region but is dominated by the discharge from Māngere WWTP. Māngere WWTP is one of four discharges to Manukau Harbour, and is largest by volume (Māngere  $390,000 \text{ m}^3 \text{ d}^{-1}$ , Waiuku  $2200 \text{ m}^3 \text{ d}^{-1}$ , Clarks Beach  $470 \text{ m}^3 \text{ d}^{-1}$ , and Kingseat  $27 \text{ m}^3 \text{ d}^{-1}$ ).

Manukau Harbour is the second largest harbour in the Auckland Region. It has extensive intertidal flats and a deep outer harbour (around 40 m). The harbour entrance is comparatively narrow and the tidal currents are rapid. The shallower and intertidal parts of the harbour are often turbid. The intertidal flats are intersected by four main channels. Two of these (Wairopa Channel and Purakau Channel) extend roughly eastward from the harbour mouth before diverging close to Puketutu Island and then extending further in a north-easterly direction into Māngere Inlet. The third arm extends in a south-easterly direction into Pahurehure Inlet. The fourth arm extends southward towards Waiuku (Figure 1-1).

The catchment of Manukau Harbour has been modified by urbanisation and changes in land use. Such changes have increased contaminant loads (including sediments, nutrients, metals and microbes) to the harbour, which in turn have affected its environmental health. The eastern part of the catchment is highly urbanised. The southern part is rural (though subject to urban expansion). Much of the northern harbour catchment is under regenerating forest.

Auckland's main wastewater treatment plant is located at Māngere. It discharges treated wastewater into the Purakau Channel close to Puketutu Island. Other wastewater discharges include Waiuku, Clarks Beach and Kingseat. These wastewater discharges were recently characterised as part of the consent renewal process (e.g. Hudson 2016).

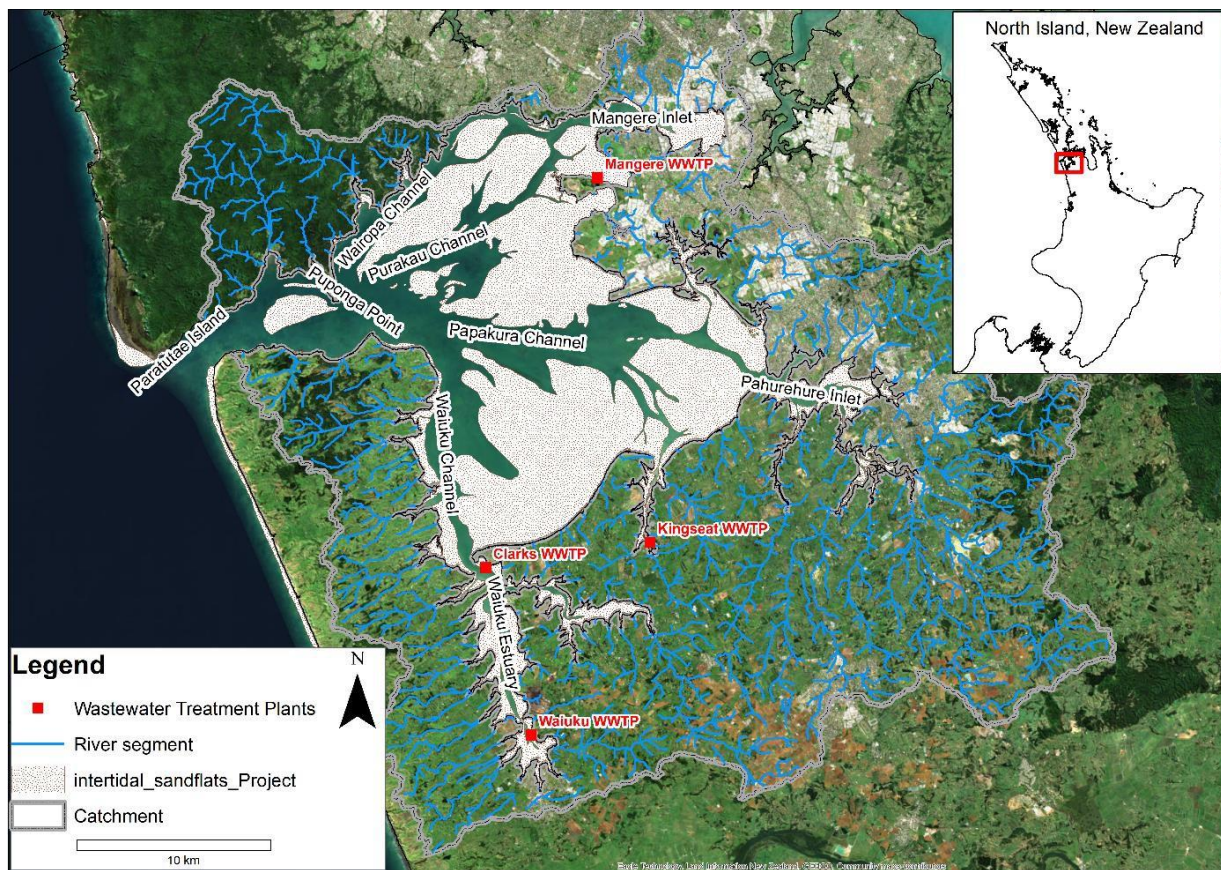


**Figure 1-1: Manukau Harbour location map, with catchment.** The red squares denote the WWTPs that discharge into the harbour. Light blue lines represent the TOPNET river segments and the thick grey line is the contributing hydrological catchment perimeter of the harbour.

Watercare commissioned NIWA to undertake this work to:

- better understand the impact on harbour water quality of discharge from the Māngere WWTP relative to other harbour inflows,
- enable Watercare to prepare for re-consenting of the Māngere WWTP discharge,
- address their duty of care to residents and harbour users,
- address community and cultural concerns regarding water quality in the harbour, and
- address the values of Manukau Harbour and assist in meeting the legal responsibility for maintaining and where necessary enhancing these values.

To assist in meeting its responsibilities, Watercare required a programme of work that established a coupled hydrodynamic and water-quality whole-of-harbour model of Manukau Harbour. The coupled whole-of-harbour model presented here builds on various models previously developed for different sectors of the harbour.

In response to Watercare’s requirements, we coupled a water-quality model (**DeIWAQ**, open-source licensed from Deltares Institute, Delft, the Netherlands) with a 3D hydrodynamic model (**DeltaFM**, also open-source licensed from Deltares Institute) of Manukau Harbour.

The coupled model incorporates three-dimensional hydrodynamics. The model simulates the effect of nutrients on harbour water quality, and allows for further applications, including assessing the effect on water quality of sediments, metals, and faecal indicator bacteria and pathogens.

The harbour model incorporates discharges of water and contaminants from tidal creeks and rivers that drain into the harbour, wastewater discharges into the harbour (Waiuku, Clarks Beach, Kingseat and Māngere), and stormwater inflows, where data exist.

The harbour model will help provide understanding regarding:

- patterns of water circulation in the harbour driven by tides, winds, freshwater runoff and saline–freshwater interactions,
- nutrient dynamics, including:
  - dispersal, transformation and sequestration of nutrients in the harbour, and the way these are affected by the harbour’s physical and biological environment, and
- the provenance of nutrients in the harbour.

The model suite will also permit scenarios to be run to assess the impact that Auckland's growth, changes in contaminant loads input to the harbour, and climate change, are likely to have on harbour water quality. Through in-house use of the model, there will be opportunities for capacity and capability building with both Watercare and Auckland Council.

This report is one of three to date which addresses the second deliverable outlined in the proposal:

- a suite of models as detailed in the Proposal,
- scientific reports documenting methodology and results along with supplementary research needed to support the further development of nutrient models, and
- simulations of results in a video format to enable sharing of results with non-technical audiences.

The DelWAQ water-quality model (described in this report) builds upon five prior pieces of work commissioned by Watercare Services Ltd as a part of this Manukau nutrient modelling project.

1. Construction, calibration and usage of a catchment model to estimate volumes of freshwater and loads of nitrogen and phosphorus from catchment sources other than wastewater treatment plants (i.e., from streams and drains) that feed directly into the harbour (Palliser et al. 2018). The catchment model was used to generate an archive of time-series of daily stream flows and nutrient concentrations spanning the period 1980–2012 for each of the streams/drains flowing into Manukau Harbour.



2. Construction, calibration, validation and usage of an unstructured grid, three-dimensional hydrodynamic model (DeltaFM) to generate an archive of spatially resolved time-series of water levels, current vectors, temperature and salinity in the harbour (Reeve and Broekhuizen 2019). The archived hydrodynamics time-series are used to drive the transport of materials within the DelWAQ model. The archive spans the period 2010–2011, but the underlying time-series of winds, insolation, stream flows etc., required to drive DeltaFM span the period of at least 1990–2012. Thus, the hydrodynamic archive could be extended (as future work under a new contract).
3. Deployment of sensors measuring currents, pressure, temperature, salinity, turbidity, dissolved oxygen, and photosynthetically active radiation in the Purakau and Wairopa Channels. These data have been used to better validate the DeltaFM hydrodynamic model in the vicinity of the Māngere WWTP (MacDonald and Broekhuizen 2018).
4. Compilation and analysis of satellite imagery of Manukau Harbour to estimate mean patterns of light attenuation and chlorophyll-*a* concentration in the harbour (Pinkerton 2017). These data were used (in part) to validate the selection of parameters to represent the background light attenuation coefficient of the water and algal biomass in the model.
5. A brief field campaign to measure benthic nutrient fluxes at several intertidal sites in the harbour (Lohrer, D. et al. 2017).

## 1.1 In this report

Herein we report on the implementation and calibration of DelWAQ and the utility of the calibrated model vis-à-vis Watercare’s aims to better understand the impact on harbour water quality of the discharge from the Māngere WWTP.

Scenario modelling will be reported subsequently in either a separate short document or in an amendment to this report.

## 2 The DelWAQ model

### 2.1 Introduction to DelWAQ

DelWAQ is a component within the Deltares software suite. It is created and maintained by Deltares Institute (Delft, the Netherlands). The suite can be used to simulate the temporal evolution of water quality (and sediment quality) in lakes, rivers, estuaries and open-marine water bodies (Bai et al. 2022). The suite has been under continuous development since the 1980s. An open-source software approach was adopted in the early 2010s. Bai et al. (2022) review several different water-quality modelling systems (AQUATOX, CE\_QUAL-W2, Deltares suite, EFDC, MIKE, WASP). Each has differing strengths and weaknesses such that there is no obvious ‘universal best choice’, but the Deltares suite does appear to be one of the most flexible tools. It has been used to simulate algal blooms and macrophyte growth. Further examples where the Deltares suite have been used are listed in Bai et al. (2022).

Figure 2-1 provides a schematic illustration of the components of the modelling system. These include contaminants (sediment, heavy metals, organic micro-pollutants, faecal bacteria), and trophic-status-related components (dissolved oxygen, nutrient concentrations, phytoplankton concentrations). Subject to some restrictions, components can be turned on or off independently of one another. In this case, we apply the DelWAQ elements that relate to trophic status<sup>2</sup> of a water body,. In the remainder of this document, phrases such as ‘water quality’ should be interpreted as referring to ‘water quality as indicated by trophic status’.

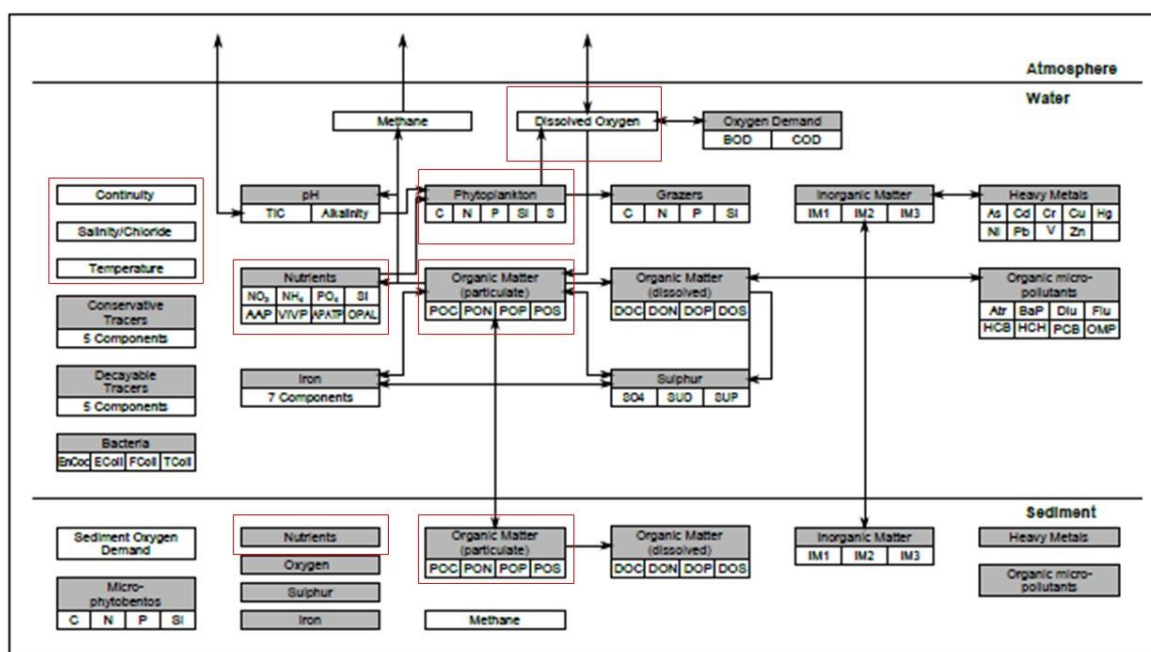


**Figure 2-1: Schematic illustration of the state-variables and relationships available within the DelWAQ suite.** Components outlined in red were active (turned on) within our Manukau model..

<sup>2</sup> As described by properties such as concentrations of key nutrients, phytoplankton biomass and dissolved oxygen.

Like any modelling suite, DelWAQ is targeted towards a comparatively narrow range of time- and space-scales. In particular, it is designed such that:

- processes operating at time-scales of hours-to-days can be resolved,
- time-spans ranging from hours to months (exceptionally, a few years) can be simulated,
- processes operating on horizontal space-scales ranging from approximately ten metres (m) to several kilometres (km) can be resolved, and
- processes operating on vertical space-scales ranging from approximately tens of centimetres (cm) to tens of metres can be resolved within the water column.

DelWAQ allows a distinction to be drawn between oxic surficial sediments and anoxic deeper sediments (but it offers no explicit vertical resolution within either the oxic or anoxic sediment layers).

The user can elect to turn some components of the overall model on or off (as a part of the initial model set-up process). For example, one can run the model with or without a seabed layer into which organic matter can settle and undergo mineralisation.

## 2.2 Phytoplankton dynamics

Phytoplankton dynamics, which are critical to water quality, can be simulated using either of two different modules that are offered within DelWAQ: **DYNAMO** or **BLOOM**. Conceptually, structurally and parametrically, DYNAMO is the simpler of the two models. However, BLOOM usually requires less calibration effort (Deltares, *pers. comm.*).

Phytoplankton growth rates of individual algal cells can vary through time as a function of their historical experiences of light intensity, nutrient concentrations and water temperature. Like many phytoplankton models, BLOOM explicitly represents several different algal taxa, but it seeks to approximate time-varying growth in an unusual manner that proved to render it fundamentally unsuited for application to Manukau Harbour, which is subject to episodic wastewater discharges and substantial periodic tidally-driven changes in water depth that affect light regime and exposure to nutrients emanating from the seabed.

DYNAMO distinguishes between two types of algae – green algae and diatoms – but makes no attempt to represent changing physiological/behavioural state within each of those two taxa. DYNAMO takes a more conventional approach than BLOOM to solving its constituent equations. This makes it better suited to the Manukau situation. Nevertheless, we were unable to achieve a satisfactory calibration with DYNAMO, which necessitated us commissioning Deltares and working with them to develop an enhanced benthic algal module<sup>3</sup> dubbed '**MICROPHYT**', which includes a phenomenological/empirical representation of microphytobenthos benthic algal self-limitation<sup>4</sup>.

---

<sup>3</sup> The module is an enhanced version of the module Deltares had previously developed and coded, but which was not incorporated into DelWAQ previously.

<sup>4</sup> The modified module assumes that the maximum weight-specific growth rate (when light, nutrients and temperature are optimal) declines linearly as the density of benthic algae increases – that is, it incorporates a form of so-called logistic growth. The maximum weight-specific growth rate falls to zero at the so-called carrying capacity ( $\text{g C m}^{-2}$ ). The user is able to specify the value associated with this coefficient.

Using the enhanced benthic algal module (MICROPHYT) together with DYNAMO in DelWAQ, a satisfactory calibration was achieved. In particular, the model ceased to be prone to exhibiting alternative stable states (in which the system became either dominated by an ever-growing benthic algal population which the water-column was almost entirely devoid of nutrient and phytoplankton, or dominated by unrealistically high phytoplankton concentrations which shaded the seabed to such an extent that plausible benthic algal populations did not develop). Further details are provided in Appendix E.

## 2.3 The operational components of DelWAQ

A DelWAQ model comprises:

- a spatial domain. This is usually sub-divided into numerous contiguous **control-volumes** or **grid-cells**. The water column can be partitioned both horizontally and vertically and DelWAQ also provides for a sediment layer under each water-column. The spatial discretisation is inherited from the hydrodynamic model, to which DelWAQ is coupled in order to drive transport of the materials being modelled,
- stored **initial conditions**. Initial conditions, which are specified by the user as a part of the model set-up, describe the state of the system at the start of the simulation. One value is required per state-variable per control-volume,
- stored time-series of **boundary conditions**. Boundary conditions, which are supplied by the user as a part of the model set-up, describe the manner in which state-variables interact with their counterparts outside the spatial domain of the model. An example is the time-series of oceanic ammoniacal-nitrogen concentrations that is applied at a seaward interface of control-volumes adjacent to the seaward periphery of the model's spatial domain,
- stored time series of **forcing data**. Forcing data, which are supplied by the user as part of the model set-up, describe the time-and-space evolution of properties which influence the time-evolution of the state-variables, but which are not themselves state-variables within the model. Examples include, solar radiation (which influences phytoplankton growth), hydrodynamic conditions (control-volume specific temperature, salinity) and water velocities at the interfaces between adjacent control-volumes,

- an (extensive) list of **state-variables** or **prognostic variables** (Figure 2-1). Some of these can be turned off, but others are obligatory. Examples include dissolved oxygen concentration, ammoniacal nitrogen concentration and diatom concentration (as carbon biomass). It is worth noting that the term ‘state-variable’ can be used in two related, but subtly different manners. Consider a model that has no spatial structure (only one control-volume) that purports to describe the evolution of a simple nutrient-phytoplankton-zooplankton system, and assume that nutrient, phytoplankton and zooplankton are each sub-divided into just one category (i.e., they are not sub-divided at all). Clearly, this model has only three state-variables. Now, let us retain the same biogeochemical structure/categorisation, but introduce some spatial structure (e.g., 1000 water columns, each composed of ten layers). In a strict mathematical sense, the model now has  $3 \times 1000 \times 10 = 30,000$  state-variables. Nonetheless, it will often be more convenient (or relevant) to describe it as a 3-state-variable biogeochemical model,
  - usually, the context of any given statement will allow the reader to determine the sense in which the term ‘state-variable’ is being used. A simple DelWAQ model may contain fewer than ten state-variables per control-volume. A complex one will contain several tens of state-variables per control-volume,
  - in the Manukau Harbour model, we provide a relatively complex model with 20 state-variables per control-volume,
- a suite of mathematical formulae which precisely specify the dependence of the instantaneous rate of change of each state-variable upon other state-variables, forcings and boundary conditions. Collectively, these equations form the set of coupled partial-differential equations that describe the time-evolution of the system of state-variables, and
- a suite of numerical integration schemes that may be used to solve the set of coupled differential equations. A DelWAQ solution consists of many time-series (one for each state-variable within each control-volume). Each of the numerical integration schemes offered by DelWAQ implies a different trade-off between computational demands (model runtime, memory requirements) and the stability, and accuracy of simulation results.

## 2.4 Viewing DelWAQ model results

By default, the user interacts with the model via a Graphical User Interface (GUI, specifically: DeltaShell). The GUI is used for setting the model up. This can include selecting amongst optional process descriptions and specifying model coefficients, forcing data, integration characteristics etc. DelWAQ results are stored in the widely used netCDF format. The GUI can also be used to view model results but the user may also view the model results in other software that supports netCDF, such as Matlab, R and Python. Many of the plots displayed within this report were generated by processing the stored netCDF results within Python rather than within the native DeltaShell GUI.

## 2.5 Operational application of DelWAQ and DeltaFM in this project

In this project we have:

- generated the files of boundary conditions, forcings that span the period 1990–2012 and initial conditions needed for a **hydrodynamic simulation** by the **DeltaFM** model spanning the period 01-01-2010 to 01-03-2011,
- created files of boundary conditions, forcings and initial conditions needed for a **water-quality simulation** by the **DelWAQ** model spanning the period 01-01-2010 to 01-03-2011, and
- generated DeltaFM and DelWAQ input files which stipulate:
  - which state-variables are to be incorporated into the (hydrodynamic or water-quality, as the case may be) simulation,
  - which process descriptions are to be incorporated into the simulation,
  - what time-period is to be simulated,
  - what files of boundary conditions, forcings and initial conditions are to be used by the simulation,
  - what integration method is to be used by the simulation, and
  - the time intervals at which the results are to be archived to file.

## 2.6 Numerical integration

The coupled differential equations that form a DelWAQ model and that are used to calculate the instantaneous rate of change (with respect to time) of each state-variable must be solved by numerical integration (as opposed to finding analytical solutions). The size of the solution time-step ( $\Delta t$ ) and the choice of numerical integration scheme both influence the likely accuracy of the eventual numerical solution, with accuracy tending to increase as  $\Delta t$  decreases.

The DelWAQ user-manual (Deltares 2011) provides brief descriptions of the various numerical integration schemes that can be implemented. Each of the schemes implies a different trade-off between runtime, stability, accuracy and memory requirements.

Together with Deltares, we ran extensive tests to determine the optimal numerical integration scheme for application to Manukau Harbour. These tests included “continuity tests” to establish the magnitudes of any volume or mass conservation errors. The DelWAQ integration scheme 15 (implicit both in vertical and horizontal) with a time-step of 5 min was selected as it was numerically stable, moderately fast (in comparison with many of the alternatives) and generated only small continuity errors (less than 5% over 3-month time-period).

See Appendix F for further details, including our use of a purpose-built continuity tracer model for testing candidate numerical integration schemes.

## 3 DelWAQ model setup

### 3.1 Spatial domain

The DelWAQ model inherits the spatial domain and discretization from the DeltaFM hydrodynamic model. The setup, calibration and performance of DeltaFM was described in Reeve and Broekhuizen (2019).

The model domain and horizontal discretisation are illustrated in Figure 3-1. The domain encompasses the entire harbour up to the high-tide spring water-level and it extends approximately 20–30 km from the harbour mouth into the Tasman Sea. The domain was discretised both horizontally and vertically into a total of 226880 tessellating (interconnected/adjoining) ‘control-volumes’<sup>5</sup>. For the horizontal discretisation, we favoured a curvilinear grid (based upon quadrilateral elements)<sup>5</sup> wherever possible but triangular elements have been used to better resolve coastal features. The (horizontal) surface areas of the grid elements range between 450 and 3,000,000 m<sup>2</sup> (side-lengths ranging between approximately 30 m and 2 km). The horizontal surface areas of water columns in shallow water tend to be much smaller where (high-tide) water depths are shallow. In the vertical, each water-column is divided into 10 discrete (sigma) layers. Each layer occupies 10% of the total instantaneous local water depth.

---

<sup>5</sup> In general, the numerical schemes that are used to simulate the advection and diffusion of materials between control-volumes are more accurate for curvilinear grids than for unstructured grids.



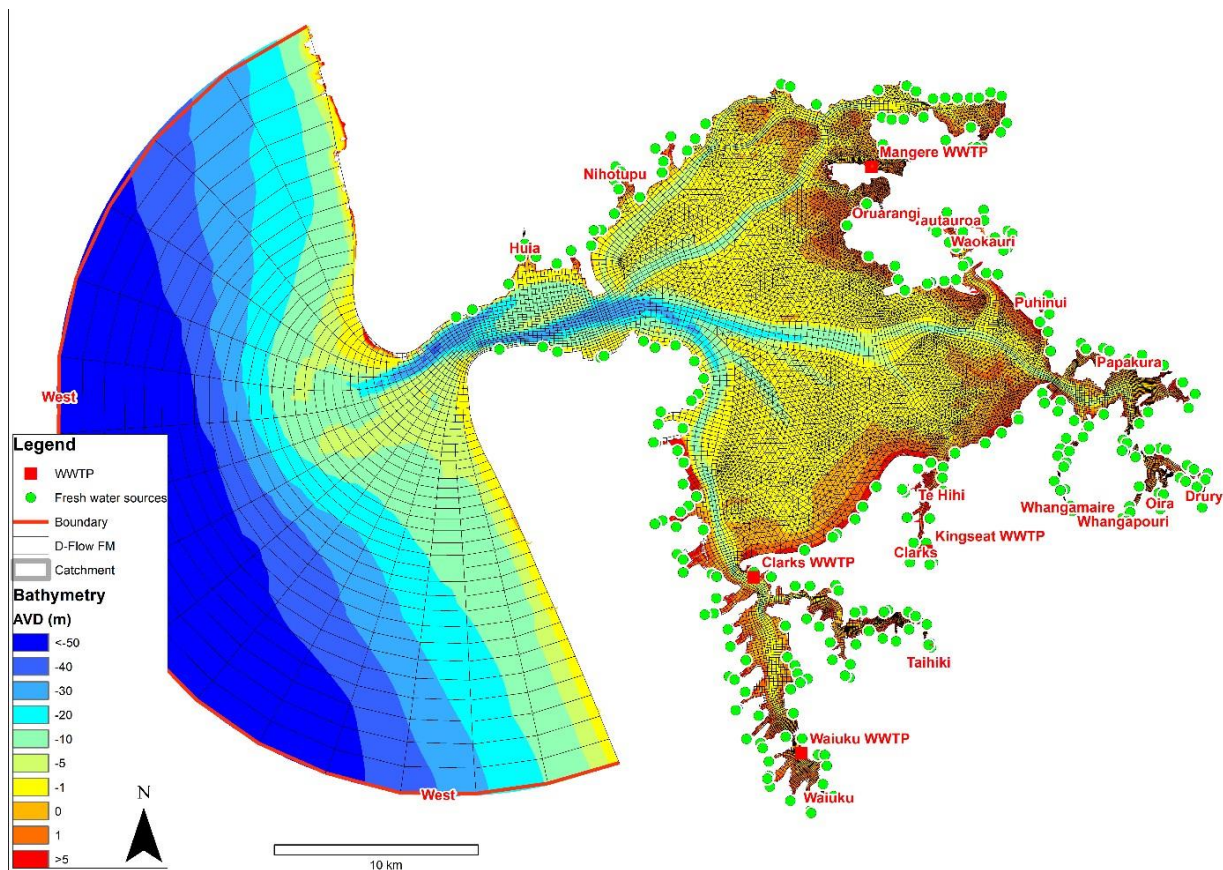


**Figure 3-1: Illustration of the spatial domain of the DelWQA model.** Green dot symbols at the coastline indicate the locations of point sources. Red squares, line symbols and names represent boundaries and WWTP sources.

### 3.2 Catchment boundary conditions (excluding WWTPs)

DeltaFM and therefore DelWQA by association, incorporates freshwater inputs from 217 distinct locations (Figure 3-1). Each is a potential source (input) of one or more of the DelWQA state-variables. The user is required to prescribe a time-series of water-flows and accompanying state-variable concentrations for each source.

Of the 217 inputs, four represent the Māngere WWTP, Clarks Beach WWTP, Kings Seat WWTP and Waiuku WWTP respectively. The Māngere WWTP has consent to discharge an average daily volume of 390,000 m<sup>3</sup> of treated wastewater per day. Clarks Beach, King Seat and Waiuku WWTPs discharge a water volume of approximately 470 m<sup>3</sup>, 27 m<sup>3</sup> and 2200 m<sup>3</sup> per day, respectively. The remainder of the 217 freshwater inputs are discharges from streams and storm-water over-flows.

DeltaFM recognises two different types of input to the model domain: (a) **point sources**, which are those that contribute water, salt, temperature and have a predefined cross-sectional area through which the water flows ; and (b) **boundary conditions**, which are those that contribute water, salt and temperature, but for which momentum is implicitly derived from the wetted area of the grid-cell wall into which the water is flowing. Our Manukau Harbour model includes 199 point sources (the first type of input green symbols in **Figure 3-2**) and 18 boundary conditions (the second type of input, purple symbols in **Figure 3-2**). Boundary conditions were used at locations where the peak discharge frequently exceeds 2 m<sup>3</sup> s<sup>-1</sup> (for example Māngere WWTP).



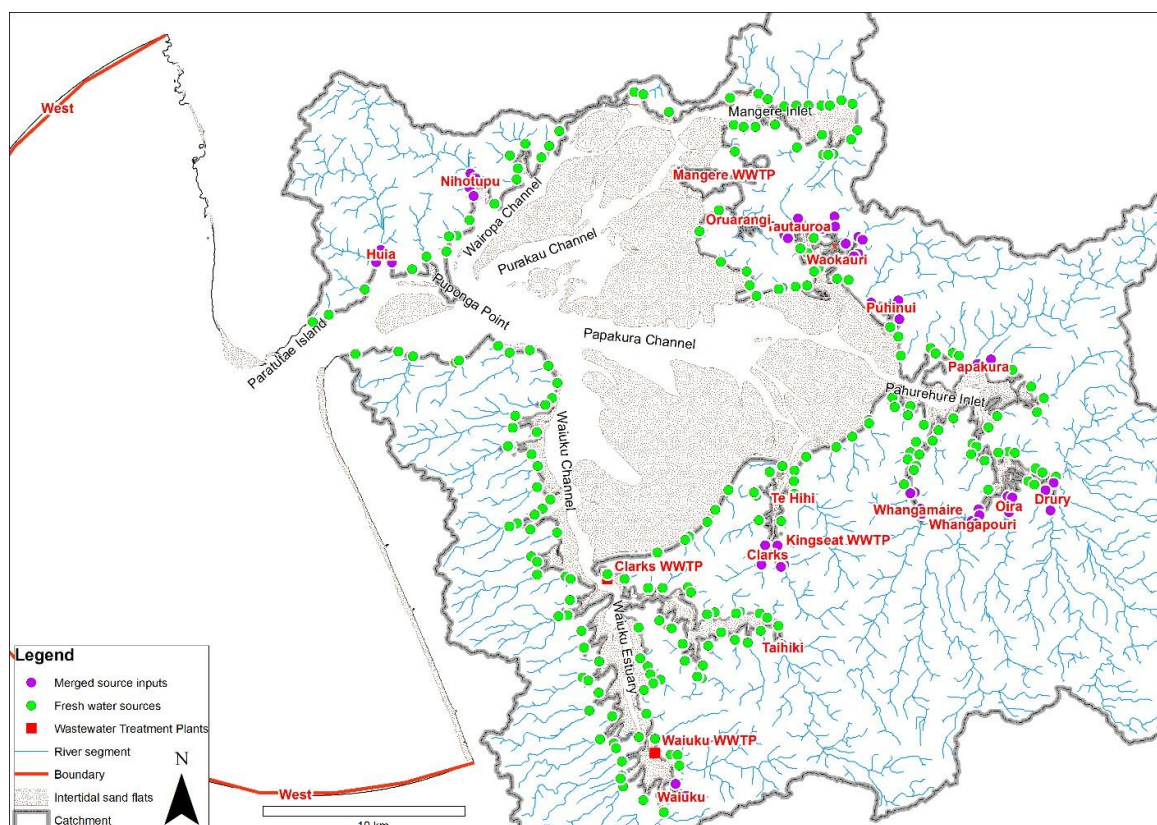


**Figure 3-2: Manukau harbour location map, with TOPNET model output (i.e., catchment derived river flow) locations showing the 217 freshwater sources.** The red names (purple dots indicate merged TOPNET stream inputs) denote freshwater sources that we have deemed to have “significant” flood flows (frequently  $>2 \text{ m}^3 \text{ s}^{-1}$ ). At these locations the model grid is changed to explicitly incorporate these flows. Green dots are the TOPNET stream locations that correspond to point source freshwater input locations with generally lower flows.

Where boundary conditions are prescribed, the discharge through said boundary must have a continuous flow (i.e., never go dry or stop running in the summer) or not be located in an intertidal area. This is because the model needs to see a water level at the boundary to calculate the momentum associated with the inflowing freshwater. Although, Māngere is not a continuous flow, a boundary condition works at this location because the discharge always starts just after high tide, therefore the model registers the water level at this boundary.

Palliser et al. (2018) describe how time-series of daily average flow and nutrient loads for the sources which do not correspond to treatment plants (i.e., streams and storm-water over-flows) were calculated. For nitrogen, they calculated time-series of: (i) total nitrogen (TN), (ii) dissolved oxidised nitrogen (nitrate+nitrite,  $\text{NO}_x\text{N}$ ), (iii) ammoniacal nitrogen ( $\text{NH}_x\text{N}$ ) and, by implication, (iv) organic N, calculated as  $[\text{TN} - \text{NO}_x\text{N} - \text{NH}_x\text{N}]^{+6}$ . For phosphorus, they calculated time-series of total phosphorus (TP) and dissolved reactive phosphorus (DRP).

Dissolved inorganic nitrogen, ammoniacal nitrogen and DRP have direct equivalents within DelWAQ (i.e., they are state-variables within DelWAQ), but organic N and the quantity  $[\text{TP} - \text{DRP}]^+$  (= dissolved organic P + sediment-bound P) have no unique equivalents.

<sup>6</sup> The superscripted ‘+’ symbol outside the square brackets indicates that zero would have been adopted whenever the term inside the bracket yielded a value less than zero.

In reality,  $[\text{TN} - \text{NO}_x\text{N} - \text{NH}_x\text{N}]^+$  represents the sum of particulate and dissolved organic nitrogen whilst  $[\text{TP} - \text{DRP}]^+$  represents the sum of dissolved organic phosphorus, particulate organic phosphorus and suspended, sediment-bound phosphorus. In turn, the particulate organic components will be comprised of both living and dead particulate organic matter.

DelWAQ requires a time-series for each of its state-variables at each source. Thus, the organic N (implicit organic P) time-series must be further sub-divided amongst the DelWAQ state-variables. Whilst DelWAQ offers separate groups of state-variables representing dissolved organic matter and particulate organic matter, we chose to exclude the former. As a corollary, we assumed that all  $[\text{TN} - \text{NO}_x\text{N} - \text{NH}_x\text{N}]^+$  and all  $[\text{TP} - \text{DRP}]^+$  in the incoming water was organic detritus (i.e., dead, particulate organic matter). This implies: (i) that the incoming water is devoid of phytoplankton etc., capable of living for extended periods in the marine environment, (ii) that any dissolved organic matter that may have been present in the incoming water behaves in the same way as any particulate organic matter (in terms of mineralisation rates, sinking speeds etc.), and (iii) any incoming sediment-bound P behaves in a manner akin to detrital P (readily mineralises into DRP regardless of the oxic state of the water/seabed).

DelWAQ also requires boundary conditions for detrital carbon, dissolved reactive silicon (DRSi) and dissolved oxygen (DO). Carbon:nitrogen ratios in organic detritus derived from living vegetation range between about 5:1 and about 180:1 (by mass, depending upon the nature of the precursor vegetation: Enríquez et al. 1993). We chose to assume that detrital carbon =  $20 \times$  detrital nitrogen. For simplicity, we chose to assume that all incoming stream and river waters would have a dissolved oxygen concentration of  $6 \text{ g m}^{-3}$  (regardless of source and temperature). This concentration implies that we assumed the water was approximately 60% saturated with oxygen. The stream/river/culvert flow rates are generally small in comparison with the volume of the receiving waters. Incoming waters are fresh (buoyant), and oxygen will readily be exchanged with the atmosphere (and less readily exchanged with the denser water below). Beyond the immediate vicinity of discharges the model has proven to be insensitive to assumptions regarding the oxygen status of the incoming water. As evidence of this, we note that, with the exception of the landward-most parts of the Pahurehure Inlet and Taikihi River arms, dissolved oxygen concentrations are well above the  $6 \text{ g m}^{-3}$  level that we chose to apply in the water entering the harbour from streams, rivers and culverts (Figure 4-8).

We know of no measurements of DRSi in waters that flow into Manukau Harbour. Consequently, we assumed that the DRSi concentration in waters flowing from the catchment (and WWTPs) was  $15 \text{ g m}^{-3}$ . This is approximately the median value recorded across a nationwide survey of rivers/streams (Close and Davies-Colley 1990). Figure 3-3 and Figure 3-4 illustrate the absolute and relative loads of water, nitrogen and phosphorus associated with each catchment input location. They also indicate the magnitudes of the nutrient-loads arising from atmospheric deposition (see next section).

### 3.3 Atmospheric nutrient loading

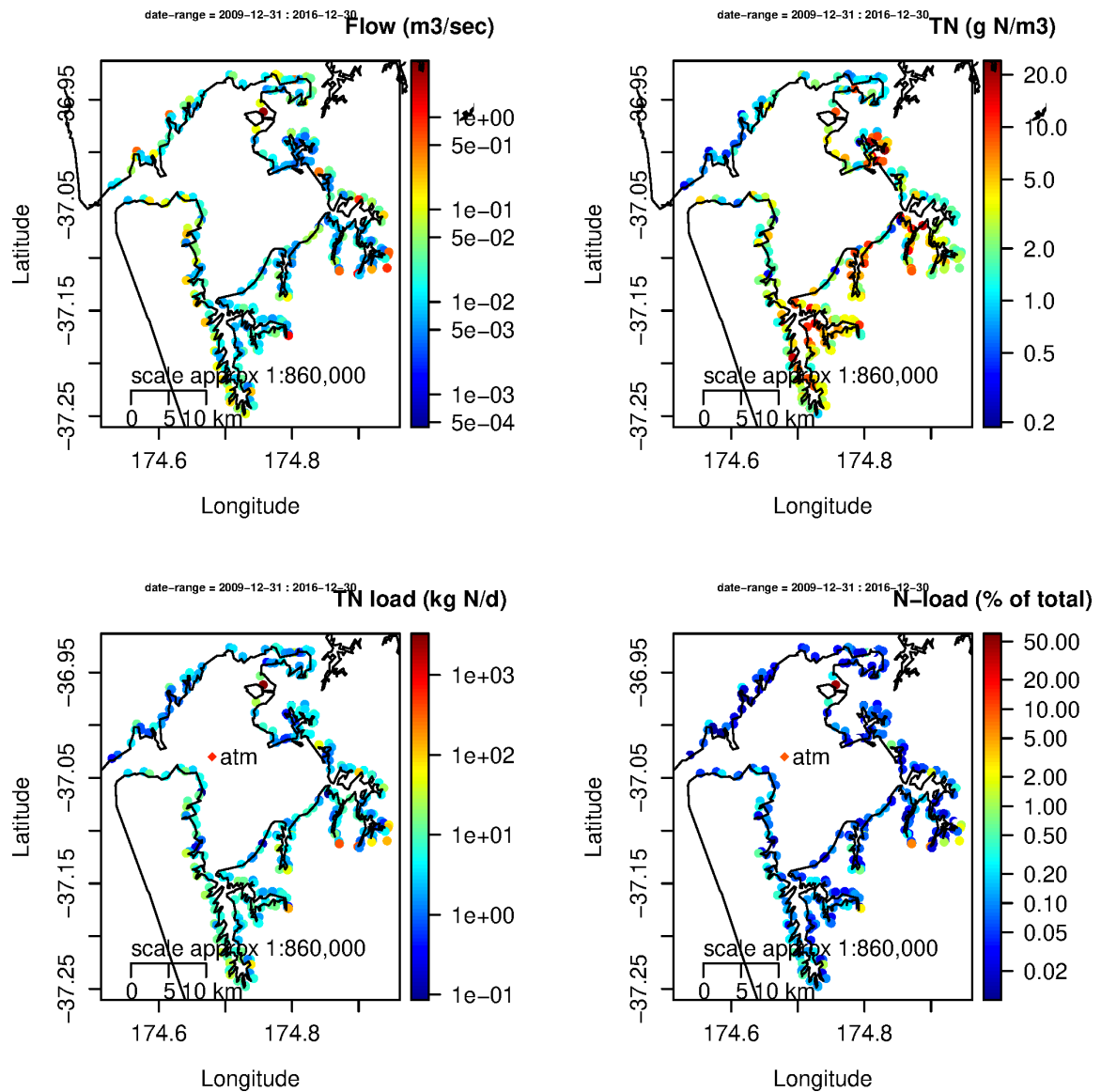
Nutrients can also enter the harbour through wet and dry deposition. The net rate of nitrogen deposition from the atmosphere in the Auckland region has been estimated to be approximately  $6 \text{ kg N ha}^{-1} \text{ y}^{-1}$  (Parfitt et al. 2006; Verburg et al. 2018), whilst North Island P-deposition rates are estimated to be around  $0.37 \text{ kg P ha}^{-1} \text{ y}^{-1}$  (Verburg et al. 2018). We apply these rates as time- and space-invariant values across the entire high-tide surface area of the harbour. We assume that all the nitrogen enters the sea-water as ammoniacal-N whilst phosphorus enters as DRP.

Figure 3-3 illustrates the long-term average flow ( $\text{m}^3 \text{s}^{-1}$ ) and nitrogen concentration, load and relative load associated with each stream, each WWTP and atmospheric deposition. Figure 3-4 provides the equivalent information for phosphorus. Both figures serve to emphasize that:

- the Māngere WWTP is (by far) the largest individual sources of water and nutrients to the harbour, providing approximately 17%, 47% and 82% of the total water, nitrogen and phosphorus loads respectively<sup>7</sup>,
- our catchment model indicates that the streams on the southern, eastern and western flanks of the harbour tend to carry larger nutrient concentrations than do those on the northern flank, and
- atmospheric nutrient deposition accounts for 5% (nitrogen) and 2% (phosphorus) of the total load to the estuary. Except for the Māngere WWTP, which generates the largest individual nutrient loads, the atmospheric load (integrated across the entire surface area of the harbour) exceeds that of any other individual WWTP, stream or culvert.

---

<sup>7</sup> Note that direct nutrient deposition to the sea-surface (e.g., through rainfall and particulates) is explicitly assumed to be negligibly small in the DelWAQ model and the budgets implied by Figure 3-3 and Figure 3-4.



**Figure 3-3: Long-term average flows and nitrogen concentrations, loads and relative contributions to Manukau Harbour.** Note the use of logarithmic colour-scales. The symbol marked 'atm' illustrates the magnitude of the nitrogen deposition from the atmosphere. In the bottom-right image, the relative loads (expressed as a percentage) loads are calculated relative to the sum of loads from all streams and WWTPs. In particular, the atmospheric deposition term does not contribute to the denominator that is used in the calculation.

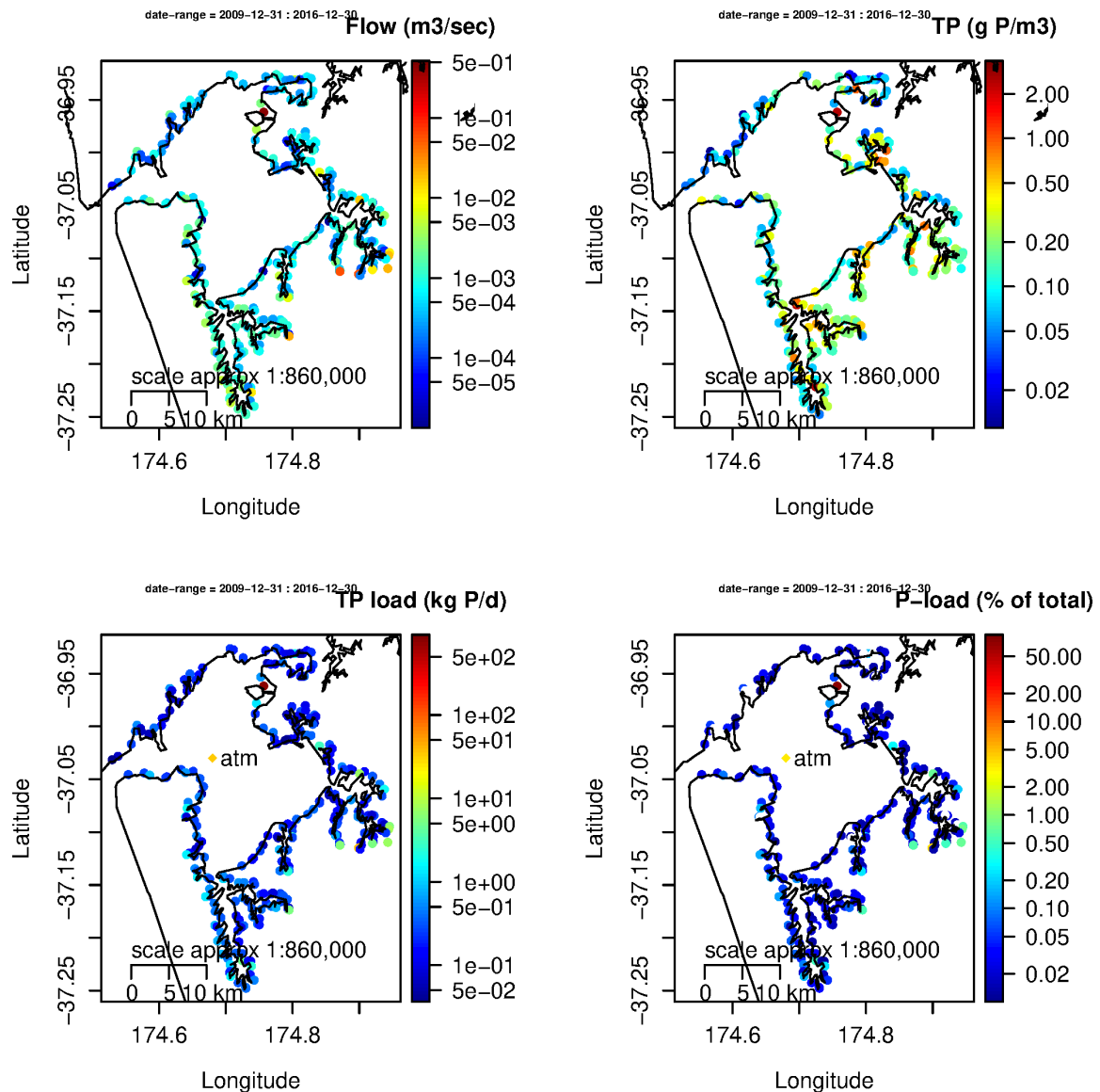


**Figure 3-4: Long-term average flows and phosphorus concentrations, loads and relative contributions to Manukau Harbour.** Note the use of logarithmic colour-scales. The symbol marked 'atm' illustrates the magnitude of the phosphorus deposition from the atmosphere. In the bottom-right image, the relative loads (expressed as a percentage) loads are calculated relative to the sum of loads from all streams and WWTPs. In particular, the atmospheric deposition term does not contribute to the denominator that is used in the calculation.

### 3.4 Māngere WWTP effluent boundary conditions

Many of the water-quality characteristics in the effluent from the Māngere WWTP have been monitored at intervals ranging from twice daily (once upon each discharge) through to weekly. Records are available for flow, temperature, pH, total suspended solids (TSS), total biological oxygen demand (TBOD), soluble biological oxygen demand (SBOD), total Kjeldahl nitrogen (TKN), ammoniacal nitrogen ( $\text{NH}_x\text{N}$ ), nitrite+nitrate ( $\text{NO}_x\text{N}$ ), total phosphorus (TP) and dissolved reactive phosphorus (DRP). Data spanning the period 2004–2018 were provided to us.

Again, some of the DelWAQ state-variables have direct equivalents in the monitoring data but others do not. The phytoplankton content of the effluent was assumed to be zero. Particulate organic nitrogen concentration was assumed to equate to  $[(TKN - NH_xN)^+ \times (1.0 - [SBOD / TBOD])]$  and dissolved organic nitrogen was calculated as  $[(TKN - NH_xN)^+ \times [SBOD / TBOD]]$ . Note however, that we expressly excluded dissolved organic matter from our DelWAQ implementation. Thus, the sum of the two time-series was used as the boundary condition for detrital organic nitrogen within DelWAQ (state variable PON). The detrital phosphorus concentration was assumed to equate to  $[TP - DRP]$ . The dissolved oxygen concentration was assumed to equate to 80% of the saturation concentration. The DRSi concentration was assumed to be  $15 \text{ g m}^{-3}$  (see above).

Where data were not available at daily resolution in the monitoring data, linear interpolation of the measured concentrations was used to generate time-series with daily resolution.

### 3.5 Clarks Beach and Waiuku WWTP effluent boundary conditions

Fewer data are available to characterise the quality of the Clarks Beach and Waiuku WWTP effluents than is the case for the Māngere plant. For Clarks Beach and Waiuku, the following are available: flow, temperature, DO, pH, BOD<sup>8</sup>, TSS, NH<sub>x</sub>N, total inorganic nitrogen (TIN) and TP. These span the period 2010–2018. Discharge volumes (hence, flow) were recorded daily, but other properties were recorded less frequently. Linear interpolation was used to derive daily values.

All of the TSS was assumed to be organic with a carbon:TSS ratio of 50% by mass. We calculated corresponding concentrations of particulate organic nitrogen and particulate organic phosphorus by assuming that the N:C and P:C ratios of this particulate organic matter amounted to 33% of the Redfield ratio (Redfield 1934), implying N:C and P:C ratios of 0.06 and 0.008 respectively (by mass).

DRP was calculated as  $[TP - \text{inferred particulate organic P}]^+$  (described earlier). Note that this method of calculating DRP ensures that the total phosphorus loading applied in the simulation would remain consistent with the observations at the plant – even if our inferred concentration of particulate organic P were proven to be incorrect.

Whilst we can make very approximate estimates of PON in the effluent (as described above), we have no reliable way of estimating dissolved organic nitrogen (DON) concentrations because neither TN, TKN nor DON were measured in the effluent. For simplicity, we have chosen to assume that there was no DON in the effluent. This implies that the total nitrogen input from these two plants may be under-estimated.

We calculated the concentration of nitrate+nitrite (NO<sub>x</sub>N) as  $[TIN - NH_xN]^+$ .

We assumed that the wastewater contained no phytoplankton capable of surviving in a marine environment.

### 3.6 Kingseat WWTP effluent boundary conditions

For Kingseat WWTP, the data are restricted to: flow, DO, BOD, TSS and NH<sub>x</sub>N. Data span the period 2010–2018. Discharge volumes (hence, flow) were recorded daily, but other properties were recorded less frequently. Linear interpolation was used to derive daily values.

---

<sup>8</sup> The data from Clarks, Waiuku & Kingseat report “BOD” – which we assume to be total BOD (TBOD).



All of the TSS was assumed to be organic with a carbon:TSS ratio of 50%. We calculated corresponding concentrations of particulate organic nitrogen and particulate organic phosphorus by assuming that the N:C and P:C ratios of this particulate organic matter amounted to 33% of the Redfield ratio (Redfield 1934), implying N:C and P:C ratios of 0.06 and 0.008 respectively (by mass).

Without measurements of TN, TKN, TP or DRP, it is difficult to establish how much dissolved inorganic and organic nitrogen or phosphorus is in the effluent, thus requiring approximation.

Nitrate+nitrite concentrations were calculated by multiplying measured Kingseat  $\text{NH}_4\text{N}$  concentrations by the median  $\text{NO}_3\text{N}:\text{NH}_4\text{N}$  ratio from either Waiuku or Clarks Beach. Dissolved organic N concentrations were assumed to be zero.

DRP concentrations were calculated by multiplying measurements of TSS measured at Kingseat by the median of all available pairwise ratios of DRP:TSS in all records from Clarks Beach and Waiuku. Dissolved organic P concentrations were assumed to be zero.

We assumed that the wastewater contained no phytoplankton capable of surviving in a marine environment.

### 3.7 Oceanic boundary conditions

For most state-variables, oceanic boundary conditions were based upon measurements from monthly samples of near-surface water gathered approximately 6 km offshore of the mouth of Manukau Harbour over the period November 2017 to February 2019. This is not the calendar period that we are aiming to simulate, but it is the only period during which the open-coastline waters outside the harbour have been sampled by means of in-situ measurements. The measurements include direct measurements of nitrate, ammonium, reactive phosphorus, reactive silicon, chlorophyll-*a* (Chl*a*), total Kjeldahl nitrogen (TKN) and dissolved oxygen.

Whilst the model has state-variables which are direct counterparts of some of these quantities, other state-variables have no direct counterparts in the field data. For example, there are no direct measurements of the carbon abundance of individual phytoplankton taxa or of organic detritus. For each state-variable in the model, we first synthesised a sequence of 12 monthly values as summarised within Table 3-1.

We know of no direct observations of the water-quality for the mid- or near-bed waters outside the harbour mouth. In the absence of such observations, and noting that current speeds and wind-driven mixing are both moderately strong on the open coastline outside the harbour, we chose to assume that the water-column at the seaward boundary of the model domain is vertically homogenous. Inspection of archived simulation results from the HYCOM global circulation model revealed that there is little or no stratification in the open coastal waters outside Manukau Harbour (albeit that we acknowledge that HYCOM has coarse horizontal resolution and lacks any freshwater inputs and as such it may not resolve near-shore features outside Manukau reliably). Consequently, we chose to apply vertically homogenous boundary conditions along the seaward boundary of our model domain.

The NIWA-SCENZ archive<sup>9</sup> provides ready access to processed satellite imagery. The archive spans the period 2002-2023. Informal inspection of data from a pixel immediately outside the harbour mouth suggests that annual maximum, month-average near-surface chlorophyll concentrations

---

<sup>9</sup> [niwa.co.nz/portal/apps/experiencebuilder/template/?id=9794f29cd417493894df99d422c30ec2&page=Timeseries](https://niwa.co.nz/portal/apps/experiencebuilder/template/?id=9794f29cd417493894df99d422c30ec2&page=Timeseries)

range between circa 1.6 and 2.8 mg Chl m<sup>-3</sup>. Annual minima range between approximately 0.3 and 0.7 mg m<sup>-3</sup>. In the scant in-situ data that do exist, measured chlorophyll concentration have ranged between 0.2 mg m<sup>-3</sup> and 2.1 mg m<sup>-3</sup> (with several other values recorded as “≤ 3 mg m<sup>-3</sup>”). Thus, there is no reason to believe that the oceanic boundary conditions which we have applied for phytoplankton in the near-surface waters are anomalously high or low. The satellite data provide no clues as to annual variability in properties such as nutrient concentrations or dissolved oxygen.



**Table 3-1: Summary of manners in which model state-variables were derived from field measurements.**

Field measurements were made at monthly (from November 2017) intervals at stations approximately 6 km outside of the mouth of Manukau Harbour. Monthly boundary conditions were estimated using the average of the (up to) two values available for each calendar month. Note that, where values were recorded as below detection limit in the raw laboratory data, the detection-limit concentration was adopted in calculations of oceanic boundary conditions. This choice was made for two reasons. Firstly, there were insufficient values in the offshore station time-series to permit meaningful imputation. Secondly, imputation involves adopting different (randomly chosen) values (that are consistent with the overall probability distribution of the data) for each non-detect upon each occasion. Thus, imputation makes it difficult to generate reproducible boundary conditions (or initial conditions).

State-variable	Method by which values were derived from field-data	Comments
Nitrate	Measured	
Ammoniacal nitrogen	Measured	
Dissolved reactive phosphorus	Measured	
Dissolved reactive silicon	Measured	
Biogenic silica (opal)	POC / Redfield <sub>Si</sub>	POC denotes the inferred particulate organic carbon concentration (see below). Redfield <sub>Si</sub> denotes the C:Si ratio within the extended Redfield ratio (3.03 g C g <sup>-1</sup> Si).
Particulate organic nitrogen (detrital N)	TKN – NHxN – (Chla × 10)	TKN is measured total Kjeldahl nitrogen. NHxN is measured ammoniacal nitrogen. Chla is measured chlorophyll- <i>a</i> . 10 is a typical ratio for algal N to chlorophyll (Bowie et al. 1985).
Particulate organic phosphorus (detrital P)	TP – TDP – (Chla × 0.5)	TP is measured total phosphorus. TDP is measured total dissolved phosphorus <sup>10</sup> . 0.5 is a typical ratio for algal P to chlorophyll.
Particulate organic carbon	$0.5 \times (\text{PON} / \text{Redfield}_N + \text{POP} / \text{Redfield}_P)$	PON is particulate organic N as above. POP is particulate organic P as above. Redfield <sub>N</sub> , Redfield <sub>P</sub> are Redfield C:N and C:P ratios by mass (Redfield 1934).
Diatom phytoplankton carbon	$(0.7 \times \text{Chla}) / (\text{Chla:C})_{\text{Diatom}}$	Assume 70% of total measured Chla is diatom chlorophyll. (Chla:C) <sub>Diatom</sub> is the default Chla:C ratio for N-limited diatoms from DelWAQ model (DYNAMO formulation).
Green phytoplankton carbon	$(0.3 \times \text{Chla}) / (\text{Chla:C})_{\text{Green}}$	Assume 30% of total measured Chla is flagellate chlorophyll. (Chla:C) <sub>Green</sub> is the default Chla:C ratio for N-limited flagellates from DelWAQ model (DYNAMO formulation).

<sup>10</sup> This is the measured total phosphorus content of water that has passed through a filter (usually, 0.45 micron pre-size). It may include both inorganic and organic phosphorus whether as solute or bound to tiny particles. In practice, most will likely be soluble reactive phosphorus (orthophosphate).

### 3.8 Initial conditions

Initial conditions are required for each of the model's state-variables. Over simulated time, a model tends to 'forget' the initial conditions and evolve towards conditions that are dictated by the catchment and oceanic boundary conditions and other aspects of the model's parameterization. This evolution time is known as the 'transient period'. Initial trials revealed that the transient period for the Manukau model is around six-to-nine months.

We draw a distinction between 'cold start initial conditions' and 'hot start initial conditions'. The former are initial conditions provided by the user at the outset of an investigation (series of simulations). The latter are the stored results from an earlier simulation (that has been run for sufficiently long that the model had forgotten the cold-start initial conditions). Hot start initial conditions are useful when one wishes to make a simulation that will require many computer hours (or days). In particular, they mitigate the costs that can arise when simulations fail to run to completion because of hardware type failures (exhaustion of storage space for model results, power outages etc.). Furthermore, when the user is making only comparatively small parametric changes, the transient period associated with hot-start initial conditions from a prior simulation (with only subtly different parameterization) will often be shorter than that associated with entirely naïve user-generated cold-start initial conditions.

Our ultimate 'production quality' simulations were generated using hot-start initial conditions. Nonetheless, in the remainder of this sub-section, we discuss our cold-start initial conditions.

Our cold-start initial conditions were spatially uniform but we emphasize that the subsequent hot-start ones contained spatial variations generated during the cold-start simulation period under the influence of the various boundary conditions etc.

For the pelagic state-variables, our cold-start were based upon the median values from the long-term monthly monitoring at the Auckland Council/Watercare monitoring station located in the mouth of the harbour (Figure 4-1). As noted above, we applied those medians throughout the pelagic domain regardless of horizontal or vertical position within the pelagic zone.

Cold-start initial conditions were also required for benthic properties: particulate organic carbon, nitrogen and phosphorus (i.e., elemental components of organic detritus); biogenic silica (BSi, the frustules ('shells') of living and dead diatomaceous-algae); and benthic algae. Measurements of the organic matter and algal content of the sediments are scarce and largely restricted to intertidal locations. We know of no estimates of the BSi content of the sediments (or overlying water).

In reality, these materials are distributed through the upper few centimetres of the seabed. Material close to the surface of the seabed will exchange with the over-lying water more readily/more rapidly than material deeper in the seabed. The model has no explicit vertical structure in the seabed layer so cannot easily accommodate any exchange process.

We chose to assume that, on the time-scales that we are simulating (up to about 18 months), material in the upper 5 cm (active layer) of the seabed can interact with the overlying water. Thus, we derived initial conditions by integrating surficial measurements of organic matter and Chla over the active layer to yield a density (mass  $\text{m}^{-2}$  over the upper 5 cm). This choice of integration depth is somewhat arbitrary. Storm events and burrowing macrofauna etc., may (intermittently but rapidly) exchange materials from this depth towards the sea-surface but passive diffusive exchange of materials through the pore-waters will do so only very slowly. The initial conditions for benthic

material play a substantial part in determining the initial nutrient content of the harbour. Nonetheless, those nutrients are ultimately displaced towards the open-ocean, or denitrified, and the model slowly ‘forgets’ the initial conditions. The initial conditions influence the duration and nature of the model’s transient behaviour (out to time-scales of several months), but we do not believe that they influence the model’s longer-term behaviour.

We summarise how we calculated benthic state-variables in Table 3-2.

.

**Table 3-2: Derivation of benthic state-variables.** In ‘Means of calculation’, unit conversions and conversions from point estimates of concentration to depth-integrated estimates of density are not shown. Scaling required to convert between e.g., cm<sup>3</sup> and m<sup>3</sup> or µg and g and from point estimates of concentration to depth-integrated estimates of density are not shown.

State-variable	Means of calculation	Comments
POC	$\frac{[(\text{AFDM:DM})_{\text{measured}} \times (\text{C:AFDM})_{\text{lit}} \times \rho_{\text{rock}} \times (1 - \phi)]}{[(1 - (\text{AFDM:DM})_{\text{measured}}) - \text{benthic algal carbon}]}$	<p>(AFDM:DM)<sub>measured</sub> is organic matter in sediment (g ash free dry mass g<sup>-1</sup> dry mass). Typical values are 0.5–2% in Manukau intertidal zone.</p> <p>(C:AFDM)<sub>lit</sub> is representative C:AFDM ratio for organic matter (g g<sup>-1</sup>).</p> <p>ρ<sub>rock</sub> is representative density for inorganic sediment (g cm<sup>-3</sup>).</p> <p>φ is representative porosity for Manukau sediments (cm<sup>3</sup> void space cm<sup>-3</sup> bulk volume).</p>
PON	0.5 × Redfield <sub>N</sub> POC	NIWA data from the Firth of Thames suggest N:C ratios in benthic organic matter range from << Redfield up to around Redfield with a median that is around 50% of Redfield.
POP	0.5 × Redfield <sub>p</sub> POC	Data from the Firth of Thames suggest P:C ratios in benthic organic matter range from << Redfield up to around Redfield with a median that is around 50% of Redfield.
BSi	$\frac{[980 \times \rho_{\text{rock}} \times (1 - \phi)]}{[1 - (\text{AFDM:DM})_{\text{measured}}]}$	Krause et al. (2017) suggest approx. 35 µmol Si g <sup>-1</sup> (980 µg Si g <sup>-1</sup> sediment) sediment in a coastal lagoon.
Benthic algal carbon	$\frac{[10^{-6} \times \rho_{\text{rock}} \times (1 - \phi)]}{[(1 - (\text{AFDM:DM})_{\text{measured}}) \times (\text{C:Chla})_{\text{lit}}]}$	Benthic chlorophyll concentrations in Manukau intertidal sediments ranged from 5–13 µg Chla g <sup>-1</sup> dry sediment in the incubation studies made to support this modelling. In the routine Harbour estuary monitoring programme the range is approx. 5–25 µg Chla g <sup>-1</sup> dry sediment (Greenfield et al. 2013). We adopted a value of 10 µg Chla g <sup>-1</sup> dry sediment.

### 3.9 Other aspects of parameterisation

DelWAQ requires numerous coefficients governing processes such as photosynthesis and nutrient uptake by algae, death of algae, decay of organic matter, nitrification of ammonium, denitrification of nitrate and gaseous exchange at the sea-surface. For these coefficients, and unless otherwise specified herein, we adopted the default values recommended by Deltares.

Light is attenuated as it passes through the water-column. Materials such as phytoplankton, organic detritus and dissolved colours and suspended sediments all contribute to this attenuation. Our model includes explicit state-variables for phytoplankton and organic detritus (and we adopted the corresponding default specific attenuation coefficients), but it does not explicitly simulate suspended sediments or dissolved colour.

To accommodate the various factors that influence attenuation, we rendered the model's 'background light attenuation coefficient' as a temporally constant but spatially varying field of values based upon the map of time-averaged attenuation coefficients inferred from satellite data of Manukau Harbour that was prepared as a part of this project (Pinkerton 2017 figure 4-14).

Since Pinkerton's values are for 'total attenuation' (including attenuation due to phytoplankton and organic detritus), we took care to discount Pinkerton's values a little to reduce the likelihood that light attenuation by Chla and organic detritus would be double counted in the DelWAQ model. The applied background attenuation coefficients range from  $0.12 \text{ m}^{-1}$  in the waters outside the harbour up to about  $1.0 \text{ m}^{-1}$  in the upper intertidal zones. In the model, the realized local, instantaneous attenuation coefficient for light is given by the sum of the local temporally constant 'background' coefficient and time-varying components proportional to the simulated, local, instantaneous concentration of phytoplankton chlorophyll and suspended particulate organic matter.

### 3.10 Wetting and drying

Approximately 60% of the seabed of Manukau Harbour is intertidal. These intertidal regions present a special problem to the hydrodynamic model related to wetting and drying of the seabed. The advection/diffusion equations become numerically much less tractable as the model mesh cell control-volumes decline. In order to maintain numerical stability in the solutions, the model time-step must shrink towards zero as the water depth reduces and the thickness of the control-volumes correspondingly declines. In common with most analogous models, the Deltares suite adopts a pragmatic solution to this for inter-tidal regions.

Advective exchange between adjacent water columns that have water depths less than a nominated drying depth (chosen by the user) are set to zero. By choosing the maximum time-step and the drying depth judiciously, the user can ensure that no water-column becomes entirely dry or, worse still, attains a negative water-mass or volume. This ensures that the integration time-step never has to shrink to zero and reduces the probability that the numerical solutions will become unstable. We adopted a drying depth of 0.1 mm.

Since DelWAQ inherits the advective rates and water depths etc., from a prior hydrodynamic simulation, DelWAQ water columns are unlikely to run dry. Note, however, that it is still possible because: (a) the archived hydrodynamics used to drive DelWAQ are likely to have coarser temporal resolution than was available within the prior hydrodynamic model and (b) DelWAQ tends to run

with a coarser time-step than the prior hydrodynamic model. The drying depth that is applied is inherited from the hydrodynamic simulation<sup>11</sup>.

---

<sup>11</sup> We adopted values of 0.1 mm and 1 mm respectively for the hydrodynamic and water quality simulations.

The advective export is set to zero when the depth of a water column falls below the drying depth, but other processes can continue. For example, dispersive exchange can continue and biogeochemical processes occurring within the water column (and in the seabed) can continue. In very shallow water columns (such as the quasi-dry ones), nutrient concentrations can climb very high while the tide is out (due to continued decay of benthic organic material). Once the tide returns, any high nutrient concentrations quickly decline as the nutrient is diluted by the large quantities (relative to the thin layer of water retained in the quasi-dry cell) of incoming sea-water.

## 4 Calibration of DelWAQ

In this section of the report, we address the calibration of the DelWAQ model for Manukau Harbour. Model calibration is used to quantify the capability of the model to predict nutrient concentrations in the harbour. Calibration is an iterative process which involves the systematic changing or tuning of model parameters to optimise the model's ability to accurately reproduce – or 'hindcast' – observations.

Whilst we have created an archive of boundary conditions and forcings (winds, insolation etc.,) that span the period 1990–2018, the model runs too slowly to enable repeated simulations of that full calendar period. Thus, for calibration purposes, we chose to focus upon just one year, 2010–2011. This period was chosen as it represents a fairly typical year (neither an exceptionally strong El Niño or La Niña year), with no persistent (weeks or longer) unusual winds, rainfall etc., (pers comm., R Bell, 2018).

### 4.1 Background

Calibration data sets are available from Watercare and Auckland Regional Council at up to 16 sites across the harbour (see Figure 4-1). These data were collected for Watercare as part of the Harbour Environment Monitoring Programme (HEMP), which was established in 1995.

HEMP measurements were generally made from a helicopter over a 4-hour period during an ebbing tide, during daylight hours (Kelly 2014). Data were collected approximately monthly from surface water. Although as many as 16 sites across the harbour have been sampled, not all 16 sites have been sampled consistently over time; much of the data are from different periods and not always for the full range of nutrients.



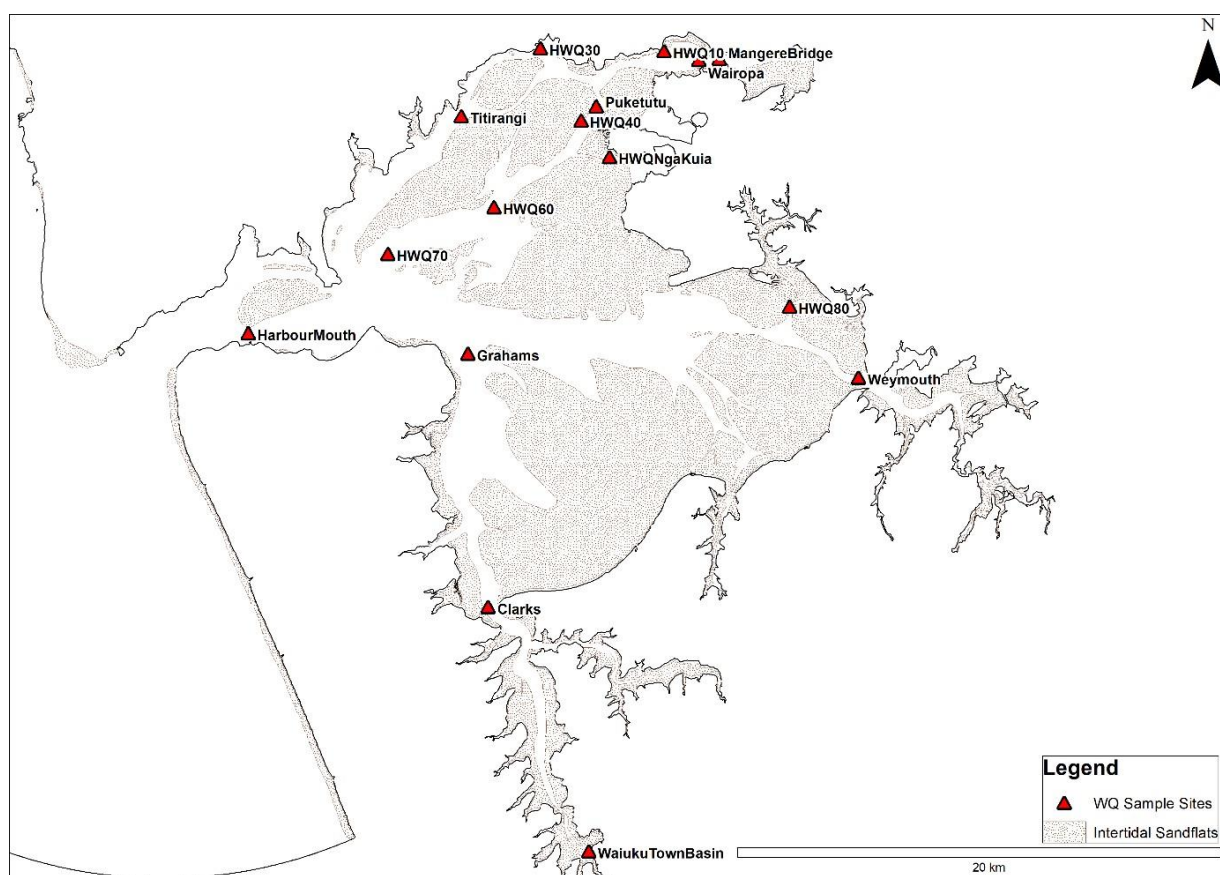


**Figure 4-1: HEMP water quality sampling sites used by Watercare and Auckland Regional Council.** Red triangles represent the locations where monthly surface water quality samples were collected.

The HEMP monitoring data cover the period from 1995 to present, but for the purpose of model calibration we only used data from 2004 onwards. Data before 2004 was not used because there appears to be a step change in the data near the end of 2003, which appears to take several years to normalise (Figure 4-2). We believe that this change occurred after the decommissioning of the Māngere WWTP retention ponds and associated upgrades to the Māngere WWTP. The model was calibrated using boundary forcing data for the period January 2010 to March 2011. Importantly, the calibration period (January 2010 to March 2011) coincided with a period of intense HEMP sampling<sup>12</sup>.

<sup>12</sup> In terms of number of sites and parameters measured.

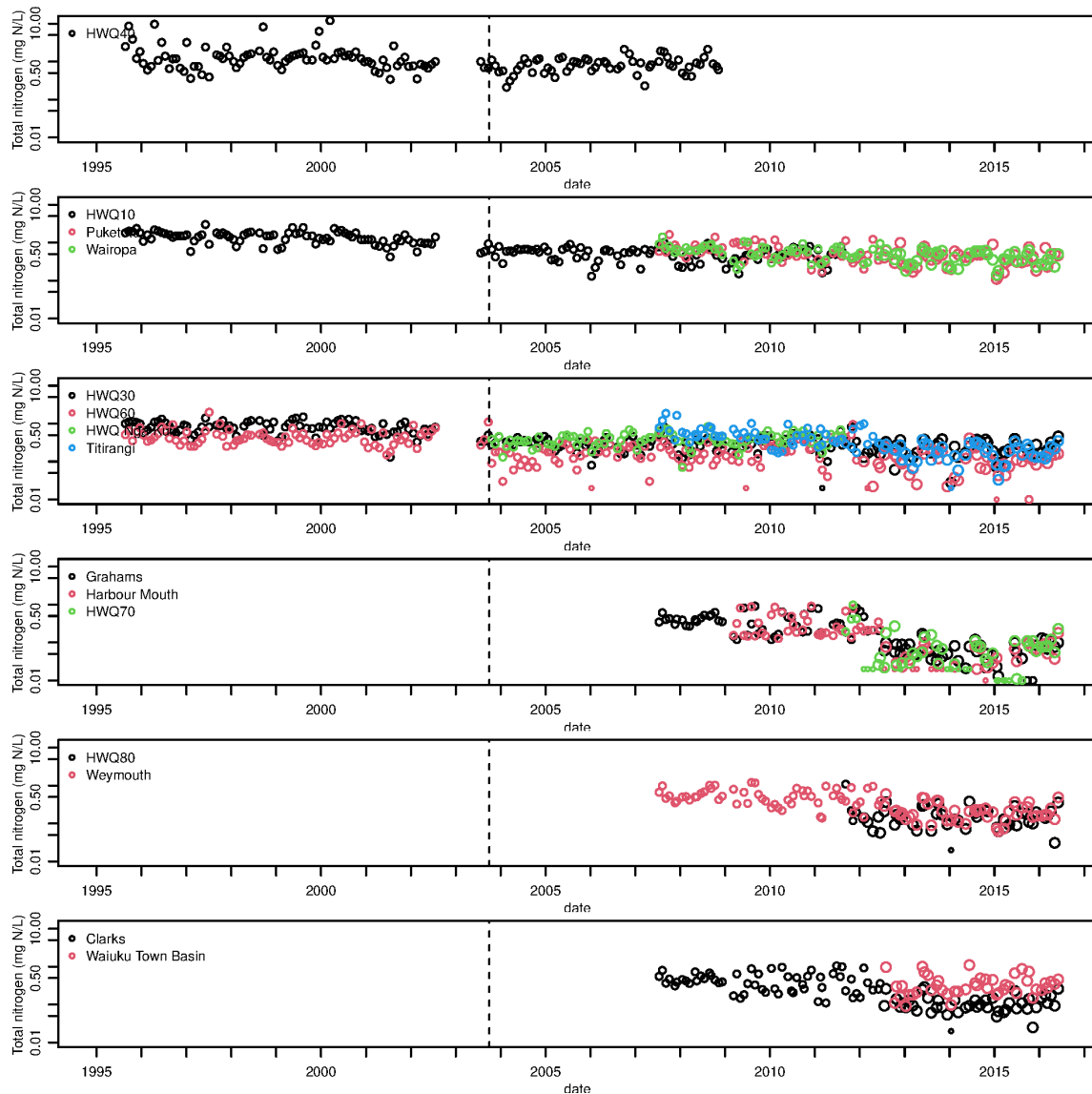


**Figure 4-2: Total nitrogen measured at Manukau Harbour (HEMP) sampling locations.** Coloured circles represent individual water quality samples; the vertical broken black line at the end of 2003 coincides with the approximate time when the wastewater storage pond was removed as part of a treatment plant upgrade.

## 4.2 Methods

The DelWAQ simulation predictions (or, more accurately in the case of a calibration exercise, hindcasts) at the HEMP monitoring locations were archived at 15-minute intervals. We endeavoured to approximate the real-world HEMP sampling scheme as follows:

1. at each of the HEMP monitoring locations, hindcast water levels were used to identify high tides, and the model state-variables were extracted over corresponding subsequent ebb tides,
2. for each model state-variable at each station, two sets of ebb-tide hindcasts per 24-hour period were extracted. Model hindcasts between 8 pm and 6 am were omitted to better align with the day-time sampling, and

3. as the observations were derived from near-surface water-samples, we compared model hindcasts from the surface layer with the observations.

We simulated the 2010–2011 year and compared the model hindcasts with a synthetic time-series. The synthetic time-series comprised 12 monthly values (January, February... December). Each monthly value in the synthetic series was the average of the data from the corresponding month in the field data spanning the period 2004–2019.

To reduce the impact of the initial conditions on the model results, the model was spun-up to quasi-equilibrium for the 1-year period January 2010 to January 2011 using our cold-start initial conditions. This gives the system time to ‘forget’ the user-supplied initial conditions and adapt towards the state that the coefficients, boundary conditions etc., dictate that it should adopt. Results from the end of this simulation were then used as ‘hot-start initial conditions’ for subsequent simulations. Those subsequent simulations spanned the period 1 January 2010- 1 March 2011..

We found that despite parametric changes introduced between the initial cold-start simulation and any subsequent hot-started calibration simulations, the hot-start initial conditions were forgotten in less than two months of simulated time. Thus, for our ultimate analyses, we discarded the hot-started simulation results from 1 January 2010-28 February 2010 and restricted our analyses to hot-started simulation results from the 1 March 2010-1 March 2011 simulation period.

#### 4.2.1 Phytoplankton carbon:chlorophyll ratios

Unlike some other phytoplankton growth, the DYNAMO growth model assumes that the taxon-specific carbon:chlorophyll ratio is constant (a user specified value). In DYNAMO, the state-variables representing phytoplankton abundance are ‘diatom carbon concentration’ and ‘green algae carbon concentration’ (non-diatom algal carbon concentration). The DYNAMO module enables the user to specify taxon-specific, constant Chl<sub>a</sub>:C ratios for diatoms and green algae. These ‘convenience coefficients’ enable the model to report inferred Chl<sub>a</sub> concentrations, but they play no dynamic role in the model’s differential equations<sup>13</sup>. Whilst differing (but constant) coefficients can be specified for DYNAMO’s diatoms and green algae, it is not possible to render them functions of the evolving local environmental conditions. Thus, there is only limited scope for the model to reproduce event-scale, seasonal-scale or spatial variations in Chl<sub>a</sub>:C ratios.

The field data do not contain estimates of phytoplankton concentration as carbon. Instead, chlorophyll-*a* concentration is measured as a proxy for phytoplankton abundance. In reality, even within an individual phytoplankter, cell-specific chlorophyll-*a*:carbon (Chl<sub>a</sub>:C) ratios evolve over time-scales of hours to days in response to the environmental characteristics that the cell has recently experienced (especially light intensity, ambient nutrient concentrations and water temperature). Furthermore, different taxa can exhibit differing Chl<sub>a</sub>:C ratios even when they have experienced similar environmental conditions.

Initial comparisons between field observations of Chl<sub>a</sub> concentration and Chl<sub>a</sub> concentrations inferred from the simulated carbon concentrations and the nominated, constant Chl<sub>a</sub>:C ratios revealed discrepancies that we believe reflect the model’s failure to explicitly represent all of the processes that influence cell-specific Chl<sub>a</sub>:C ratios. We found that the fit between observed and simulated Chl<sub>a</sub> could be improved by applying a seasonally varying Chl<sub>a</sub>:C ratio (as a post-processing operation after the simulation had completed). More specifically, we assume that the Chl<sub>a</sub>:C ratio

---

<sup>13</sup> Phytoplankton-dependent light attenuation is specified through a coefficient that relates attenuation to phytoplankton carbon concentration rather than phytoplankton chlorophyll concentration.

varies sinusoidally through the year, being higher in summer (maximum Chla:C = 55) than in winter (maximum Chla:C = 48). The phase and amplitude of the yearly cycle were chosen to be consistent with data from the Marlborough District Council (MDC) monthly monitoring programme in Pelorus Sound (the monitoring programme and data data from early years of it are summarized in Broekhuizen and Plew 2018). Note that, in the MDC data, there are some subtle differences amongst sites in the annual means and the phases and amplitudes of the annual Chla:C cycles. In particular, the amplitudes are smaller at the inner-Sound sites (PLS-1, PLS-2, Mahau and Kenepuru arms of Pelorus respectively). It is probable that the spatial patterns reflect differing turbidities or proximity to river influences etc. Whilst Manukau Harbour has much more extensive intertidal zones than Pelorus Sound has, it is possible that analogous spatial differences exist inside the Manukau Harbour. Nonetheless, we have restricted ourselves to imposing only a seasonal Chla:C cycle in the Manukau model.

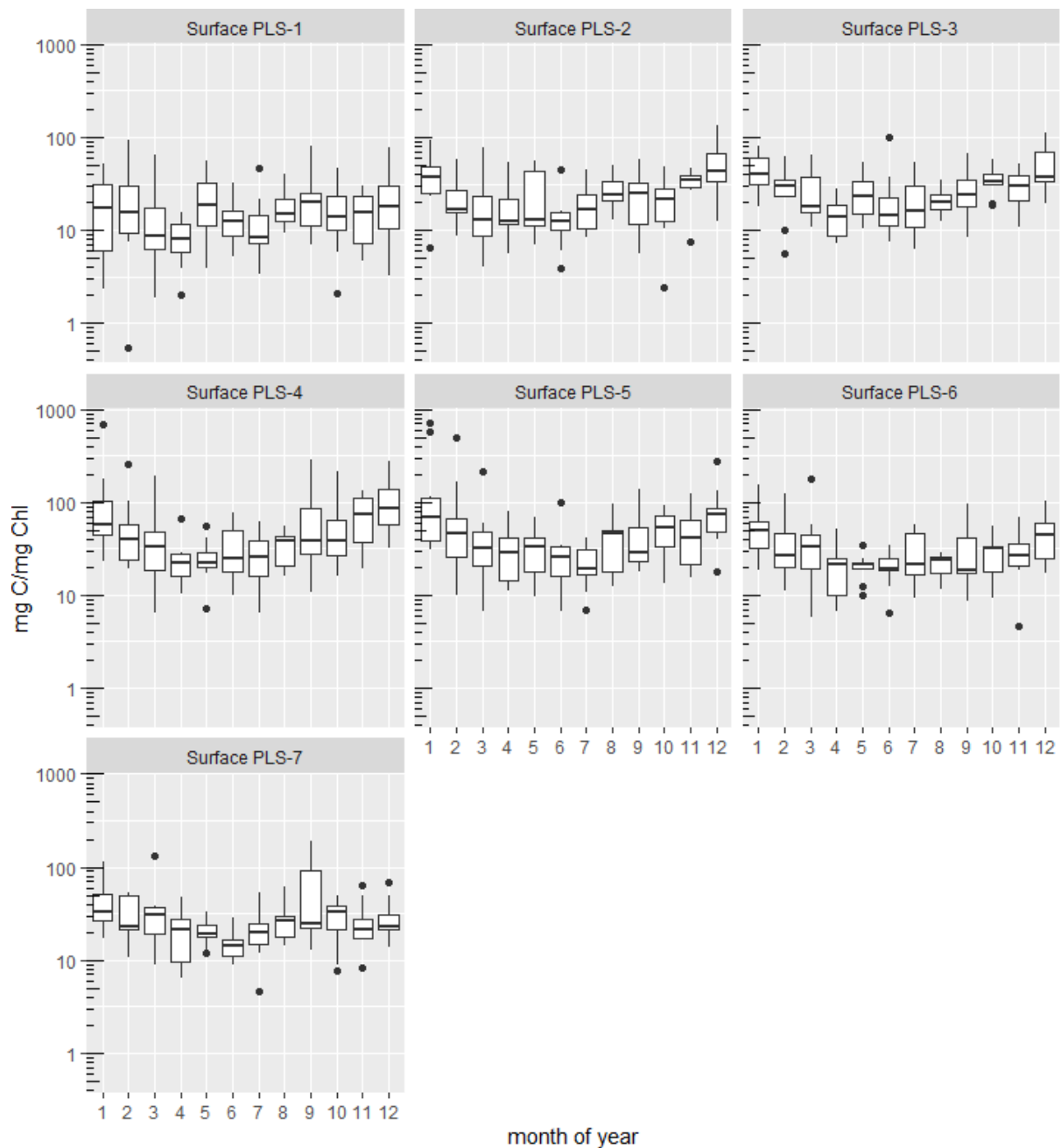


**Figure 4-3: Boxplots of phytoplankton carbon:Chla ratios measured at seven sites in Pelorus Sound.** Data are from the Marlborough District Council monthly monitoring programme. The sites have been sampled at approximately monthly intervals since July 2012. An open hose is lowered to approximately 12 m depth, closed and recovered to yield a depth-averaged surface water sample. Chlorophyll-*a* (Chla) concentrations were measured on a GFC filter. Lugols-preserved phytoplankton were identified, counted and cell dimensions were measured. Cell biomass was estimated using taxon-specific relationships between carbon content and cell volume (approximated using geometrical shapes). The heavy line within each box denotes the median. The boxes extend out to the 25<sup>th</sup> and 75<sup>th</sup> percentiles and the lines extend from the 25<sup>th</sup> (75<sup>th</sup>) percentile to no further than  $1.5 \times$  inter-quartile range.

### 4.3 Model performance measures

Target diagrams (Jolliff et al. (2009); Los, Blaas (2010)), which display model normalised bias  $B^*$  and normalised, unbiased root-mean-squared difference  $RMSD^*$  between model hindcasts and observations, were used to assess model performance.

$B^*$  is a measure of the difference between the time-averages of the model hind-cast and the time-average of the target data (field observations) scaled by the standard-deviation within the target data-set. Similarly,  $RMSD^*$  derives from the squared-differences between corresponding values in paired time-series of hind-cast and observed values normalised against the standard deviation of the observed values. It provides an indication of how successfully the model is reproducing the magnitudes and/or phases of any shorter-term oscillations/fluctuations that may be present in the target time-series (field data).

Normalisation ensures that all the error measures are non-dimensional – making it easier to compare, say, Chla performance with total-nitrogen performance.

Following Jolliff et al. (2009); Los, Blaas (2010):

$$B^* = \frac{\bar{M} - \bar{D}}{\sigma_D} \quad (1)$$

where  $B^*$  is normalised  $B$ ;  $\bar{D}$  is the time-average of the observations;  $\bar{M}$  is the time-average of the corresponding model hindcasts; and  $\sigma_D$  is the standard deviation of the observations<sup>14</sup>.  $B^*$  is non-dimensional.

Also:

$$RMSD^* = \frac{\sigma_M}{\sigma_D} * \frac{\text{sgn}(\sigma_M - \sigma_D)^{1/2}}{[(M_n - \bar{M}) - (D_n - \bar{D})]} \quad (2)$$

where  $RMSD^*$  is normalised  $RMSD$ ;  $\sigma_M$  is the standard deviation of the model hindcasts;  $M_n$  is the  $n$ th observation;  $D_n$  is the  $n$ th hindcast; and  $\text{sgn}$  is the sign operator.

The sign of  $B^*$  is positive if the time-average of the hind-cast exceeds the time-average of the target (observed) values. Conversely, the sign is negative if the time-average of the hind-cast is less than that of the observations. If the absolute difference between mean of the hindcast and the mean of the observations is smaller than the standard deviation of the observations, the absolute value of  $B^*$  will be inside the range  $0 \leq B^* < \pm 1$ .

Small values for  $B^*$  indicate that the model is reproducing the time-mean of the observed time-series well (because the discrepancies between the time-means of the hind-cast time-series and observed time-series are small relative to the differences across the observed time-series).

$RMSD^*$  may be regarded as an overall measure of disagreement between observations and hindcasts that arises from differences in amplitude or phase, as opposed to any difference in time-series averages. The sign of  $RMSD^*$  is positive if the standard-deviation the hind-cast exceeds or is equal to the standard-deviation of the target (observed) values. As with  $B^*$ , values of  $RMSD^*$  that are close to zero indicate good model performance.

<sup>14</sup> For consistency, we normalised performance scores by the standard deviation of the 12-value monthly synthetic time-series, rather than by the standard deviation of the 2004–2019 field-data time-series.

An example target plot is given in Figure 4-4, which suggests that hindcasts at site A are ‘good’ (because  $RMSD'^* < \pm 1$ ) but at site B they are ‘poor’ (because  $RMSD'^* > \pm 1$ ). At both sites,  $B^*$  is positive, indicating that the time-averaged hindcast is greater than the time-averaged observation.

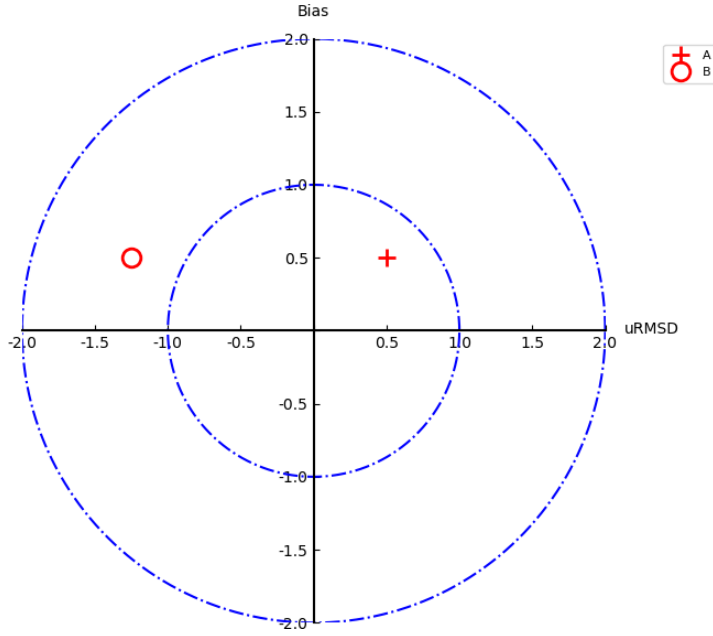


**Figure 4-4:** Example target diagram: y-axis is normalised bias ( $B^*$ ) and x-axis is normalised RMSD ( $RMSD'^*$ ). (where:  $uRMSD = RMSD'^*$ ). Site A (red plus symbols) and site B (red circle symbols).

We use the error radius:

$$E_{s,v} = \sqrt{RMSD'^*{}^2_{s,v} + B^{*2}_{s,v}} \quad (4)$$

as a compact (inverse) measure of the congruence, or ‘goodness-of-fit’ between observations and hindcasts for the  $v$ -th state-variable at the  $s$ -th monitoring station. (Note that we frequently talk about the ‘model best fit’ by which we really mean configuring the model in the way that model hindcasts most nearly match field observations).  $E_{i,s}$  takes account of discrepancies arising from any inability of the model to reproduce either or both of (i) the long-term mean of the state-variable, and (ii) the amplitudes and phases of fluctuations in the state-variable. The smaller the value of  $E_{i,s}$ , the closer the congruence between observations and hindcasts.

The total error radius is given by:

$$E_{tot} = \sum_{s=1}^{15} \sum_{v=1}^8 E_{s,v} \quad (5)$$

where  $E_{tot}$  so calculated gives all stations and all state-variables equal weight in the estimate of goodness-of-fit.  $E_{tot}$  also weights  $B^*$  and  $RMSD'^*{}^2$  equally.

We calculated  $E_{tot}$  from eight state-variables (or derivatives thereof: oxygen, nitrate, ammoniacal-N, total phosphorus, soluble reactive phosphorus, total nitrogen, Chla and salinity) for which field observations exist<sup>15</sup> and 15 monitoring stations.

The calibration process is an iterative process which involves the systematic changing or tuning of model parameters to optimise the model predictive capability. We sought the model configuration that results in the lowest  $E_{tot}$ . This implies that we sought to optimise the fit of the model across all monitoring sites and all monitored water properties (rather than favouring some sites and/or properties at the expense of others).

#### 4.4 Model calibration

Ecological models are characterised by large uncertainties in their parameters and DelWAQ is no exception. Whilst simple models can often be calibrated to data using automated parameter optimisation methods, those methods are computationally prohibitive to apply to models as complex as this one. Furthermore, it is our impression<sup>16</sup> that, for models as complex as this one, these formal optimisation methods usually fail to converge upon a solution<sup>17</sup>. In part, this reflects the fact that most response-variables are influenced by several processes, and many of those processes are dependent upon the states of other response-variables. The former means that it is difficult (either through manual calibration or automated techniques) to determine which process(es) to focus calibration efforts upon in order to tune to any single response variable, whilst the latter implies that it is rarely possible to tune any one response variable in isolation from others.

Improving the model's ability to reproduce (or hindcast) one state-variable sometimes had counter-intuitive, adverse influences upon the reproduction of another state-variable. Similarly, we sometimes found that achieving an improved fit for one (or more) state-variable(s) in one part of the harbour, worsened the fit(s) in another part of the harbour.

We also sometimes found that a parametric change which yielded improved model fits when applied in isolation from other parametric changes sometimes worsened the model fit when applied with one other parametric changes that had also proven beneficial when applied in isolation.

We undertook a total of 44 formal calibration trials with the final configuration of the model (and many prior shorter simulations during the initial model setup). Each simulation spanned 14 months of model time, and required around 7–8 computer-days to complete. Based upon this experience, we are confident that it would be possible to improve the fit of the model to one (or a few) state-variables in some specific region of the harbour by adopting a differing parameterisation, but we are not confident that one could achieve a meaningfully better fit to the collective, harbour wide data. We believe that many different (and currently confounding) factors would need simultaneous adjustment to improve harbour wide calibration substantially - the knowledge required to guide such optimisation does not exist at present.

---

<sup>15</sup>Strictly, salinity (which is a component of the archived forcing data), is generated by the hydrodynamic model, not by DelWAQ. Therefore, the  $B^*$  and  $\text{RMSD}^*$  scores for salinity reflect the performance of the hydrodynamic model rather than the performance of DelWAQ. Inevitably, the performance scores remained the same across all DelWAQ simulations. Thus, the ranking of the various DelWAQ simulations (as measured by the error radius) is independent of salinity and derives only from the fidelity with which DelWAQ reproduces the dynamics of the remaining seven state-variables (or properties derived from DelWAQ state-variables).

<sup>16</sup> Based upon a combination of limited personal experience and wider reading/discussion with other practitioners.

<sup>17</sup> Whether a local optimum or a global one.



## 4.5 Results

### 4.5.1 Iterative calibration

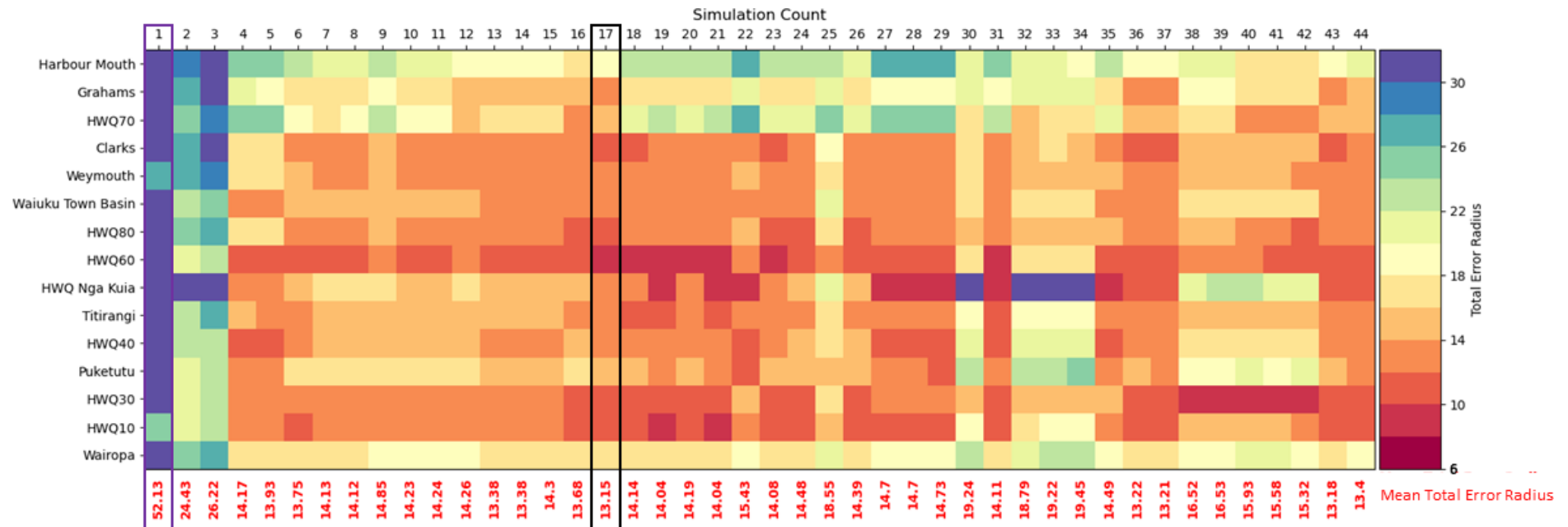
The error-radius scores at each station (and the mean score for all stations) for sequential calibration trials made using the ultimate model variant (that used the DYNAMO phytoplankton module and the updated microphytobenthos module that Deltares delivered during the course of the project) are displayed in Figure 4-5<sup>18</sup>. After adopting the DYNAMO phytoplankton and revised MICROPHYT benthic algal modules (see Section 2.2 and Appendix E), the model predictions were found to be particularly sensitive to changes in the background light attenuation, optimal daylength for growth, and the nitrogen half-saturation for diatoms.

Figure 4-5 illustrates how  $E_{tot}$  evolved across sequential simulations and across stations.

- Simulation 1 from Figure 4-5 is a DYNAMO simulation before the implementation of the new MICROPHYT enhanced benthic algal module. All the subsequent simulations adopted the enhanced module.

---

<sup>18</sup> Figure 4-5 does not include data from the large number of simulations that we conducted done using the BLOOM module of the DelWAQ model or the simulations undertaken with DYNAMO with the much simpler default microphytobenthos benthic diatom module.



**Figure 4-5: Graphical representation of the performance of DelWAQ water-quality simulations undertaken using DYNAMO.** Simulation 1 (outlined with purple box) represents the DelWAQ model results before the updated MICROPHYT model was implemented. Simulations numbers from 2-44 include the enhanced benthic algal module MICROPHYT. Each numeral on the top x-axis identifies an individual simulation; simulations were run sequentially, from left-to-right. Each numeral on the lower x-axis indicates the mean of all  $E_{tot}$  for the HEMP monitoring site shown on the y-axis. The individual pixel colours indicate  $E_{tot}$  associated with each individual station. Simulation 17 (outlined with black box), represents the model with the best overall fit.

- In simulation 1, the mean  $E_{tot}$  across the 15 sampling sites and seven state-variables is 52.13. Adopting the enhanced benthic algal module that we commissioned Deltares to implement led to a dramatic improvement in model performance – the error score for simulation 2 (and all subsequent ones) was reduced by almost 50% (Figure 4-5).

Within our trials, simulation 17, hereafter referred to as MS17, yielded the best overall fit, with  $E_{tot} = 13.15$  (Figure 4-5). (Again, we note that ‘best fit’, means the configuration of the model that yields the closest match between model hindcasts and field observations – giving all stations and all state-variables (for which there are field data) equal weight.)

- Appendix D presents a summary of the model coefficients that were used in MS17.
- The station-specific results for MS17 are shown as a time-series overlaid upon the field data in Appendix A.
- The target-plot illustrations of model performance are presented in Appendix B.

Table 4-1 shows  $B^*$ ,  $RMSD'^*$  and  $E_{i,s}$  for simulation MS17.

- $|B^*| \leq 1.0$  in 69 out of 120 cases.
- $RMSD'^* \leq 1.0$  in 61 cases.
- $E_{i,s} \leq 1.0$  in 42 cases.
- There are no state-variables for which both  $B^*$  and  $RMSD'^*$  are  $\leq 1.0$  at all stations.

As for particular state-variables:

- the model performs best for salinity ( $|B^*| \leq 1.0$  and  $RMSD'^* > 1.0$  only at Weymouth),
- second-best is nitrate ( $|B^*| \leq 1.0$  in 13 of 15 cases and  $RMSD'^* \leq 1.0$  in 10 of 15 cases),
- third-best is dissolved oxygen ( $|B^*| \leq 1.0$  in eight of 15 cases and  $RMSD'^* \leq 1.0$  in 7 of 15 cases,
- Figure 4-6, Figure 4-8, Figure 4-9),
- concentrations of nitrate and phosphorus are predicted more reliably than are the concentrations of total nitrogen and total phosphorus<sup>19</sup>, and
- the model performs most poorly for ammoniacal nitrogen, total phosphorus (
- Figure 4-7, Figure 4-8, Figure 4-9) and Chla.
- In general,  $|B^*|$  tends to be smaller than  $RMSD'^*$ , implying that the model hindcasts long-term station averages better than it hindcasts phases and/or amplitudes of shorter-term fluctuations.
- The site with the best overall error radius across the seven state-variables is Weymouth with a station-specific  $E_{tot} = 8.74$ , followed by Titirangi with  $E_{tot} = 9.06$ .

<sup>19</sup> For total nitrogen: ammonium, nitrate, algal nitrogen, detrital nitrogen; for total phosphorus: dissolved reactive phosphorus, detrital phosphorus and algal phosphorus.

**Table 4-1: Summary of model performance measures.** The same information is presented graphically in Appendix B.

Substance	OXY			NO3			NH4			PO4			Chl-a			TN			TP			Salinity		
Sites	B <sup>+</sup>	RMSD <sup>+</sup>	Error radius	B <sup>+</sup>	RMSD <sup>+</sup>	Error radius	B <sup>+</sup>	RMSD <sup>+</sup>	Error radius	B <sup>+</sup>	RMSD <sup>+</sup>	Error radius	B <sup>+</sup>	RMSD <sup>+</sup>	Error radius	B <sup>+</sup>	RMSD <sup>+</sup>	Error radius	B <sup>+</sup>	RMSD <sup>+</sup>	Error radius	B <sup>+</sup>	RMSD <sup>+</sup>	Error radius
Clarks	0.57	0.4	0.7	0.53	0.41	0.68	-2.32	-2.33	3.29	-0.48	0.92	1.04	-0.17	1.21	1.22	-1.05	0.69	1.26	-1.93	1.35	2.36	-0.38	0.52	0.64
Grahams	-0.24	-0.53	0.58	1.08	0.41	1.15	2.23	-2.33	2.23	-0.38	0.98	1.05	-0.31	1.01	1.05	-0.76	1.08	1.32	-1.75	1.34	2.820	0.78	-0.87	1.17
Harbour Mouth	-1.13	-0.52	1.24	1.85	0.65	1.96	2.23	-1.22	2.54	-0.43	0.85	0.95	-1.27	1.1	1.68	-0.51	-1.62	1.7	-0.8	0.91	1.21	0.9	-02.33	2.498
HWQ 10	2.23	-1.05	2.47	0.59	0.52	0.79	-2.32	-1.46	2.74	1.01	0.93	1.37	0.05	-0.6	0.61	-0.26	0.75	0.79	0.01	1.24	1.24	-0.46	-0.67	0.81
HWQ 30	1.31	-0.73	1.5	0.57	0.64	0.86	-2.32	-2.33	3.29	0.81	0.82	1.15	0.57	0.7	0.9	0.28	0.75	0.8	0.2	0.99	1.01	-0.95	-0.74	1.02
HWQ 40	2.23	-0.85	2.39	-2.32	-1.7	2.8	-2.32	-2.33	3.29	-2.32	-2.33	3.29	0.68	1.2	1.38	-2.32	-2.33	3.29	-2.32	-2.33	3.29	1.33	-1.05	1.70
HWQ 60	0.44	0.48	0.65	0.7	0.63	0.94	-2.32	-2.33	3.29	-0.7	0.98	1.20	0.33	1.1	1.15	0.23	0.77	0.8	-1.77	1.41	2.26	-0.60	-0.82	1.02
HWQ 70	-0.73	0.46	0.86	1.4	0.69	1.56	2.23	-1.37	2.62	-0.26	1.1	1.13	-0.12	1.15	1.16	1.94	0.94	2.16	-0.17	1.29	1.3	-0.49	-1.27	1.36
HWQ 80	0.53	-0.67	0.85	0.53	0.6	0.8	-1.41	-1.95	2.41	-0.53	0.99	1.12	-0.08	1.08	1.08	0.45	0.76	0.88	-1.21	1.58	1.99	-0.73	0.69	0.97
HWQ Nga Kuia	1.63	-0.87	1.85	0.38	0.62	0.73	-2.32	-2.33	3.29	-0.17	1.02	1.03	0.85	0.82	1.18	-0.44	0.86	0.97	-1.15	1.27	1.71	-0.69	-0.64	0.94
Puketutu	0.95	-0.77	1.22	-0.15	0.8	0.81	-2.32	-2.33	3.29	-0.65	1.34	1.49	0.61	1.01	1.18	-1.15	0.89	1.45	-0.93	1.51	1.77	0.10	-0.66	0.67
Titirangi	0.67	0.58	0.89	0.36	0.62	0.72	-2.32	-2.33	3.29	0.03	0.95	0.95	0.55	0.89	1.05	-0.69	0.86	1.1	-0.48	0.88	1.00	-0.12	-0.66	0.67
Wairopa	1.08	-1.13	1.56	0.81	0.52	0.96	-1.43	-1.28	1.92	1.74	1.14	2.08	-0.03	0.59	0.59	-0.11	0.72	0.73	1.15	1.12	1.61	-0.35	0.76	0.84
Waiuku Town Basin	1.01	-0.52	1.14	-0.56	-1.13	1.27	-1.74	-1.51	2.30	-0.38	0.73	0.82	-1.4	-1.65	2.16	-1.43	-0.74	1.61	-2.32	-1.87	2.9	-0.12	0.54	0.55
Weymouth	0.46	-0.64	0.79	0.41	0.63	0.75	-0.9	1	1.34	-0.56	0.96	1.11	-0.44	1.07	1.16	-0.17	0.69	0.71	-1.07	1.19	1.6	-0.47	0.66	0.808
Number of cases where unsigned score <=1.0	8	13	7	11	13	10	1	1	0	12	10	3	13	5	3	10	12	7	3	6	0	14	13	9
Number of cases where test score is positive	12	4		12	13		3	1		4	13		7	13		3	12		2	13		4	5	

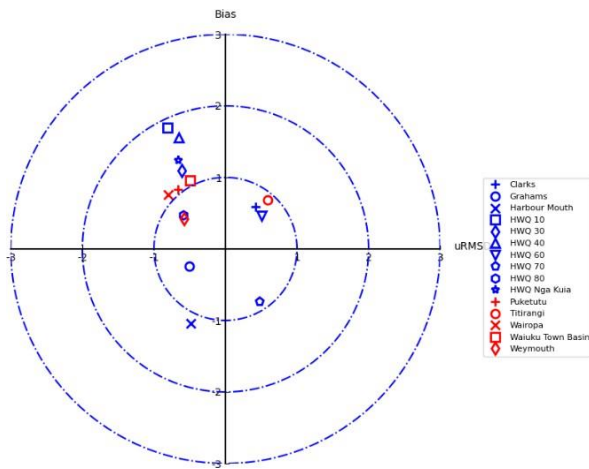


**Figure 4-6: Target diagram for dissolved oxygen at all sample sites.** Where: y-axis is normalised bias ( $B^*$ ) and x-axis is normalised RMSD ( $uRMSD = RMSD^*$ ).

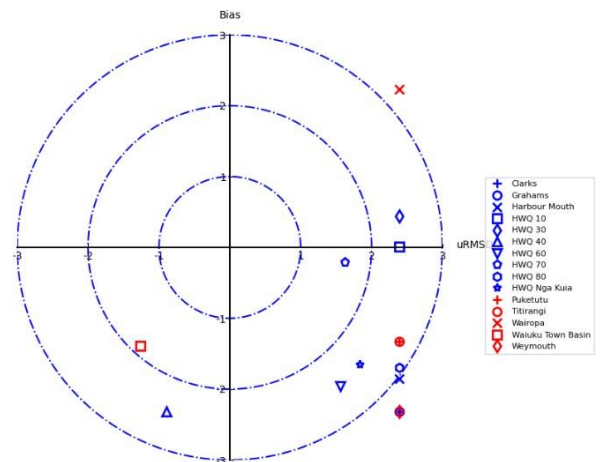


**Figure 4-7: Target diagram for total phosphorus at all sample sites.** Where: y-axis is normalised bias ( $B^*$ ) and x-axis is normalised RMSD ( $uRMSD = RMSD^*$ ).



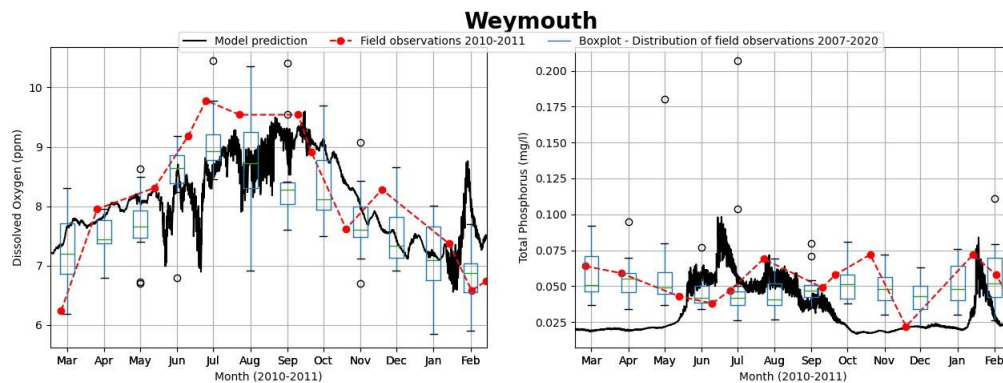


**Figure 4-8: Measured and hindcast dissolved oxygen and total phosphorus: station Weymouth.** The boxplots summarise all the measured data. Black line is the ebb-tide model hindcast. Red symbols denote the monthly HEMP data for the 2010–2011 year (where available). Boxplots illustrate the spread of the monthly HEMP data for the period 2004–2019 (or a lesser period in cases where sampling did not extend over that full calendar period). Green line = median, box limits are 25<sup>th</sup> and 75<sup>th</sup> percentiles of the samples, and distance between is the interquartile range. Whisker lines extend to 1.5 × interquartile range and correspond to approximately  $\pm 2.7$  sigma and 99.3% coverage if the data are normally distributed. Observations beyond the whisker length are marked as outliers (black circles). Further explanation of the symbology used in these graphs is provided in Appendix C.

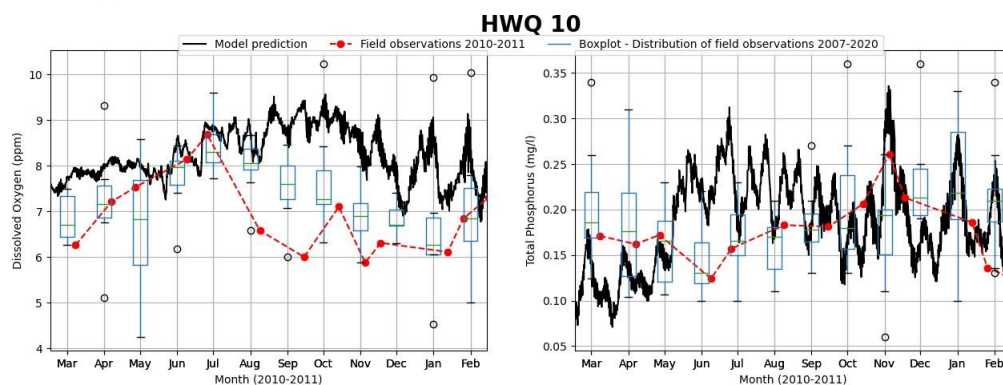


**Figure 4-9: Measured and hindcast dissolved oxygen and total phosphorus: station HQW 10.** The boxplots show all the measured data. Black line is the ebb-tide model prediction. Red symbols denote the monthly HEMP data for the 2010–2011 year (where available). Boxplots illustrate the spread of the monthly HEMP data for the period 2004–2019 (or a lesser period in cases where sampling did not extend over that full calendar period). Green line = median, box limits are 25<sup>th</sup> and 75<sup>th</sup> percentiles of the samples, and distance between is the interquartile range. Whisker lines extend to 1.5 × interquartile range and correspond to approximately  $\pm 2.7$  sigma and 99.3% coverage if the data are normally distributed. Observations beyond the whisker length are marked as outliers (black circles). Further explanation of the symbology used in these graphs is provided in Appendix C.

#### 4.5.2 Spatial patterns

Figure 4-10 to Figure 4-17 (figures assembled on pages after following remarks) show spatial (harbour-wide) patterns of hindcast and observed seasonal-average water-quality properties.

Regarding **salinity** (Figure 4-10):

- salinity in the wider body of the harbour is strongly affected by inputs from the Māngere WWTP, and in the Waiuku and Pahurehure sub-estuaries by the riverine plumes from the Taihiki River and the streams (Ngakoroa, Oira, Hingaia and Whangapouri) that feed Drury Creek, respectively,
- spatial patterns of salinity vary seasonally, with inner parts of the harbour being less saline during winter, reflecting higher winter-time inflows of freshwater and lesser winter-time evaporation at the sea-surface,
- the Māngere WWTP is, on average, the largest freshwater source; salinity in the northern harbour is often ~3 ppt less than at the harbour mouth, and
- at most of the monitoring locations, the model reproduces the seasonal change in salinity well.

Regarding **dissolved oxygen** (Figure 4-11):

- near-surface DO is high throughout the harbour, being higher in shallow water and during the seasons in which water is cooler,
- observed and hindcast seasonal-average DO in the vicinities of Puketutu, Māngere and Pahurehure inlets and the Taihiki River inlet tend to be a little lower than elsewhere in the harbour, and
- the model does a good job hindcasting DO.

Regarding **total nitrogen** (Figure 4-12):

- much like salinity, TN is strongly affected by inputs from the Māngere WWTP and in the Waiuku and Pahurehure sub-estuaries by the riverine plumes from the Taihiki River and the streams (Ngakoroa, Oira, Hingaia and Whangapouri) that feed Drury Creek,
- like salinity, TN also shows strong seasonal variability, and
- the model does a moderately good job of hindcasting TN.

Regarding **total phosphorus** (Figure 4-13):

- hindcast TP is high in the NE of the harbour and (to lesser degrees) in the upper reaches of the Pahurehure and Waiuku/Taihiki arms,
- hindcast TP tends to be higher in winter than in summer, and
- the model appears to reproduce the spatial patterns in TP a qualitative sense, but it over-estimates the degree of enrichment in the NE part of the harbour.



Regarding **ammoniacal nitrogen** (Figure 4-14):

- the field data reveal that the spatial extent of ammonium enrichment reduced markedly following the upgrade of the Māngere WWTP in the early 2000s,
- nonetheless, there is some evidence that ammonium concentrations in the vicinity of the Māngere outlet (and at the downstream end of the Pahurehure inlet) are a little higher than at other monitoring sites. They also tend to be a little higher during autumn than at other times of the year,
- hind cast ammonium concentrations are higher in the NE part of the harbour and Pahurehure inlet than in the main body of the harbour. They also tend to be a little higher in the autumn/winter than in the summer, and
- thus, the model is reproducing the dynamics of ammonium at least in a semi-quantitative sense.

Regarding **nitrate** (Figure 4-15):

- nitrate tends to be higher in winter months than in summer months,
- nitrate tends to be higher in the NE region of the harbour than else, and
- in a qualitative sense, the model reproduces both seasonal and spatial patterns in nitrate.

Regarding **dissolved reactive phosphorus** (Figure 4-16):

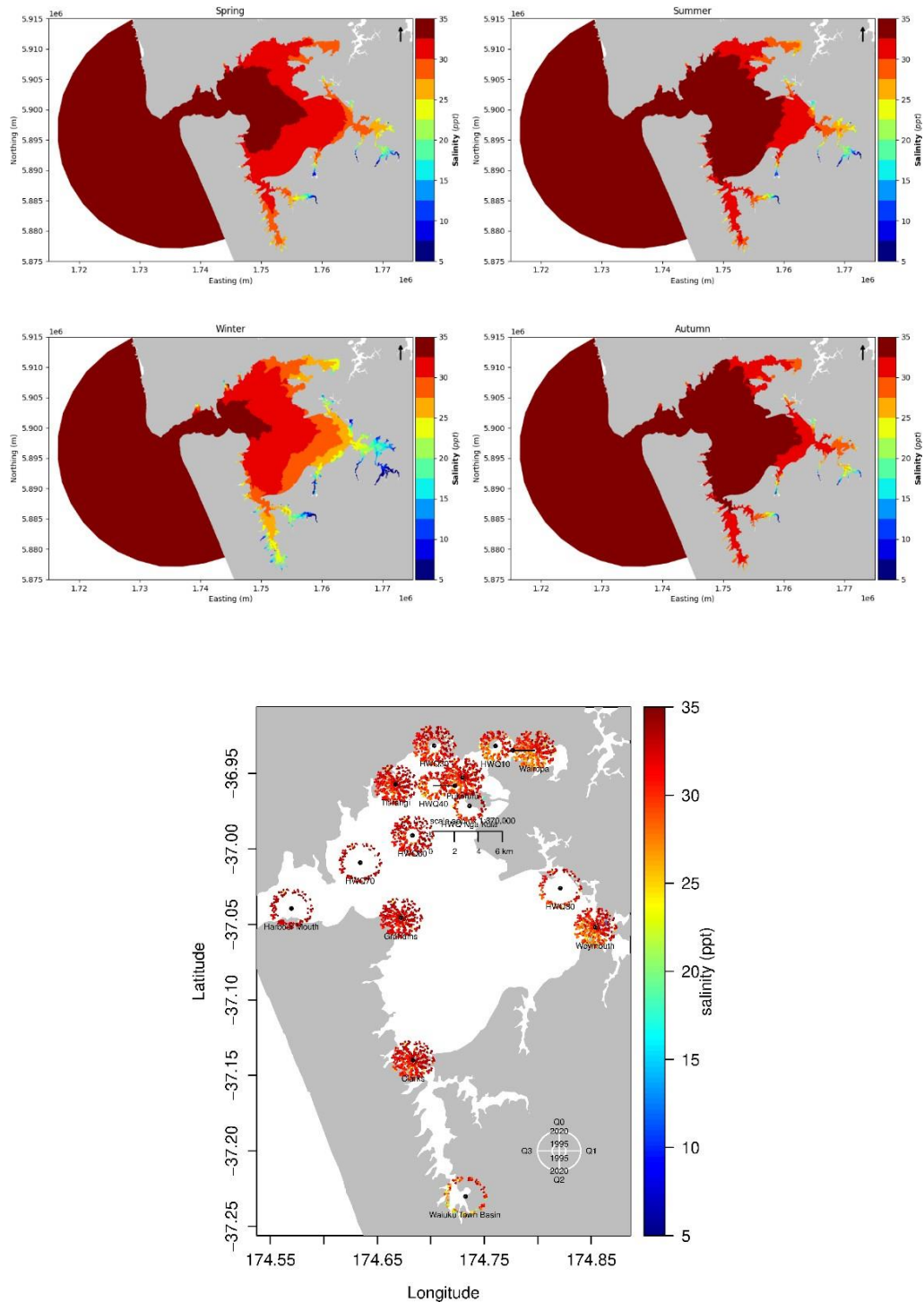
- hindcast phosphorus is clearly elevated only in the NE region of the harbour, more so in winter than in other seasons, and
- there are comparatively few field measurements, but they too indicate that phosphorus tends to be higher in the NE region of the harbour.

Regarding **Chla** (Figure 4-17):

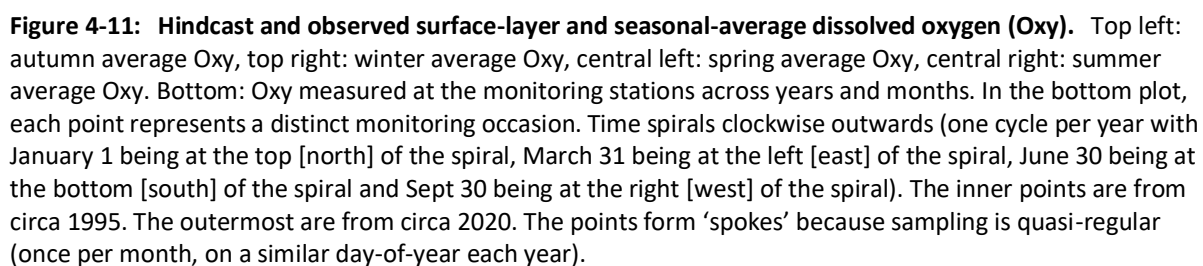
- Chla tends to be relatively uniform and highest across the intertidal flats during the winter months,
- especially spring and summer, Chla tends to be highest in the N and NE regions of the harbour and in the headwaters of the Pahurehure, Clarks Creek, Taihiki and Waiuku inlets, and
- hindcast patterns are qualitatively consistent with the observations.

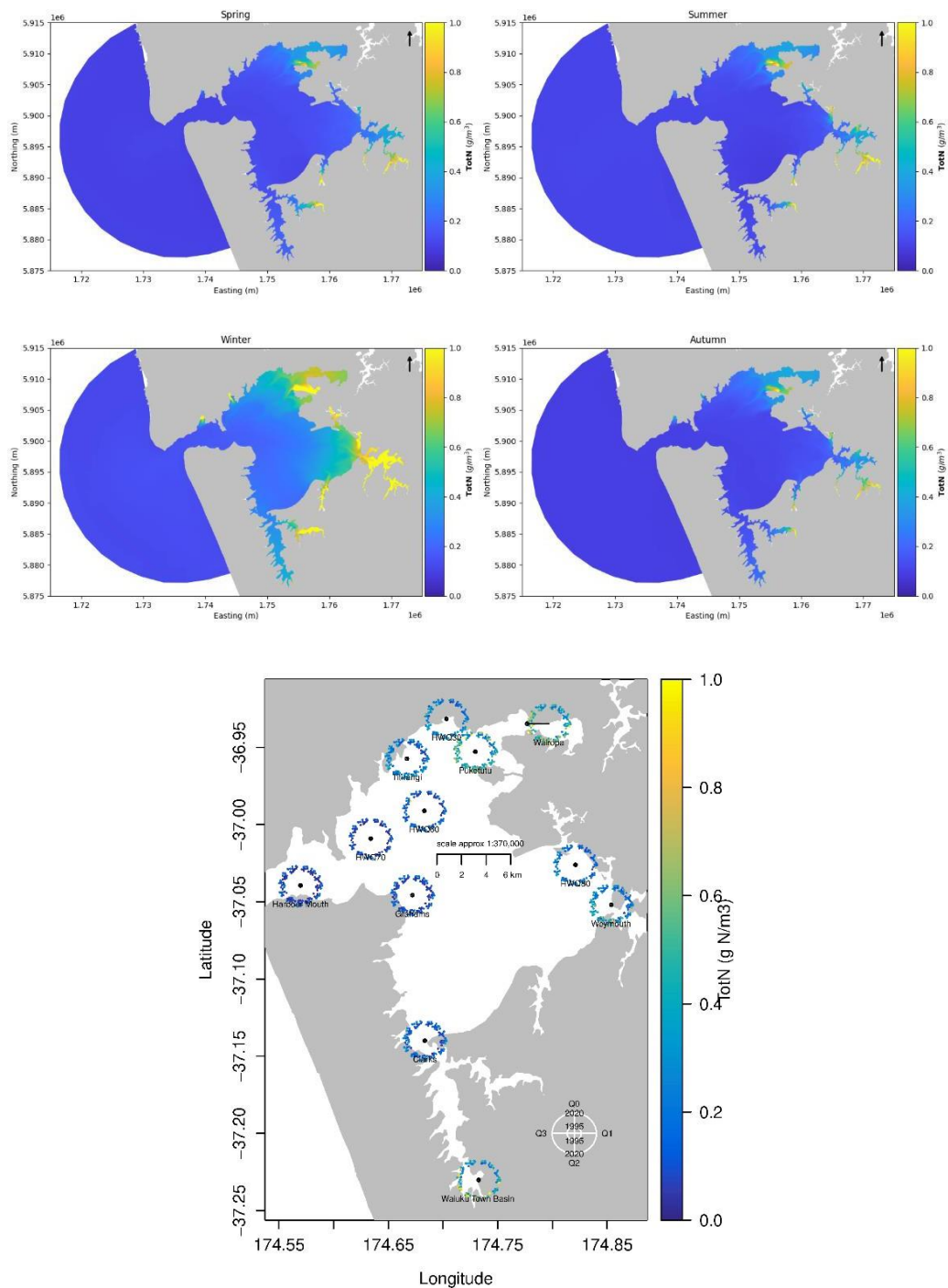
Regardless of season, most water-quality properties exhibit gradients between the upper reaches of individual arms (Waiuku, Taihihi, Clarks Creek, Pahurehure Inlet/Drury Creek, Māngere Inlet). For some of these, there are field-data from the central-upper parts of the arms. Across the spatial resolution implied by the field sampling locations, the spatial gradients evident in the simulations are similar to those evident in the field data. Thus, we believe that the model does distinguish the arms from the open waters of the central harbour basin and that the model can be usefully applied to address questions down to those sub-regional/arm-scales. The spatial gradients for salinity can only be driven by the freshwater inputs to the harbour. It is also likely that the gradients in other

properties are driven by the freshwater inputs (perhaps, acting in concert with local biogeochemical transformations).



**Figure 4-10: Hindcast and observed surface-layer and seasonal-average salinity.** Top left: autumn average salinity, top right: winter average salinity, central left: spring average salinity, central right: summer average salinity. Bottom: salinity measured at the monitoring stations across years and months. In the bottom plot, each point represents a distinct monitoring occasion. Time spirals clockwise outwards (one cycle per year with January 1 being at the top [north] of the spiral; March 31 being at the left [east] of the spiral; June 30 being at the bottom [south] of the spiral; and Sept 30 being at the right [west] of the spiral). The inner points are from











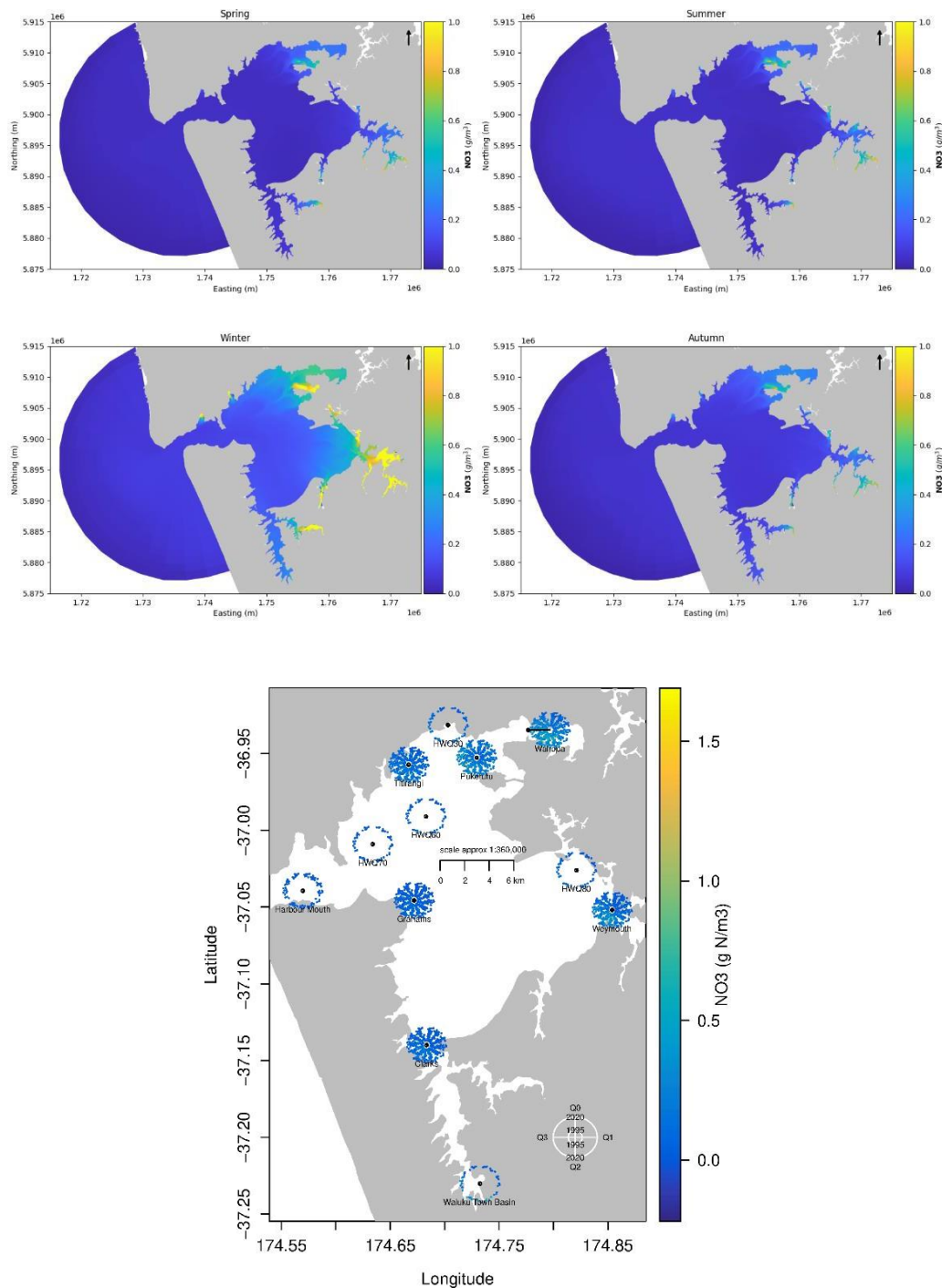


**Figure 4-15: Hindcast and observed surface-layer and seasonal-average nitrate ( $\text{NO}_3$ ).** Top left: autumn average  $\text{NO}_3$ , top right: winter average  $\text{NO}_3$ , central left: spring average  $\text{NO}_3$ , central right: summer average  $\text{NO}_3$ . Bottom:  $\text{NO}_3$  measured at the monitoring stations across years and months. In the bottom-plot, each point represents a distinct monitoring occasion. Time spirals clockwise outwards (one cycle per year with January 1 being at the top [north] of the spiral, March 31 being at the left [east] of the spiral, June 30 being at the bottom [south] of the spiral and Sept 30 being at the right [west] of the spiral). The inner points are from circa 1995. The outermost are from circa 2020. The points form ‘spokes’ because sampling is quasi-regular (once per month, on a similar day-of-year each year).





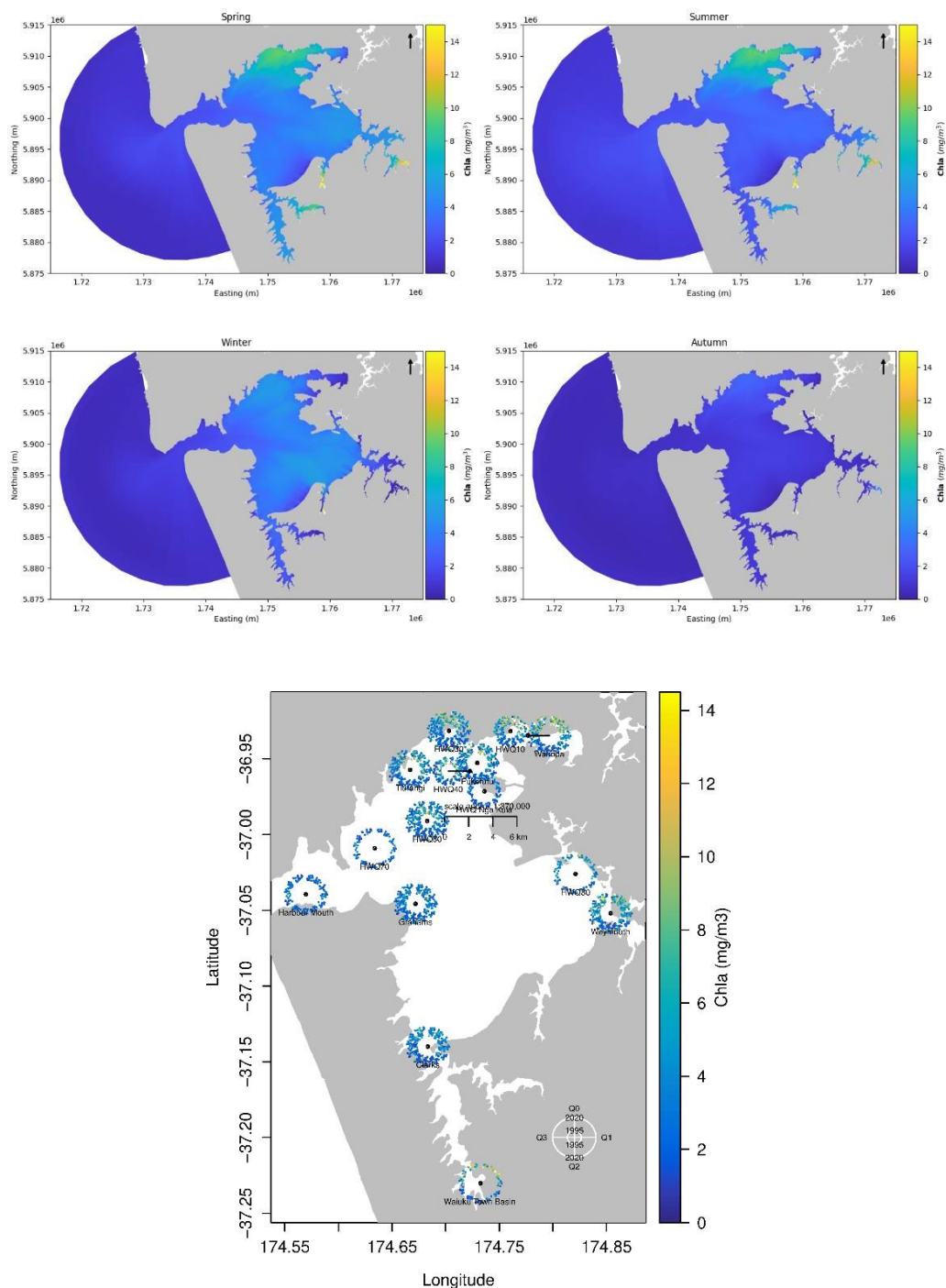


**Figure 4-17: Hindcast and observed surface-layer and seasonal-average chlorophyll-a (Chla).** Top left: autumn average Chla, top right: winter average Chla central left: spring average Chla, central right: summer average Chla. Bottom: Concentrations measured at the monitoring stations across years and months. In the bottom-plot, each point represents a distinct monitoring occasion. Time spirals clockwise outwards (one cycle per year with January 1 being at the top [north] of the spiral, March 31 being at the left [east] of the spiral, June 30 being at the bottom [south] of the spiral and Sept 30 being at the right [west] of the spiral). The inner points are from circa 1995. The outermost are from circa 2020. The points form ‘spokes’ because sampling is quasi-regular (once per month, on a similar day-of-year each year).

### 4.5.3 Seasonal cycles

The time-series plots (Appendix A) reveal seasonal cycles in most state-variables at most stations.

Observed **dissolved oxygen** concentrations tend to be greatest in winter. This is because (i) surface waters remain close to saturated throughout the year and (ii) oxygen saturation concentrations increase as water temperature falls. The model successfully reproduces the mean, phase and amplitude of the seasonal cycle at all stations. This suggests that oxygen exchange across the air–sea interface is fast relative to the rate at which oxygen is produced or consumed within the water column and at the seabed (even when simulated concentrations of phytoplankton are erroneously high or low, see below).

Observed concentrations of **inorganic nutrients** nitrate, ammonium, phosphorus and silicate all tend to be higher during the winter than during the summer. Again, the model reproduces the seasonal cycles, albeit often with some error in phase and/or amplitude. In particular, simulated concentrations of ammoniacal-N are too low during the summer months at most stations. Conversely, simulated winter-time nitrate concentrations are too high at many of the stations. Soluble phosphorus concentrations are reproduced well at some stations and poorly at others.

### 4.5.4 Weather and tidal-scale fluctuations

Thus far, we have focussed upon seasonal-scale and annual-scale variability, but water quality fluctuates on a variety of time-scales that are too short to be evident in monthly monitoring data.

Casual inspection of the time-series of simulated state-variables at the monitoring stations reveals fluctuations that are consistent with the dominant tidal cycle (approx. two cycles per day), and we suspect that a more detailed and formal analysis would reveal subtler fluctuations related to other tidal constituents (e.g., spring/neap cycle).

Perhaps more importantly, less regular but sometimes larger-amplitude fluctuations with quasi-periods of a few days are also evident. Whilst we have not formally sought to determine their causes, we believe these relate to the passage of weather systems. Weather will influence rainfall (hence, delivery of water and nutrients) to the harbour. It will also influence the quantity of solar radiation impinging upon the sea-surface, air temperature (hence water temperature), and winds (hence vertical mixing and residual – non-tidal – currents). Through these various intermediaries, weather will influence rates of primary production, rates of organic matter mineralisation, patterns of resuspension and deposition, and the manners in which solutes and particulates are transported around the harbour.

For example, ex-tropical cyclone Wilma moved across the north-east of the North Island over the course of 28–29 January 2011, bringing strong winds and heavy rain. This event was not captured in the HEMP monitoring, but the simulation results reveal patterns that are consistent with those expected to be associated with Wilma’s passage. There was a clear drop in salinity and increase in nutrients during this event (Figure 4-18). In fact, the model suggests that nutrient concentrations across much of the north-eastern harbour increased well above the normal range for several days (illustrated by predicted total nitrogen concentrations in the right-hand image within Figure 4-18).

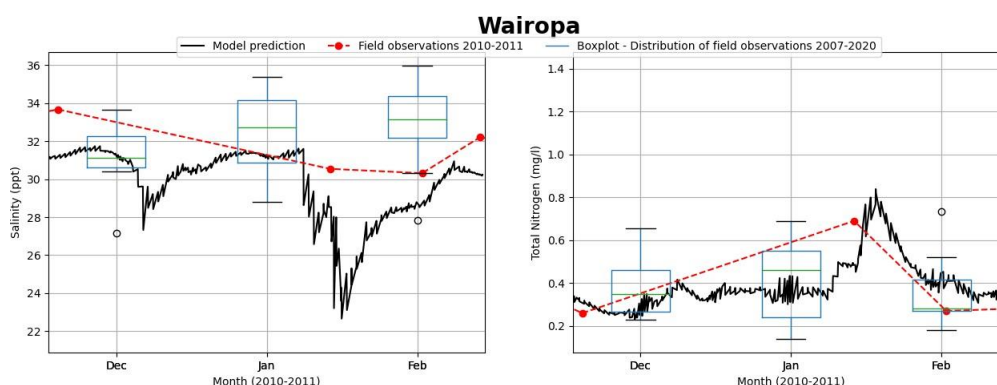


**Figure 4-18: Drop in salinity and increase in total nitrogen associated with the passage of ex-tropical cyclone Wilma.** Black line is the ebb-tide model prediction. Red symbols denote monthly HEMP data for the 2010–2011 year (where available). Boxplots illustrate the spread of the monthly HEMP data for the 2004–2019 period (or a lesser period in cases where sampling did not extend over that full calendar period). Green line = median, box limits are 25<sup>th</sup> and 75<sup>th</sup> percentiles of the samples, and distance between is the interquartile range. Whisker lines extend to 1.5 × interquartile range and correspond to approximately ± 2.7 sigma and 99.3% coverage if the data are normally distributed. Observations beyond the whisker length are marked as outliers and are black circle. Further explanation of the symbology used in these graphs is provided in Appendix C.

#### 4.5.5 Statistical performance of the model

In general, the ‘best-fit simulation’ (as measured by  $E_{tot}$ ) (simulation MS17) tends to:

- slightly over-predict near-surface salinity in some parts of the harbour and under-predict it in others (Figure 4-19, outer annulus). The magnitudes of the biases are smallest at the two stations closest to the harbour mouth (Harbour Mouth and Grahams). Elsewhere, there is little or no obvious correlation with water depth, proximity to wastewater plants etc.,
- over-predict DO concentration in the NE of the harbour and under-predict it in the vicinity of the harbour mouth (Figure 4-20, outer annulus),
- over-predict TN concentration around the harbour mouth, in the immediate vicinity of the Māngere WWTP outfall and in the Waiuku inlet (Figure 4-21, outer annulus),
- under-predict TP concentration at most sites, but over-predict it at the Wairopa site (Figure 4-22, outer annulus),
- over-predict ammonium at the three stations closest to the open ocean (Harbour Mouth, Grahams and HWQ70, Figure 4-23), but under-predict it elsewhere (especially in the NE harbour and Waiuku inlet),
- under-predict nitrate-N at the two stations closest to Māngere (Puketutu and HWQ40, Figure 4-24, outer annulus) and at the Waiuku Town Basin site, but over-predict it elsewhere. The greatest over-prediction is at two of the stations close to the harbour mouth (Harbour Mouth and HWQ70),
- under-predict dissolved reactive phosphorus at the two stations closest to the Māngere WWTP discharge (Puketutu, HWQ40, Figure 4-25, outer annulus), but over-predict it at the three stations in the NE-most part of the harbour (Wairopa, HWQ10, HWQ30),

- over-predict Chla at most stations in the NE harbour but under-predict it elsewhere (Figure 4-26, outer annulus),
- under-estimate the amplitude of fluctuations about the mean for salinity and dissolved oxygen (intermediate annuli in Figure 4-19 and Figure 4-20), but over-estimate the amplitude and/or mis-represent the phase of fluctuations for the remaining variables (Figure 4-21 to Figure 4-26, intermediate annulus), and
- even where the model hindcasts are biased, or have a tendency to exaggerate the amplitude of fluctuations, the discrepancies are not so large that it is impossible to usefully display both hindcasts and observations on the same scales (seasonal plots of Figure 4-8 to Figure 4-17 and Appendix A). Whilst this is only a very crude measure of goodness-of-fit, it does at least imply that model and data are in agreement to better than an order of magnitude. Indeed,  $B^*$  and  $RMSD^*$  scores suggest that hindcasts and observations rarely persistently disagree by more than a factor of two.

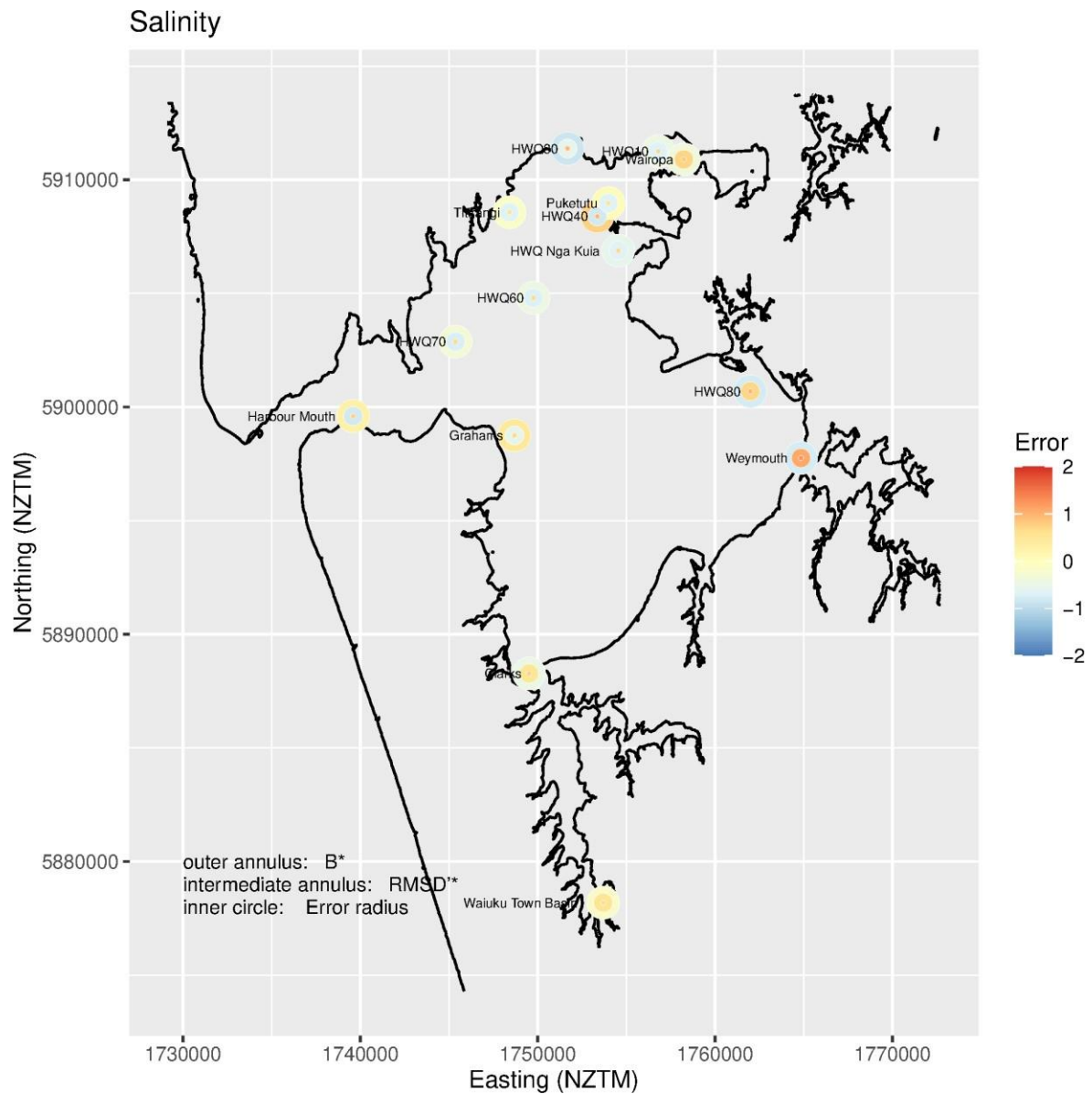


**Figure 4-19: False colour maps illustrating model performance for salinity at each monitoring station.** The colour of each outer annulus denotes  $B^*$ . The colour of each intermediate annulus denotes  $RMSD^*$ . The colour of each central circle illustrates  $E_{i, \text{salinity}}$ . A performance metric that is close to zero indicates that the model has performed well for the characteristic of which the metric is indicative.

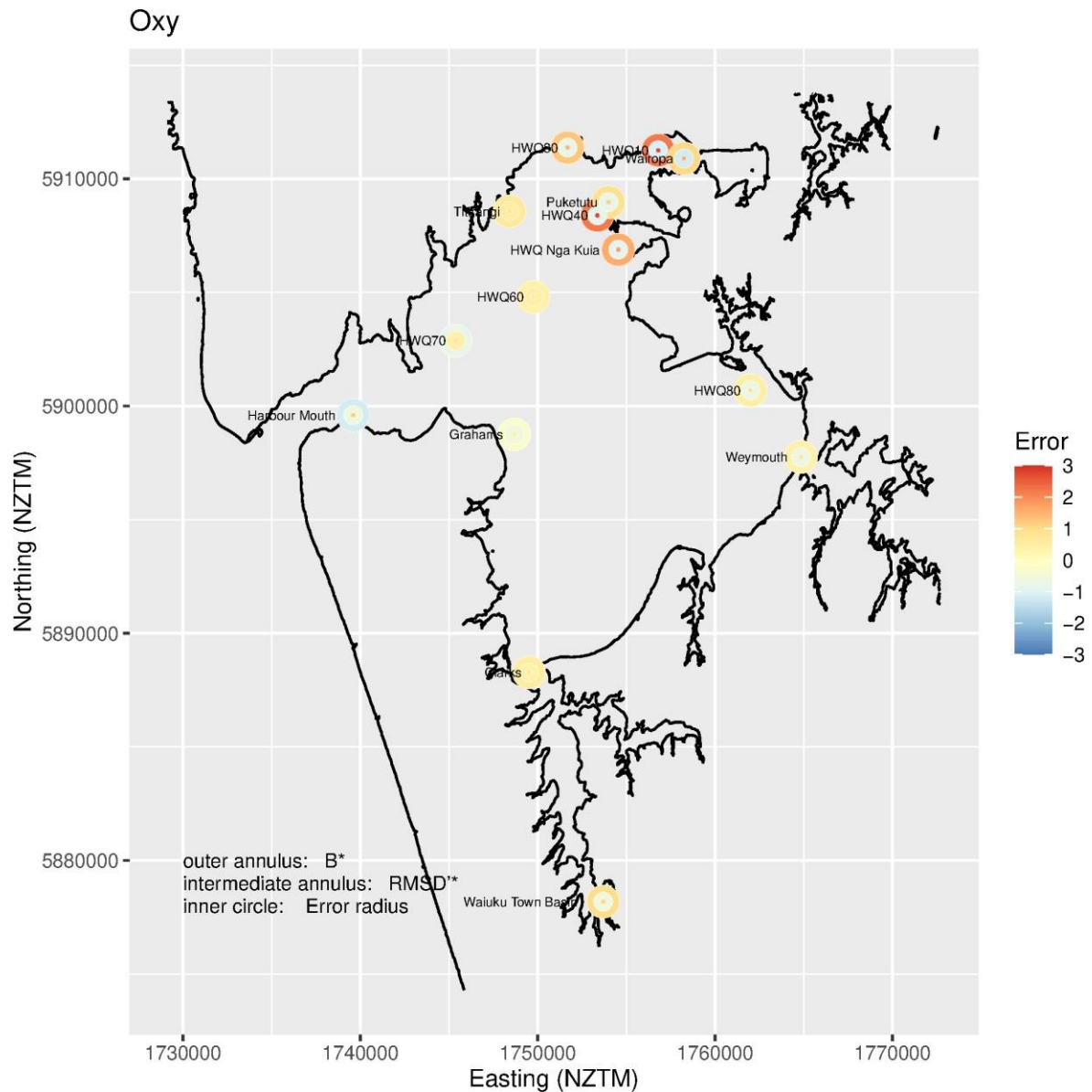


**Figure 4-20: False colour maps illustrating model performance for dissolved oxygen at each monitoring station.** The colour of each outer annulus denotes  $B^*$ . The colour of each intermediate annulus denotes  $RMSD^{**}$ . The colour of each central circle illustrates  $E_{i,O_{xys}}$ . A performance metric that is close to zero indicates that the model has performed well for the characteristic of which the metric is indicative.



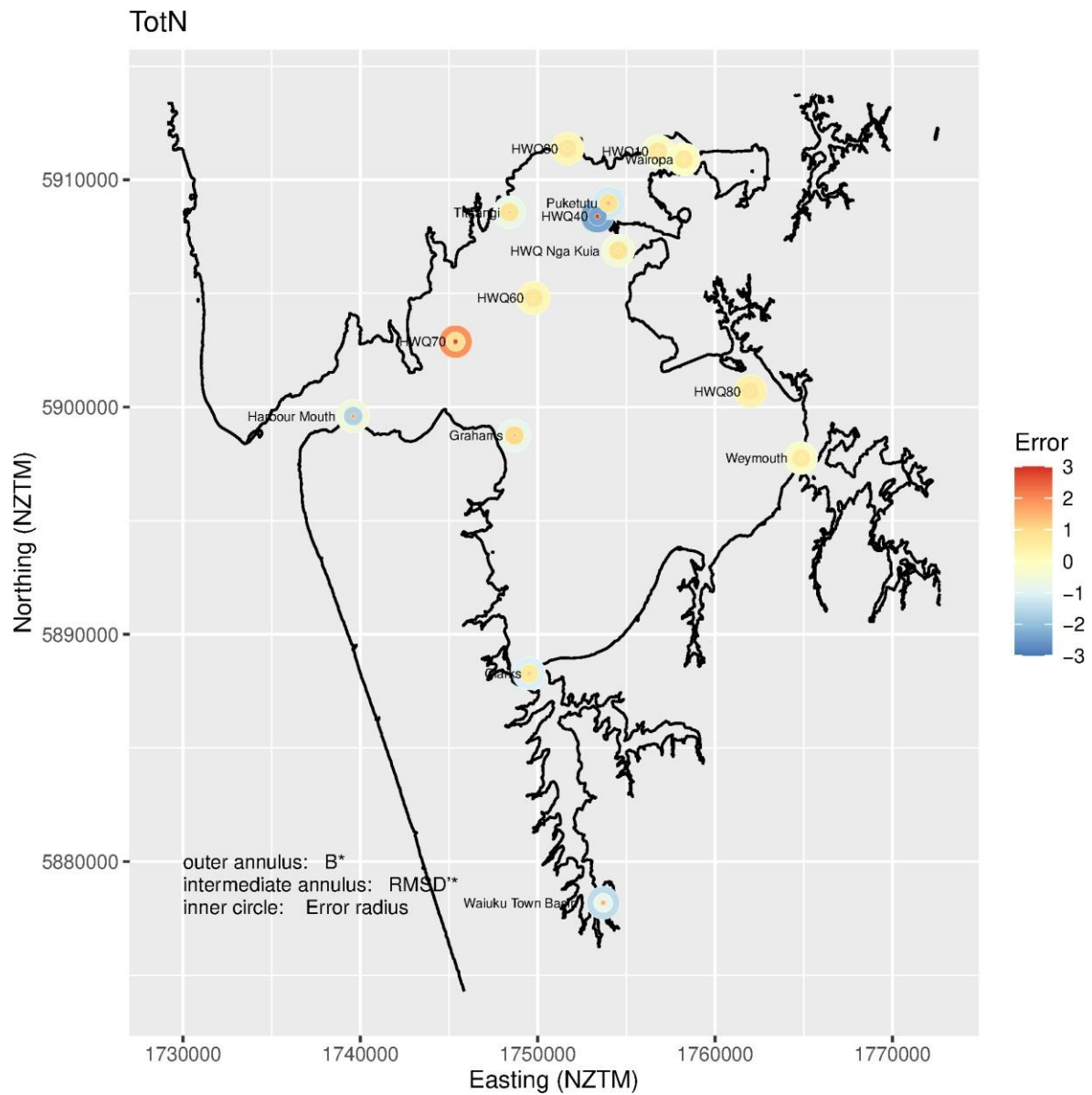


**Figure 4-21: False colour maps illustrating model performance for total nitrogen at each monitoring station.** The colour of each outer annulus denotes  $B^*$ . The colour of each intermediate annulus denotes  $RMSD^{**}$ . The colour of each central circle illustrates  $E_{i,TotNs}$ . A performance metric that is close to zero indicates that the model has performed well in characteristic of which the metric is indicative.



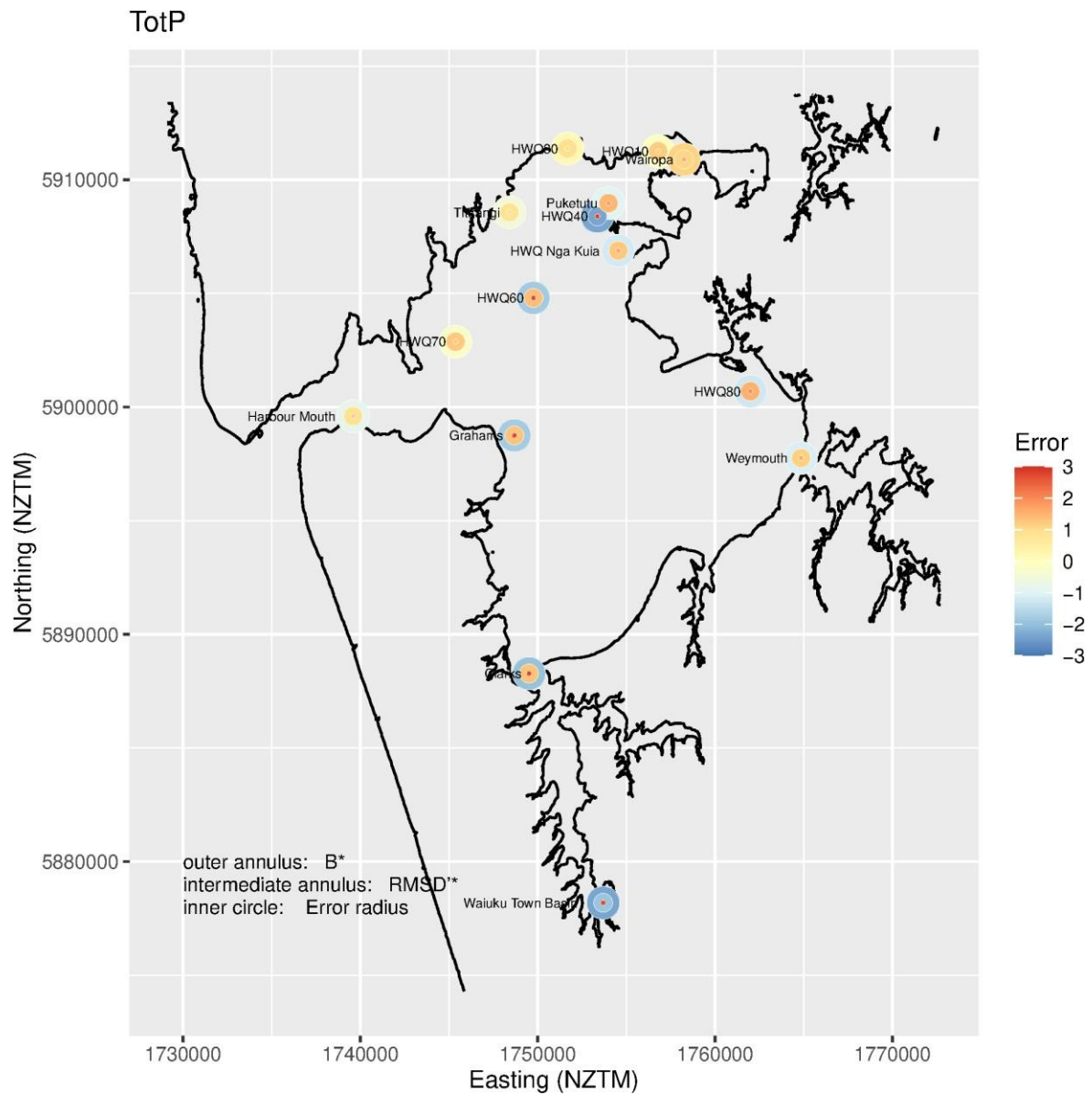


**Figure 4-22: False colour maps illustrating model performance for total phosphorus at each monitoring station.** The colour of each outer annulus denotes  $B^*$ . The colour of each intermediate annulus denotes  $RMSD^*$ . The colour of each central circle illustrates  $E_{i,TotPs}$ . A performance metric that is close to zero indicates that the model has performed well for the characteristic of which the metric is indicative.

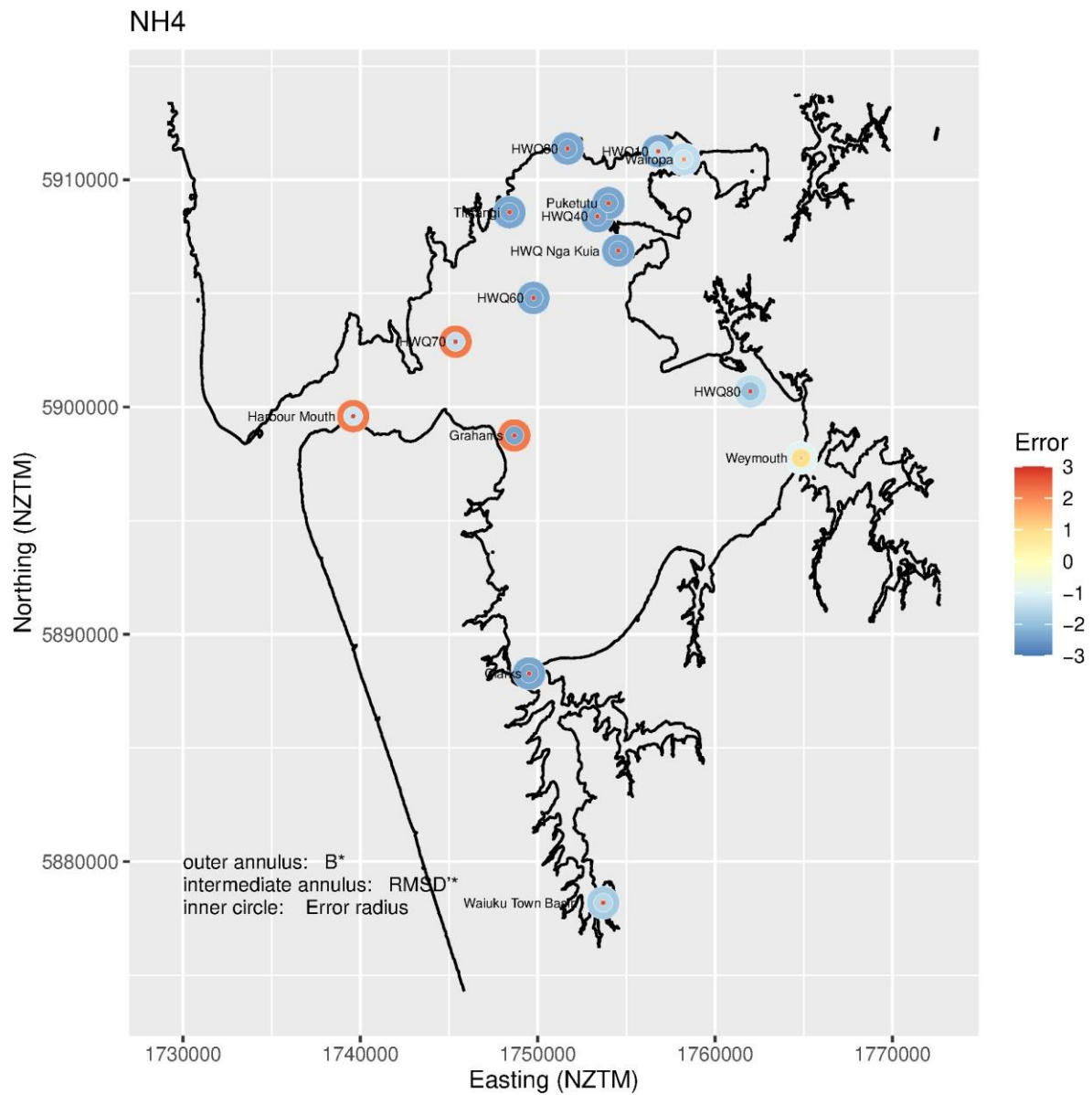


**Figure 4-23: False colour maps illustrating model performance for ammonium at each monitoring station.** The colour of each outer annulus denotes  $B^*$ . The colour of each intermediate annulus denotes  $RMSD^{**}$ . The colour of each central circle illustrates  $E_{i,NH4S}$ . A performance metric that is close to zero indicates that the model has performed well for the characteristic of which the metric is indicative.

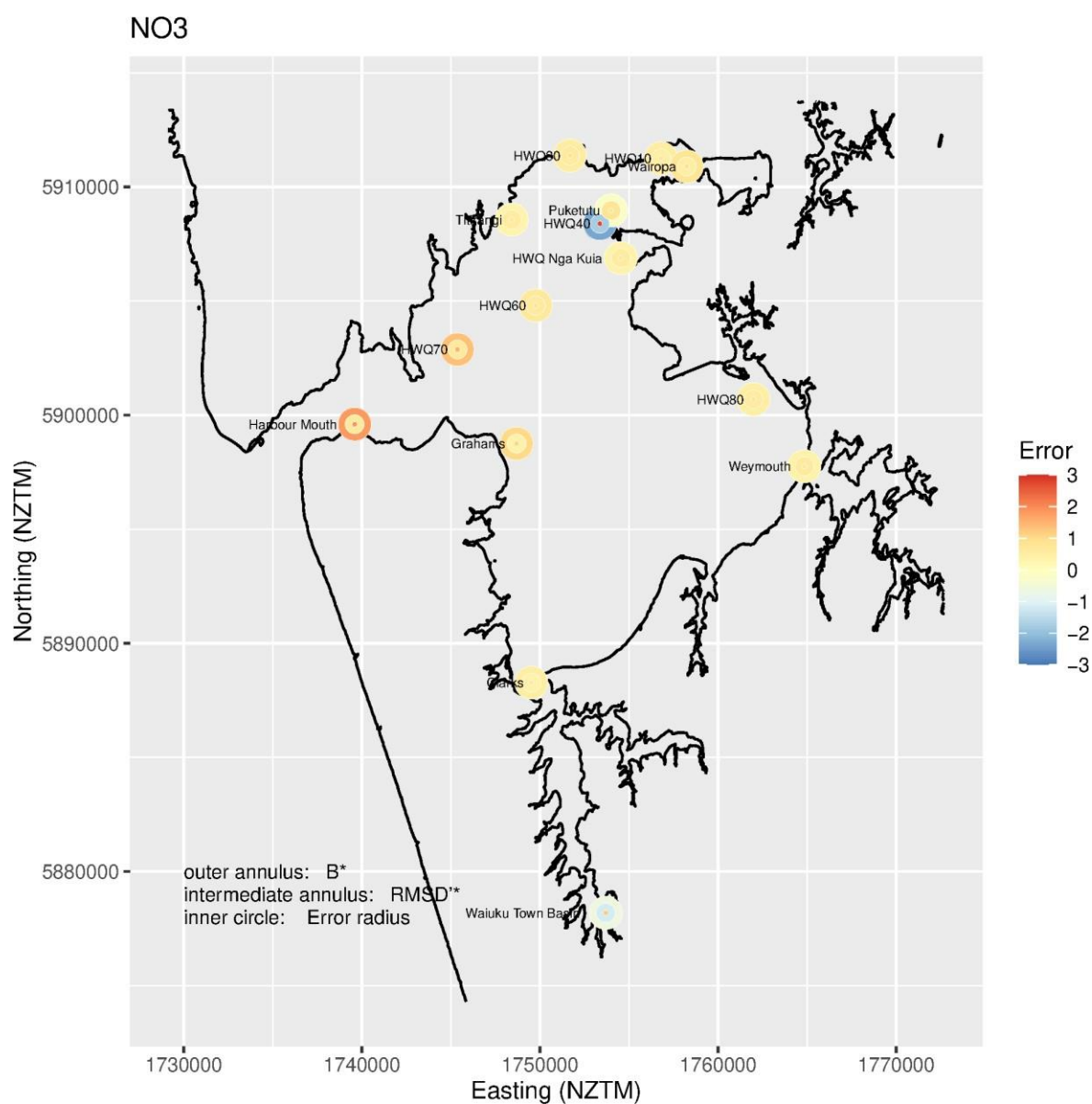


**Figure 4-24: False colour maps illustrating model performance for nitrate at each monitoring station.** The colour of each outer annulus denotes  $B^*$ . The colour of each intermediate annulus denotes  $RMSD^*$ . The colour of each central circle illustrates  $E_{i,NO3s}$ . A performance metric that is close to zero indicates that the model has performed well for the characteristic of which the metric is indicative.

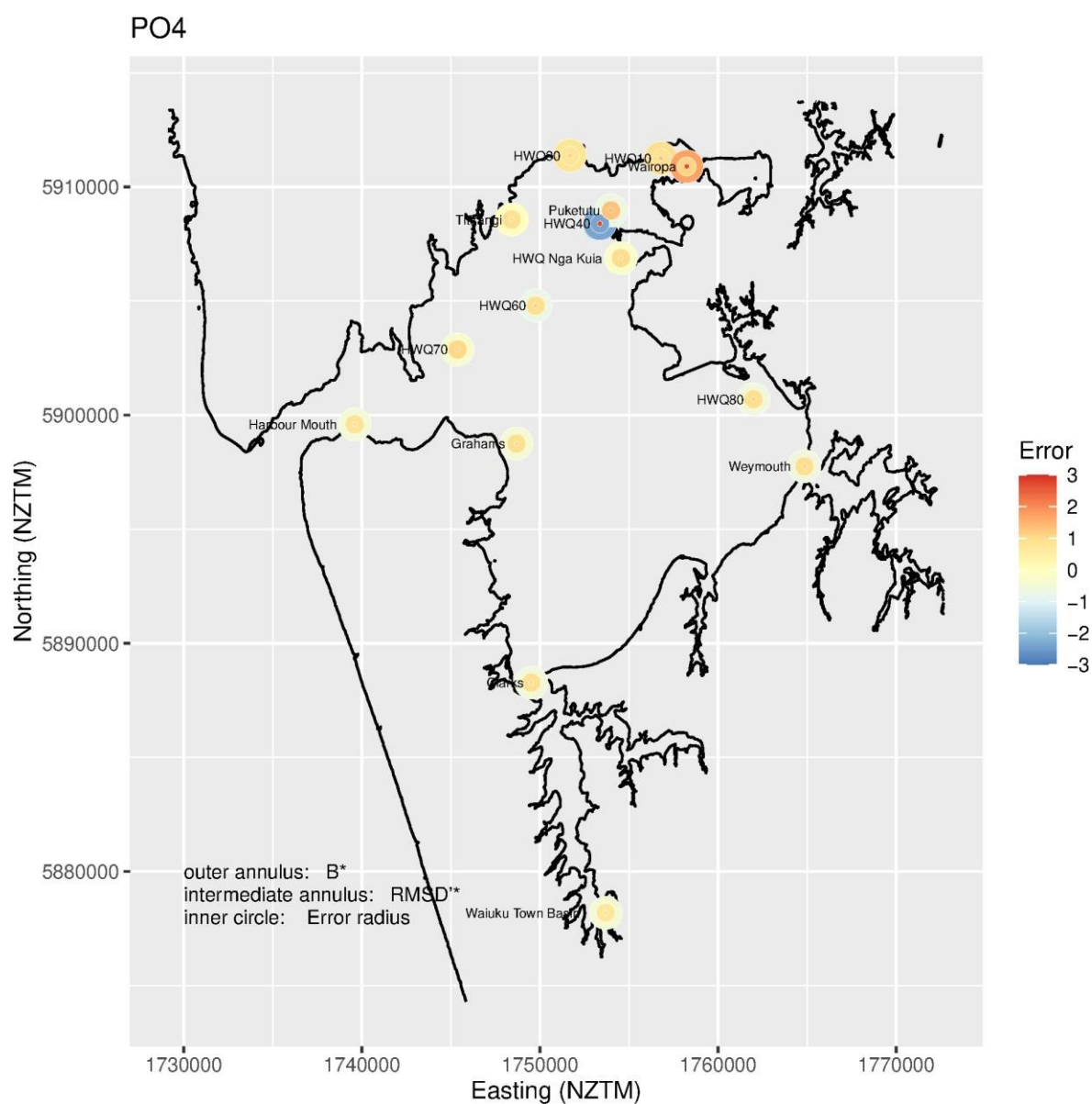


**Figure 4-25: False colour maps illustrating model performance for dissolved reactive phosphorus at each monitoring station.** The colour of each outer annulus denotes  $B^*$ . The colour of each intermediate annulus denotes  $RMSD^*$ . The colour of each central circle illustrates  $E_{i,PO4s}$ . A performance metric that is close to zero indicates that the model has performed well for the characteristic of which the metric is indicative.

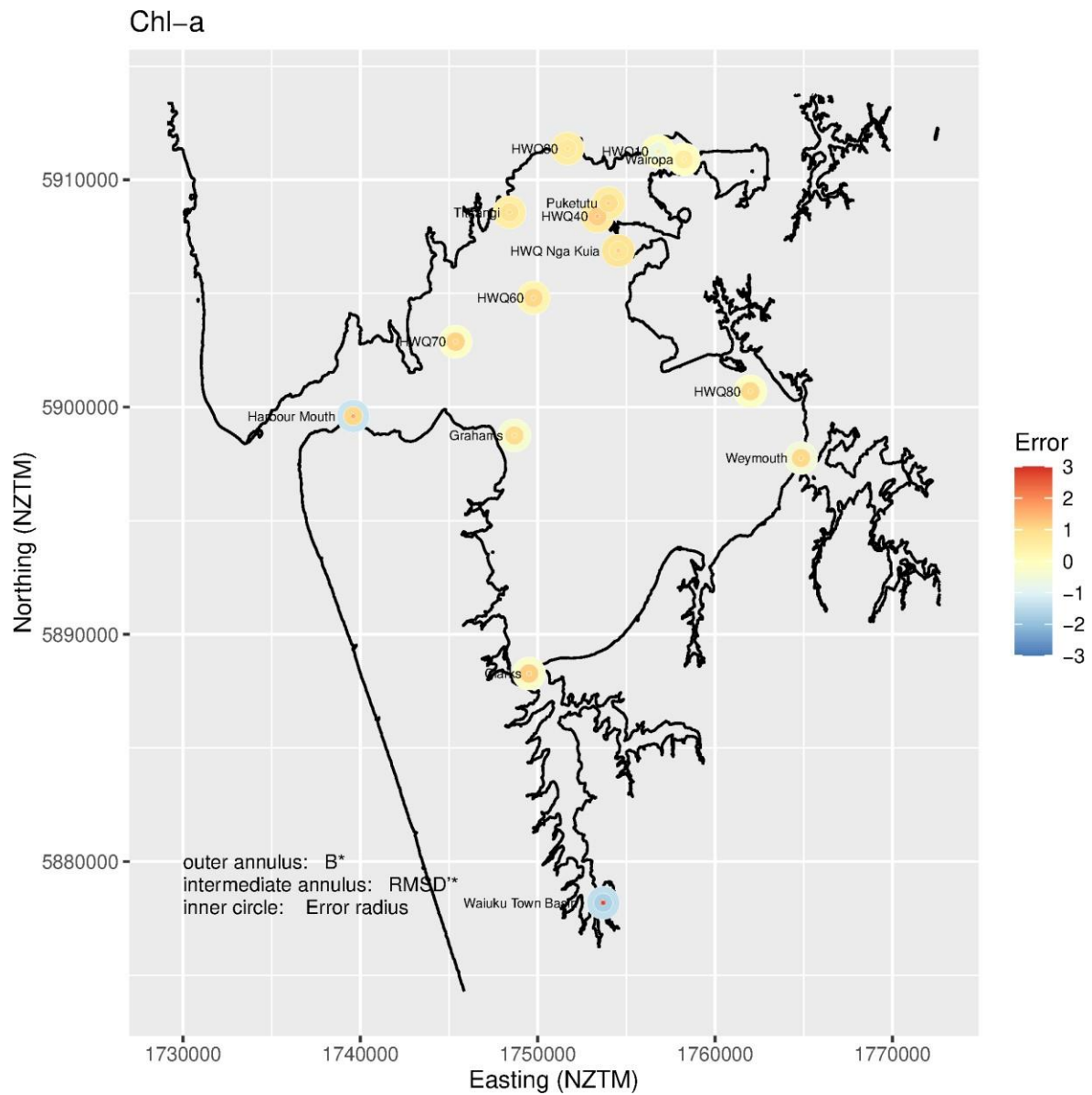


**Figure 4-26: False colour maps illustrating model performance for chlorophyll-a at each monitoring station.** The colour of each outer annulus denotes  $B^*$ . The colour of each intermediate annulus denotes  $RMSD^*$ . The colour of each central circle illustrates  $E_{i,Chl}$ . A performance metric that is close to zero indicates that the model has performed well in characteristic that the metric is indicative of.

## 5 Discussion

### 5.1 Overall performance of the model

The model and data are in agreement to better than an order of magnitude. Indeed, only in rare instances do the hindcasts and observations persistently disagree by more than a factor of two.

Overall:

- the model reproduces the qualitative characteristics (presence of seasonal cycles and spatial trends) of all the state-variables used in the calibration adequately,
- the model reproduces the quantitative dynamics of salinity, nitrate and dissolved oxygen well,
- not unexpectedly, the model is less successful at reproducing the quantitative dynamics of particulate and solute nutrient components other than nitrate (particularly, those of phosphorus), and
- for total nitrogen, total phosphorus and dissolved reactive phosphorus, performance (as  $B^*$ ,  $RMSD'^*$  and station-specific  $E_{tot}$ ) at the HWQ40 site (close to Puketutu Island) is markedly different from those at other nearby stations.

Despite the concerted efforts that both NIWA and Deltares have put into modifying details of the model formulation and performing numerous calibration trials, the fourth of the points above likely indicates that some detail(s) of our implementation of the Māngere waste-water outflows or simulated monitoring is incorrect. Several possible factors (and combinations of these and other factors) present themselves as candidate explanations. These include:

- In the real-world the Māngere discharge has probably carved a channel in the seabed. In the model, we chose to carve such a channel, but (i) the model does not have sufficient spatial resolution to accurately represent the likely width and depth of the real-world channel, and (ii) our choice of where to put the channel was somewhat arbitrary.
- Even if the direction of advective flow is 'about right', the model may not be accurately representing near-field dispersive mixing processes.
- Because the Māngere discharge is tidally staged, any discrepancies between the times or locations of real-world and virtual sampling are likely to have a disproportionately large influence upon inferred goodness of model fit.

## 5.2 Performance expectations

Manukau Harbour has features that will complicate and even frustrate any modelling endeavour. In addition, there are particular issues that our DelWAQ water-quality model (and the DeltaFM hydrodynamic model before it) has to deal with.

- In comparison with many other estuaries, Manukau Harbour is physically complex in that it contains both extensive intertidal regions and an extensive deep-water region. To successfully reproduce water-quality dynamics throughout the harbour, any model will likely need to mimic both: (a) processes that operate in the water column and (b) processes that operate at/within the seabed. The need to successfully incorporate both sets of processes adds to the complexity of the water-quality model that must be adopted. In turn, this makes calibration more difficult (see below).
- The large tidal exchange through the harbour mouth implies that oceanic conditions are likely to have a material influence on the harbour dynamics. The oceanic boundary conditions are based upon less than two years' (2017–2019) worth of monthly-resolution near-surface data. Given the limited data, the model assumes vertically homogeneous temperature, salinity and nutrient boundary conditions. It is also not clear whether the 2017–2019 period was typical, exceptional or representative of the 2010–2011 period against which we are calibrating. Furthermore, it is not certain that the near-surface values that were measured are representative of those which would have been found deeper in the water column outside the harbour mouth.
- More than 210 streams and culverts drain into the harbour, but there are almost no field observations of the nature (flow rates, water quality) of these inputs. The time-series of freshwater flow and accompanying nutrient concentrations applied at the mouths of the many streams and culverts that flow into the harbour derive from a catchment model that itself has been calibrated using very scant data from fewer than ten locations, all of which were in the eastern or southern parts of, and comparatively high up in, the Manukau catchment. The DeltaFM hydrodynamic (and DelWAQ water-quality) model reproduces (hindcasts) salinities at least moderately well at the time- and space scales of the field data. This suggests that the catchment model is generating plausible water-flows on time-scales of days-to-weeks. Nonetheless, whilst the associated estimates of nutrient concentration in the inputs are 'best efforts', it is not clear how reliable they are at even the annual-scale, let alone seasonal or event-scales.
- The harbour also receives inputs from several wastewater plants. The Māngere WWTP is, by far, the largest individual source of water and nutrients to the harbour. Whilst the characteristics (quantities of water and nutrient) of the Māngere discharge are better characterised than those of other wastewater inputs and those of streams and culverts, we still found it necessary to make some assumptions when formulating DelWAQ boundary conditions from the Māngere WWTP data. Even more assumptions were required to derive DelWAQ boundary conditions from the data available for other WWTPs.



- We know of no measurements of aerial nutrient deposition onto Manukau Harbour. We have applied a space-and-time invariant deposition rates that equated to estimates made elsewhere in New Zealand. Given that the Auckland region is much more urbanised than other parts of New Zealand, the rates which we have applied may be biased. Furthermore, because we have assumed the rates to be time-invariant, the model harbour is buffered against the influence that individual weather cycles/events may have upon aerial delivery of nutrients.
- In some parts of the model domain, there are high-frequency fluctuations in properties such as nutrient concentration. These arise because the tide advects steep concentration gradients to-and-fro across the location in question. Whilst we acknowledge that there are no relevant high-frequency data to verify the existence of the tidally-driven fluctuations evident in the model, we consider them plausible. Since we know the times of individual sampling events only very approximately (“sometime during the day-time ebb-tide”), we resorted to a “virtual sampling scheme” that involved calculating ebb-tide averages from our hindcasts and comparing those with the observations. This raises the possibility that some of the discrepancies between hindcasts and observations may have arisen because we have compared ebbing-tide time-average hindcast values with instantaneous real-world values. In regions where there are large-amplitude fluctuations in modelled water-quality across the tidal-cycle, our virtual sampling scheme will be prone to masking/damping these fluctuations. Perhaps more importantly, if the real-world stations were sampled at much the same stage of the falling tide on every sampling occasion, the ebb-tide averages calculated from the virtually-sampled hindcasts could be consistently biased one way or the other (that is, towards under-prediction or overprediction).

### 5.3 Model simplifications

By definition, any model is a simplification of reality. In the context of an implementation of a generic model (such as DelWAQ) to a specific instance (such as Manukau Harbour), there are two types of simplification: (a) those embodied within the structure/formulation of the generic model, and (b) those adopted by the practitioners when implementing the generic model for the specific application/instance.

We have already discussed some of the simplifications present within the generic DelWAQ model in earlier parts of this report. Here, we describe some of the other simplifications that we consciously made when implementing DelWAQ for Manukau Harbour.

- We assumed that all non-living organic matter would be present in particulate form only. In reality, at least some would be present in solute form. In practice, however, the two types of material perform functionally similar roles. Subject to parameterization choices, both can attenuate light and both serve to render nutrient temporarily unavailable to phytoplankton (by delaying the recycling of newly dead organic material into inorganic solute form). The user does have the option to cause particulate organic detritus to sink (whereas dissolved organic matter can only ever be neutrally buoyant). This distinction can have dynamically important implications if the sinking speeds are high relative to rates of vertical mixing, but preliminary trials (in which organic material was assumed to be present only in solute form) yielded quantitatively very similar results (for nutrient and phytoplankton concentrations) to



those stemming from a model in which this organic matter was assumed to be present as slowly-sinking ( $0.5 \text{ m d}^{-1}$ ) particulate material. Thus, we elected to simplify the model by assuming all non-living organic matter would be particulate. We suggest that our decision subtly nudges the model towards ‘worst-case’ in terms of tendency to retain reactive nutrients within the harbour. There are two reasons for this. Firstly, there is a weak estuarine flow in the harbour – meaning that near-surface waters have a tendency to flow seaward (in the long-term average) whilst near-bed ones have a tendency to flow landward. Thus, even slowly sinking material will tend to be retained inside the harbour for longer than strictly neutrally buoyant material. Secondly, fresh-dead material passes overwhelmingly into the particulate pool – and much of this fresh material is labile (readily mineralizing to inorganic solute form). Those parts which are not readily assimilated by macro-and micro-organisms (and, thereafter rapidly, into inorganic solute form) slowly degrade into ever more refractory solute organic forms from which inorganic solute nutrient emerges only very slowly.

- Sediment in the side-arms of the harbour (Pahurehure and Waiuku inlets etc.,) is finer (muddier) than that in the central harbour basin; additionally, there are gradients in sediment texture across the central basin. Different sediments will support differing biota, and nutrient dynamics may be profoundly different in different sediment types. Our modelling ignores these differences, and assumes the seabed to be uniform in some (potentially) important aspects.
- The carrying capacity<sup>20</sup> for benthic micro-algae is assumed to be spatially (and temporally) invariant. Certainly, spatial variations in realised benthic micro-algal density do emerge from the running of the model, but these are ‘dynamic’ variations, driven by factors such as quantities of light reaching the seabed (influenced by water depth and prescribed in-water light attenuation coefficient) and near-bed current speeds (influencing erosion and deposition of micro-algae and organic matter that can serve as a source of nutrient to the benthic algae).
- The fundamental capacity of the seabed to denitrify inorganic solute nitrogen is assumed to be spatially invariant. If the emergent benthic denitrification rates that the model yields vary spatially (we have not examined them), they do so only because of spatial variations in near-bed water speeds, near-bed solute concentrations, and net organic matter accrual at the seabed etc., rather than also being influenced by explicitly prescribed variations in porosity, benthic burrowing activity or denitrifier activity etc.
- After we had developed and calibrated our model, some measurements of dissolved oxygen concentrations at a small number of sites in the upper parts of the southern Manukau catchment were published (Morgenstern et al. 2023). Those authors report dissolved oxygen concentrations that range from  $< 2 \text{ g O}_2 \text{ m}^{-3}$  to  $> 9 \text{ g O}_2 \text{ m}^{-3}$  – but most were larger than the  $6 \text{ g O}_2 \text{ m}^{-3}$  that we assumed streams, rivers and culverts would deliver to the harbour. Whilst the measurements reported by Morgenstern et al. (2023) were made high in the catchment rather than at the stream mouths (i.e. close to the points where they discharge into the harbour), this may imply that our catchment boundary conditions for dissolved oxygen may be underestimates.

---

<sup>20</sup> The maximum density to which the micro-algae can accrue even under ideal conditions.

Nonetheless, as noted in Section 3.2, we believe that choices regarding the oxygen concentration in these tributary flows have no perceptible influence upon simulated in-harbour dissolved oxygen concentrations except very close to the tributary sources.

- Morgenstern et al. (2023) also present some new measurements of nutrient concentrations in the waters of the upper parts of the southern Manukau catchment. These were not available at the time that nutrient boundary conditions were derived for our model. We have not made a formal comparison between the boundary conditions that we have applied and these new data but our impression is that they are broadly consistent with one another (to within a factor of around two). Given that our boundary conditions derived from very scant historical data, we consider this level of agreement to be very encouraging. In particular, there is nothing in the new data to suggest that the Māngere WWTP discharge is unlikely to be the largest individual contributor of nutrients to the harbour.

Sediment grain size (and porosity etc.) influences benthic biogeochemical processes and faunal assemblages (Lohrer, A. M. et al. 2020; Petersen et al. 2022). Indeed, there may be a quasi-step-like change in denitrification activity as the mud content of the sediments increases across the range 20%-40% (Petersen et al. 2022). A sediment map for Manukau harbour (Gregory et al. 1994) reveals that even the side-arms of Manukau harbour (Waiuku, Pahurehure and Māngere) are predominantly muddy sand (c.f. pure mud). The inter-tidal flats of the open central harbour open, are dominated by sands and the sub-tidal areas are largely comprised of sand- and gravel-sand patches (with some patches of muddy sand). At the whole-of-harbour-scale, muds are relatively scarce and we speculate that our failure to explicitly impose a differing area-specific denitrification capacity in muddy parts of the harbour will not have induced serious bias in harbour-scale benthic nutrient processing budgets.

It is important to recognise that the realized simulated standing stocks of benthic algae and benthic detrital organic matter inputs varied in both space and time – influenced by a combination of seasonally and spatially varying near bed light intensities and erosion probabilities. In particular, simulated densities of benthic algae and sediment organic matter tended to be lower in deeper parts of the harbour including in the channels between intertidal regions. These variations will have influenced realized area-specific benthic diagenetic rates – despite the assumption that mass-and-temperature specific rates were spatially invariant.

- Whilst we chose to replicate the oyster beds that exist in the upper intertidal regions of the north-eastern part of the harbour, we did not place any benthic filter feeders elsewhere in the harbour. By their very nature, benthic filter feeders are constrained to filtering only near-bed waters. Thus, on a depth-averaged basis, a given density of benthic filter feeders will impose a lesser depth-averaged filtration demand in deeper waters. Whilst we suspect that there may be sufficient data / expert knowledge to allow qualitative maps of benthic filtration activity to be prescribed, we opted for model simplicity rather than introducing model complexity that would be informed only by comparatively scant data<sup>21</sup>.
- Our modelling makes some assumptions that apply higher in the water column that may be dynamically important. In particular, mortality of phytoplankton (and any resuspended benthic micro-algae) is assumed to vary only as a function of water temperature. One can speculate that, in reality, mortality fluctuates on time-scales of days-to-weeks as zooplankton populations wax and wane. Mortality may also evolve on space-scales of km (driven by factors such as proximity to ocean, freshwater and benthic filter-feeders etc.). Whilst the DelWAQ suite does enable the user to prescribe an explicit (and, potentially, spatially varying) time-series of zooplankton-induced mortality, we chose not to exploit the feature because, as above, this would have implied adding more model complexity informed by very scant data.

## 5.4 Model utility

The value of any tool is determined by the purpose to which it will be put.

We understand that our DelWAQ model will be used to explore the consequences of moderately large-scale change in nutrient loading from the catchment and/or wastewater treatment plants. It will be used in a ‘**scenario mode**’ rather than as an ‘**operational forecast model**’. As such, we infer that the emphasis will be on qualitative/relative change at seasonal temporal scales and ‘harbour octant’ (that is, regions or compartments of the harbour) spatial scales, as opposed to shorter time and space scales.

The model reproduces relative temporal and spatial patterns better than it does absolute quantities, and so it is better suited to scenario modelling than it is to operational forecasting. Since the model reproduces observations within a factor of two or so, it would be inappropriate to believe that any scenario forecasts will be more accurate than that.

A key result that sets the scene for the anticipated scenario modelling is that nutrient loads discharged from Māngere WWTP are having a readily discernible influence (in the model results) throughout much of the NE harbour (Māngere inlet and the waters of the open harbour around Puketutu Island), the upper reaches of Pahurehure inlet, and even some distance into the open harbour. Whilst Māngere WWTP is contributing around 50% of the total nitrogen load to the harbour, the largest source in Pahurehure contributes only around 5% of the total nitrogen load.

---

<sup>21</sup> Indeed, we introduced the oysters only to satisfy ourselves that it would be possible to incorporate benthic filter-feeders as a forcing/boundary condition if deemed necessary. Since the oysters were introduced only to the high intertidal region and occupy only a few tens of percent of the embayments in which they had been placed, they had only a subtle effect upon partial abundances in those embayments and an entirely negligible influence upon dynamics elsewhere. Placing significant quantities of benthic filter-feeders across e.g., the intertidal flats of the central open harbour may have a more dramatic influence.

We infer that changes of a few tens of percent to either of these individual sources, when entered into the model, will yield changes in water quality in the harbour that will be readily discernible at the scenario time (seasonal) and space (harbour octant) scales.

Furthermore, the model generates plausible responses to weather-scale events, which indicates that it will also generate plausible responses to brief, large-scale changes in discharge characteristics from individual point sources.

## 6 Conclusions and recommendations

We believe that the DelWAQ water-quality model described herein is fit for:

- scenario modelling at seasonal temporal scales and harbour large-scale sub-regions of the harbour (eg quadrant or octant), with a focus on qualitative changes of magnitude (cf absolute magnitudes) and relative changes in water quality,
- exploring the consequences of moderately large-scale change in nutrient loading from the catchment and/or wastewater treatment plants, and
- exploring responses to one-off, large-scale changes in individual point sources.

The DelWAQ model might be improved by the following:

- assembling more data on input (streams, culverts) flows and nutrients (concentrations of TN and TP and their respective constituent forms). Benefits (improved confidence and/or accuracy in model predictions) are likely be realised close to discharge points,
- better quantifying rates of aerial deposition of nutrients into the harbour,
- better establishing the absolute and relative abundances of differing constituent nutrients within WWTP outflows. Greatest benefits are likely to be realised in the vicinity of the associated WWTP,
- better establishing a longer baseline of oceanic monitoring data to inform the oceanic boundary conditions. Greatest benefits are likely to be realised in the subtidal central and outer regions of the harbour,
- determining how well the model can reproduce monitoring data gathered before and after the upgrade of the Māngere WWTP in the early 2000s. The benefit will be increased confidence in the model's ability to forecast the consequences of changes to catchment nutrient loading, and
- introducing explicit spatial variation in seabed-related properties (carrying capacity for benthic micro-algae, benthic filter-feeder activity, nutrient-regeneration capacity). Extensive and repeated field-work may be required to adequately characterise some of these properties

## 7 Acknowledgements

We are grateful to Chris Garton (Watercare Ltd) and Auckland Council staff (particularly Dr Coral Grant) for facilitating delivery of harbour and WWTP water-quality monitoring data.

We gratefully acknowledge Deltares Institute (notably Arjen Markus, Tineke Troost and Björn Backeberg) for the support they have provided – answering numerous questions and modifying the DelWAQ code to provide alternative process formulations etc.

We acknowledge Watercare Ltd for their unstinting support during the model development. Equally, we acknowledge the support that Neale Hudson, Iain MacDonald and other senior NIWA managers have provided during the course of this project. We are especially appreciative of the tolerance and active support they have all exhibited in the face of the many delays associated with overcoming unforeseen technical difficulties that delayed successful delivery of the model.



## 8 Glossary of abbreviations and terms

AFDM	ash free dry mass
BLOOM	DelWAQ phytoplankton model
BSi	biogenic silica
C	carbon
Chla	chlorophyll- <i>a</i>
DeltaFM	Deltares hydrodynamic model
DelWAQ	Deltares water-quality model
DO	dissolved oxygen
DM	dry mass
DON	dissolved organic nitrogen
DRP	dissolved reactive phosphorus (= soluble reactive phosphorus)
DRSi	dissolved reactive silicon
DYNAMO	DelWAQ phytoplankton model
GUI	graphical user interface
HEMP	harbour environment monitoring programme
MICROPHYT	enhanced benthic algal model
N	nitrogen
NH <sub>4</sub>	ammonium
NH <sub>x</sub> N	ammoniacal nitrogen
NO <sub>3</sub>	nitrate
NO <sub>x</sub> N	nitrogen in the form nitrate plus nitrite
P	phosphorus
PO <sub>4</sub>	dissolved phosphate (=SRP=DRP)
POC	particulate organic carbon
PON	particulate organic nitrogen
POP	particulate organic phosphorus
SBOD	soluble biological oxygen demand
Si	silica
SRP	soluble reactive phosphorus (= dissolved reactive phosphorus)
TBOD	total biological oxygen demand
TDP	total dissolved phosphorus
TIN	total inorganic nitrogen
TKN	total Kjeldahl nitrogen
TN	total nitrogen
TP	total phosphorus
TSS	total suspended solids
WWTP	wastewater treatment plant
<i>B</i> *	normalized bias
<i>RMSD'</i> *	unbiased root mean square difference
<i>E</i> <sub>tot</sub>	total error radius



## 9 References

- Bai, J., Zhao, J., Zhang, Z., Tian, Z. (2022) Assessment and a review of research on surface water quality modeling. *Ecological Modelling*, 466. 10.1016/j.ecolmodel.2022.109888
- Bowie, G.L., Mills, W.B., Porcella, D.B., Campbell, C.L., Pagenkopf, J.R., Rupp, G.L., Johnson, K.M., Chan, P.W.H., Gherini, S.A., Chamberlin, C.E. (1985) *Rates, constants, and formulations in surface water quality modelling*. United States Environmental Protection Agency, Athens, Georgia: 455.
- Broekhuizen, N., Plew, D. (2018) Marlborough Sounds Water Quality Monitoring: review of Marlborough District Council monitoring data 2011-2018: 186.  
<https://www.marlborough.govt.nz/environment/coastal/coastal-water-quality>
- Close, M.E., Davies-Colley, R.J. (1990) Baseflow water chemistry in New Zealand rivers. 1. Characterisation. *New Zealand Journal of Marine and Freshwater Research*, 24: 319-341. 10.1080/00288330.1990.9516428
- Deltares (2011) Delft3D WAQ User Manual - versatile water quality modelling in 1D, 2D, or 3D systems including physical, (bio)chemical and biological processes, Version 4.03. Revision 15587: 320.
- Enríquez, S., Duarte, C.M., Sand-Jensen, K. (1993) Patterns in decomposition rates among photosynthetic organisms: the importance of detritus C:N:P content. *Oecologia*, 94: 457-471.
- Greenfield, B.L., Hewitt, J.E., Hailes, S.F. (2013) Manukau harbour ecological monitoring programme: report on data collected up until February 2013. *NIWA Client Report (for Auckland Regional Council; report number HAM2013-044; project number ARC13206)*, HAM2013-044 (project number ARC1320\_6: 51.
- Gregory, M.R., Blackmore, N.A., Glasby, G.P., Burrows, M.W. (1994) Manukau and Waitemata Harbours sediments. New Zealand Oceanographic Institute.
- Hudson, N. (2016) Southern Manukau Harbour WWTPs: Wastewater characterisation and assessment of microbial effects. NIWA client report prepared for Watercare Services Limited, HAM2016-031: 52.
- Jolliff, J.K., Kindle, J.C., Shulman, I., Penta, B., Friedrichs, M.A.M., Helber, R., Arnone, R.A. (2009) Summary diagrams for coupled hydrodynamic-ecosystem model skill assessment. *Journal of Marine Systems*, 76(1): 64-82. <https://doi.org/10.1016/j.jmarsys.2008.05.014>
- Kelly, S. (2014) Mangere Wastewater Treatment Plant: harbour monitoring 2013-14: 79.  
<http://www.watercare.co.nz/SiteCollectionDocuments/AllPDFs/Mangere%20Wastewater%20Treatment%20Plant%202013-14%20Monitoring%20Report%20Final.pdf>  
<http://www.watercare.co.nz/SiteCollectionDocuments/AllPDFs/Mangere%20plant%20info/%20Kelly%202013-14%20Watercare%20Monitoring%20Presentation.pdf>
- Kelly, S. (2014) Mangere Wastewater Treatment Plant.

- Krause, J.W., Darrow, E.S., Pickering, R.A., Carmichael, R.H., Larson, A.M., Basaldua, J.L. (2017) Reactive silica fractions in coastal lagoon sediments from the northern Gulf of Mexico. *Continental Shelf Research*, 151: 8-14. 10.1016/j.csr.2017.09.014
- Lohrer, A.M., Stephenson, F., Douglas, E.J., Townsend, M. (2020) Mapping the estuarine ecosystem service of pollutant removal using empirically validated boosted regression tree models. *Ecol Appl*, 30(5): e02105. 10.1002/eap.2105
- Lohrer, D., Townsend, M., Broekhuizen, N. (2017) Manukau Harbour: nutrient flux measurements. National Institute for Water & Atmospheric Research Ltd., Hamilton.
- Los, F.J., Blaas, M. (2010) Complexity, accuracy and practical applicability of different biogeochemical model versions. *Journal of Marine Systems*, 81(1): 44-74. <https://doi.org/10.1016/j.jmarsys.2009.12.011>
- MacDonald, I., Broekhuizen, N. (2018) Moored instrument measurements of hydrodynamic and water-quality properties in the northern Manukau harbour.
- Morgenstern, U., Moreau, M., Cole, M.A., Johnson, K., Townsend, D.B. (2023) Groundwater and surface water conceptual flow from environmental tracer signatures in the Pukekohe and Bombay Area. *GNS Science Report*, 2022/63: 97. 10.21420/VNBF-3X96
- Palliser, C., Zammit, C., Ren, J., Semadeni-Davies, A., Yalden, S., Wadhwa, S., Hudson, N. (2018) Manukau harbour water quality model: stream flows, and loads and concentrations of nitrogen and phosphorus delivered from the catchment to the harbour. *NIWA Client Reports*, 2018030HN (project WSL16205): 99.
- Parfitt, R.L., Schipper, L.A., Baisden, W.T., Elliott, A.H. (2006) Nitrogen inputs and outputs for New Zealand in 2001 at national and regional scales. *Biogeochemistry*, 80(1): 71-88. 10.1007/s10533-006-0002-y
- Petersen, G.L., Lohrer, A.M., Bulmer, R.H., Pilditch, C.A. (2022) Altered nitrogen transformation pathways and a legacy of sediment organic matter enrichment. *Marine Pollution Bulletin*, 182: 114014. 10.1016/j.marpolbul.2022.114014
- Pinkerton, M. (2017) Satellite remote sensing of water quality and temperature in Manukau Harbour. *NIWA Client Report (for Watercare Services Ltd.)*.
- Redfield, A.C. (1934) On the proportions of organic derivatives in sea water and their relation to the composition of plankton. *James Johnstone Memorial Volume*. Liverpool University Press, Liverpool.
- Reeve, G., Broekhuizen, N. (2019) Manukau Harbour Hydrodynamic Model - Calibration and Validation. *NIWA Client Report*, 2019124HN: 49.
- Verburg, P., Schallenberg, M., Elliott, S., McBride, C.G. (2018) Nutrient budgets in lakes. In: D.P. Hamilton, K.J. Collier, C. Howard-Williams & J.M. Quinn (Eds). *Lake restoration handbook*. Springer: 129-163.

## Appendix A Time series boxplots

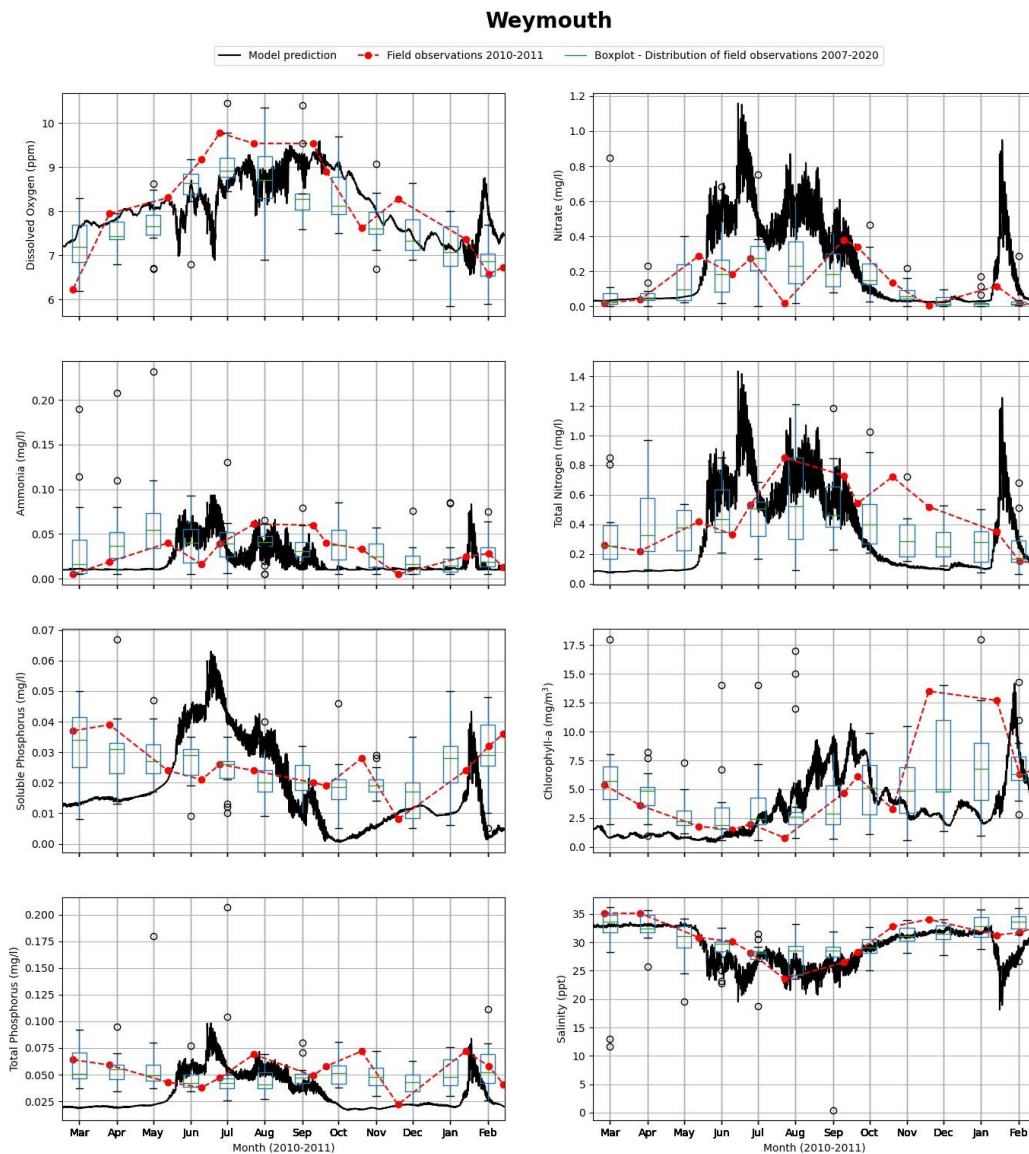


**Figure A-1: Measured and modelled data from Weymouth. The boxplots show all the measured data.** Black line is the ebb-tide model prediction. Red line (red marker dot) is measured monthly HEMP data for the 2010–2011 year (if sampled). Boxplots illustrate the spread of monthly HEMP data for the 2004–2019 period (or a lesser period in cases where sampling did not extend over that full calendar period). Green line = median, box limits are 25<sup>th</sup> and 75<sup>th</sup> percentiles of the samples, and distance between is the interquartile range. Whisker lines extend to  $1.5 \times$  interquartile range and correspond to approximately  $\pm 2.7$  sigma and 99.3% coverage if the data are normally distributed.

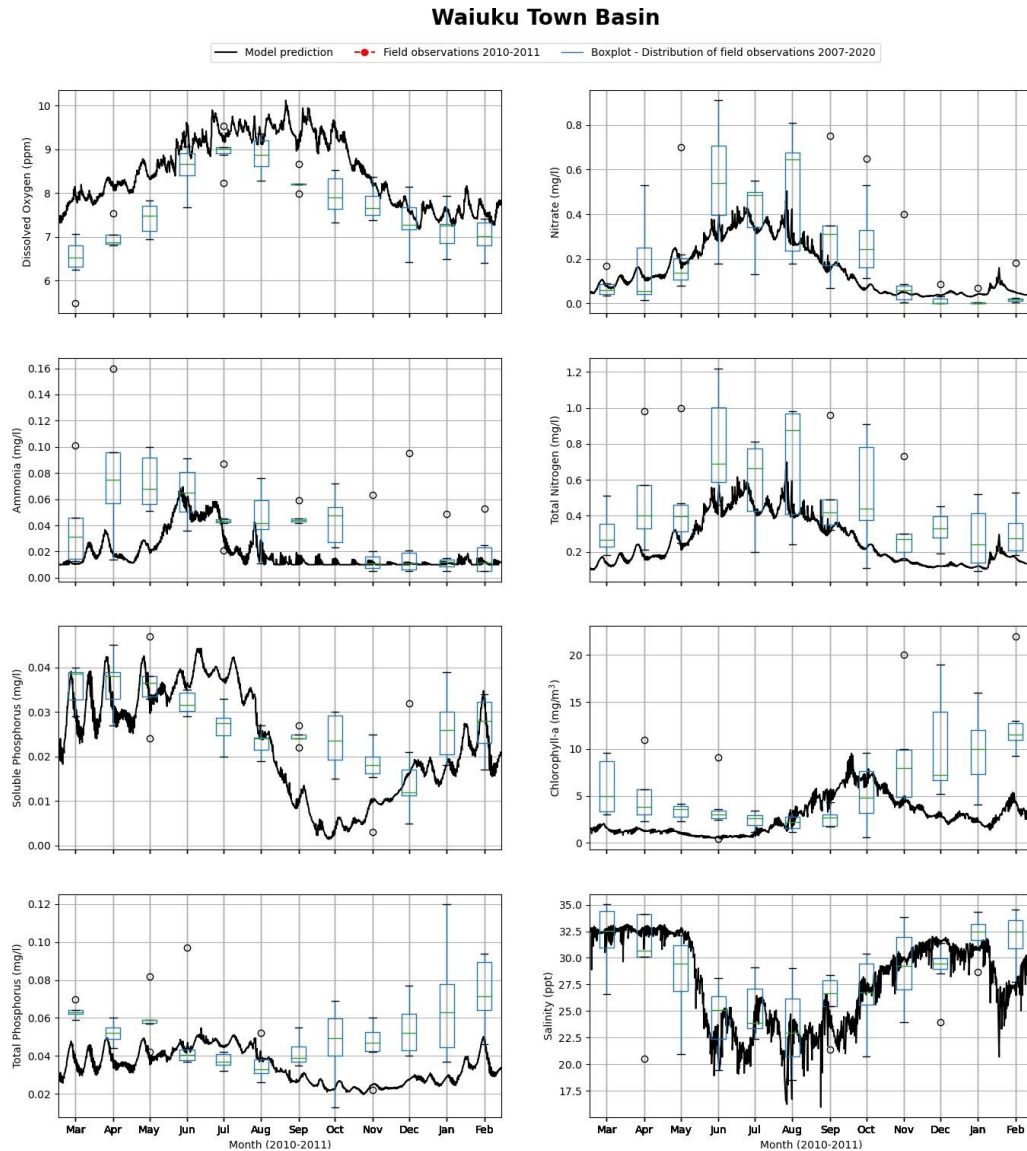


**Figure A-2: Measured and modelled data from Waiuku Town Basin.** The boxplots show all the measured data. Black line is the ebb-tide model prediction. Red symbols denote the monthly HEMP data for the 2010–2011 year (where available). Boxplots illustrate the spread of monthly HEMP data for the 2004–2019 period (or a lesser period in cases where sampling did not extend over that full calendar period). Green line = median, box limits are 25<sup>th</sup> and 75<sup>th</sup> percentiles of the samples, and distance between is the interquartile range. Whisker lines extend to  $1.5 \times$  interquartile range and correspond to approximately  $\pm 2.7$  sigma and 99.3% coverage if the data are normally distributed.

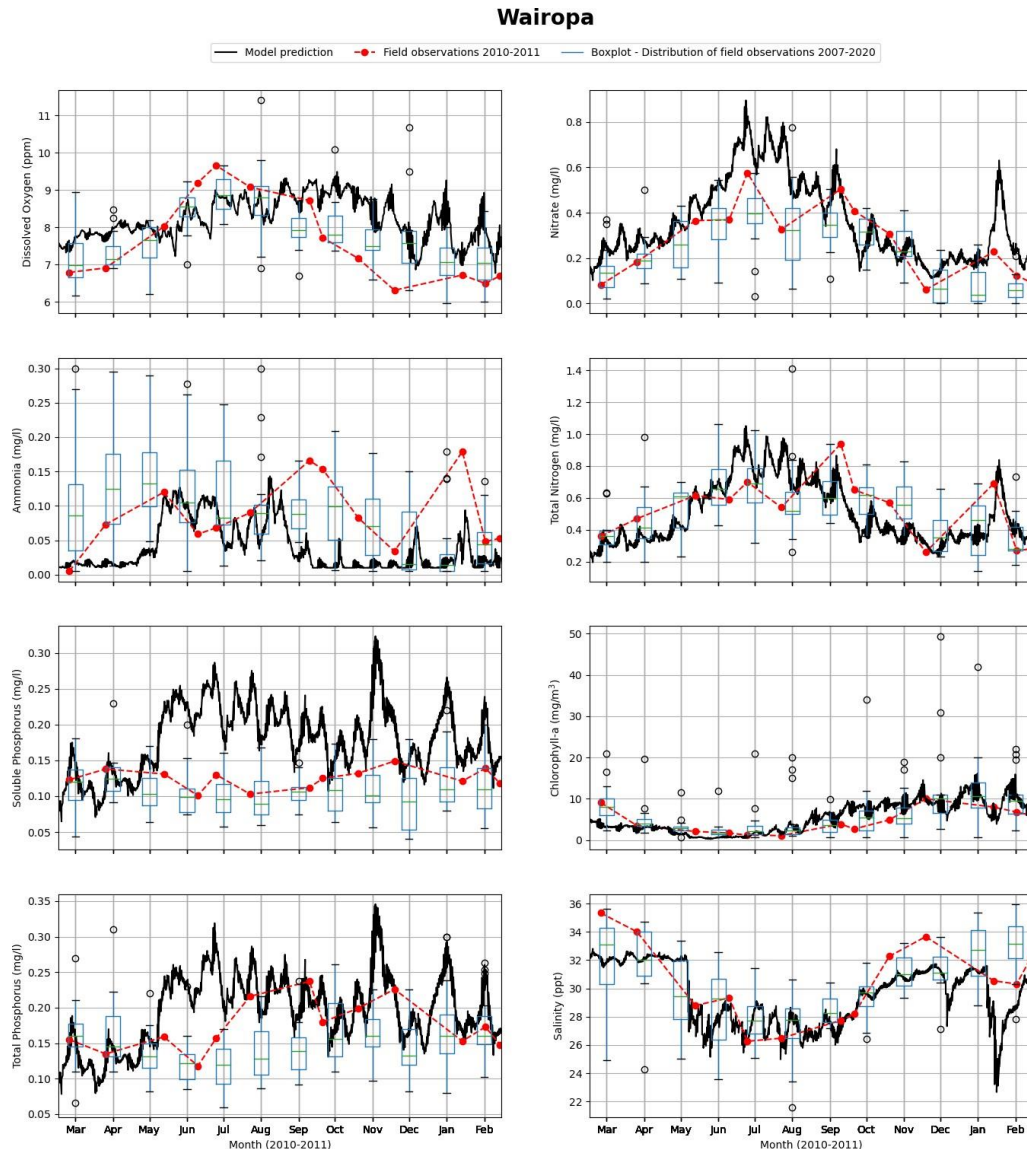


**Figure A-3: Measured and modelled data from Wairoa.** The boxplots show all the measured data. Black line is the ebb-tide model prediction. Red symbols denote the monthly HEMP data for the 2010–2011 year (where available). Boxplots illustrate the spread of monthly HEMP data for the 2004–2019 period (or a lesser period in cases where sampling did not extend over that full calendar period). Green line = median, box limits are 25<sup>th</sup> and 75<sup>th</sup> percentiles of the samples, and distance between is the interquartile range. Whisker lines extend to  $1.5 \times$  interquartile range and correspond to approximately  $\pm 2.7$  sigma and 99.3% coverage if the data are normally distributed.

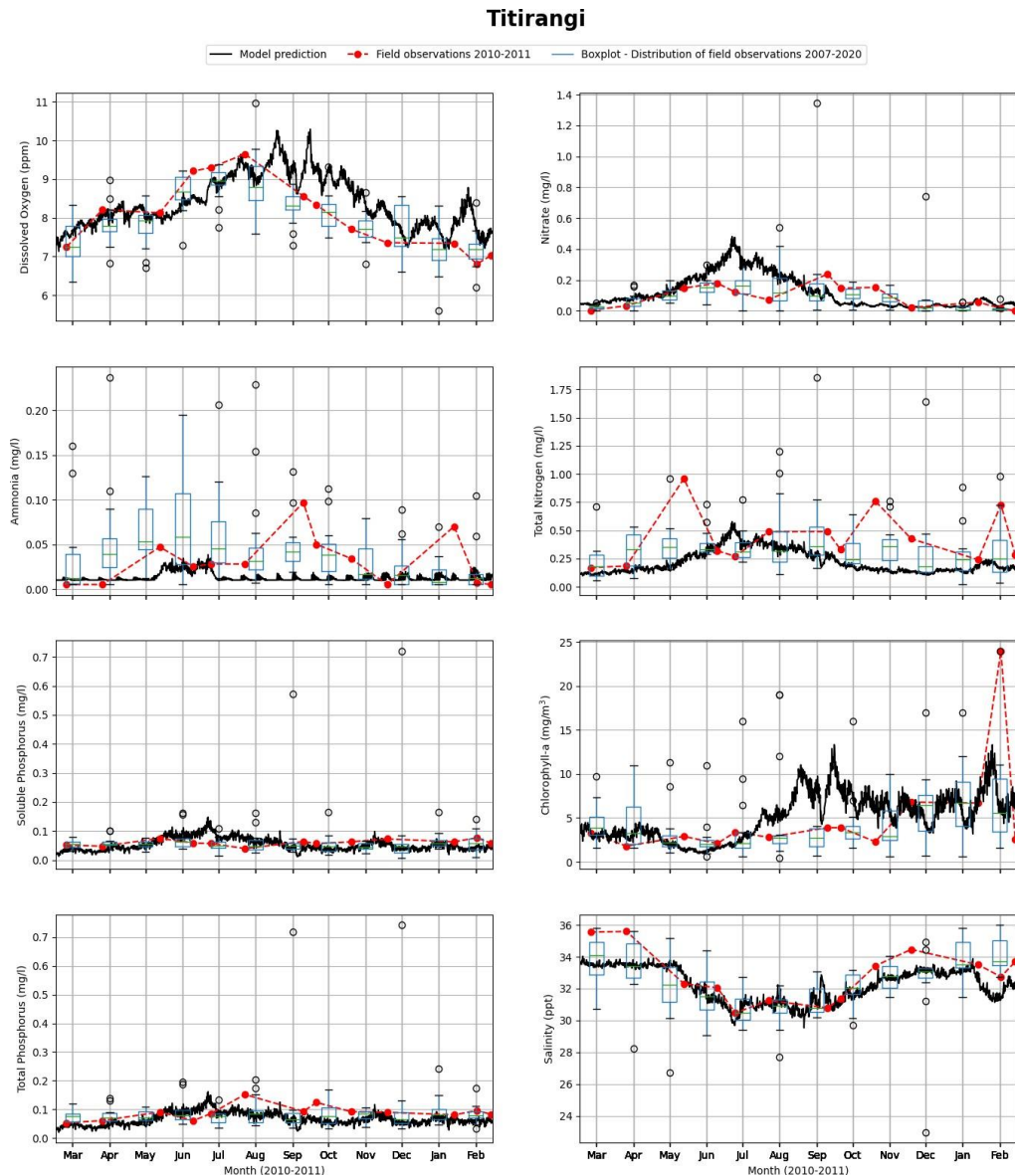


**Figure A-4: Measured and modelled data from Titirangi.** The boxplots show all the measured data. Black line is the ebb-tide model prediction. Red symbols denote the monthly HEMP data for the 2010–2011 year (where available). Boxplots illustrate the spread of monthly HEMP data for the 2004–2019 period (or a lesser period in cases where sampling did not extend over that full calendar period). Green line = median, box limits are 25<sup>th</sup> and 75<sup>th</sup> percentiles of the samples, and distance between is the interquartile range. Whisker lines extend to  $1.5 \times$  interquartile range and correspond to approximately  $\pm 2.7$  sigma and 99.3% coverage if the data are normally distributed.



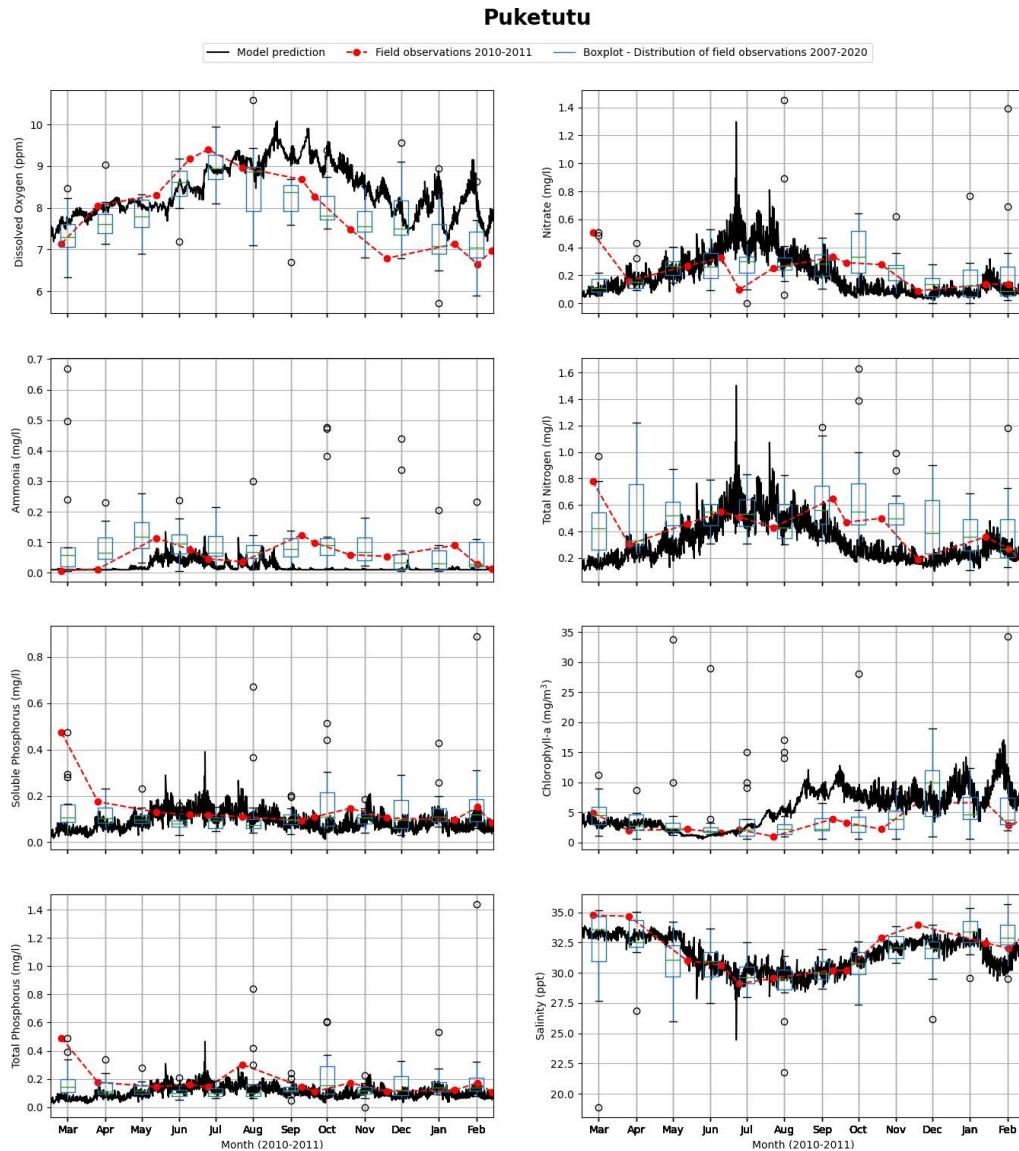


**Figure A-5: Measured and modelled data from Puketutu.** The boxplots show all the measured data. Black line is the ebb-tide model prediction. Red symbols denote the monthly HEMP data for the 2010–2011 year (where available). Boxplots illustrate the spread of monthly HEMP data for the 2004–2019 period (or a lesser period in cases where sampling did not extend over that full calendar period). Green line = median, box limits are 25<sup>th</sup> and 75<sup>th</sup> percentiles of the samples, and distance between is the interquartile range. Whisker lines extend to  $1.5 \times$  interquartile range and correspond to approximately  $\pm 2.7$  sigma and 99.3% coverage if the data are normally distributed.

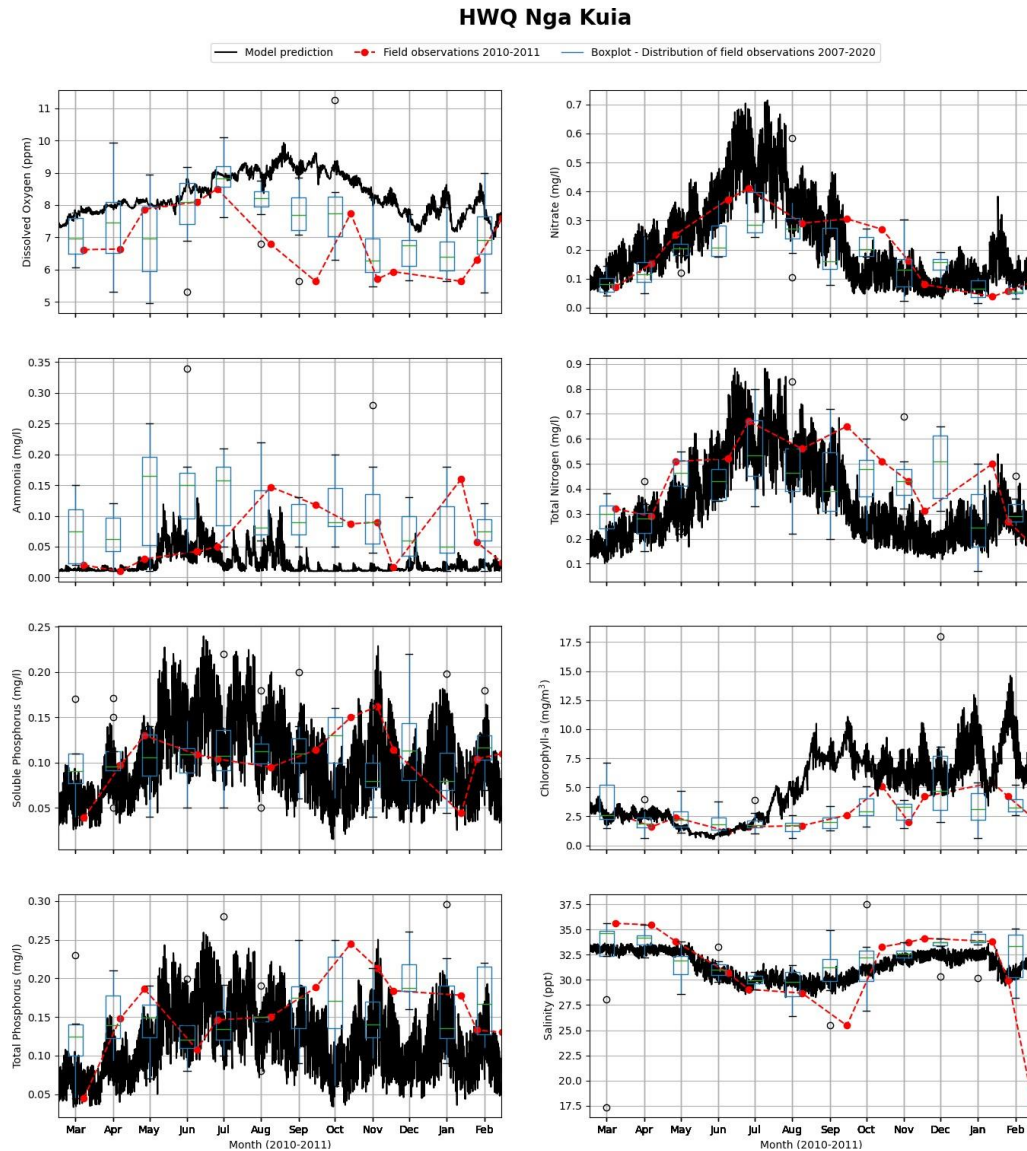


**Figure A-6: Measured and modelled data from HWQ Nga Kuia.** The boxplots show all the measured data. Black line is the ebb-tide model prediction. Red symbols denote the monthly HEMP data for the 2010–2011 year (where available). Boxplots illustrate the spread of monthly HEMP data for the 2004–2019 period (or a lesser period in cases where sampling did not extend over that full calendar period). Green line = median, box limits are 25<sup>th</sup> and 75<sup>th</sup> percentiles of the samples, and distance between is the interquartile range. Whisker lines extend to  $1.5 \times$  interquartile range and correspond to approximately  $\pm 2.7$  sigma and 99.3% coverage if the data are normally distributed.



## HWQ 80

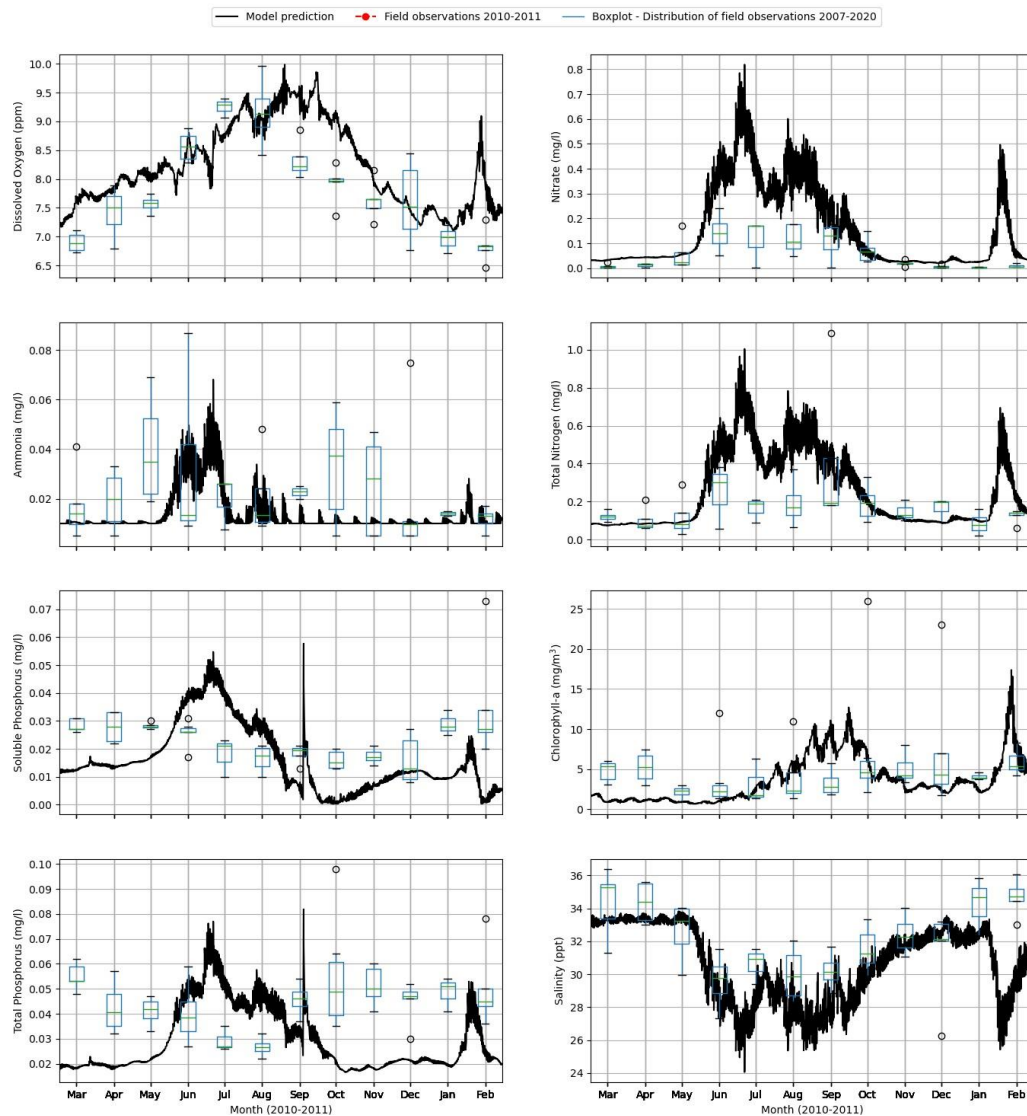


**Figure A-7: Measured and modelled data from HWQ 80. The boxplots show all the measured data.** Black line is the ebb-tide model prediction. Red symbols denote the monthly HEMP data for the 2010–2011 year (where available). Boxplots illustrate the spread of monthly HEMP data for the 2004–2019 period (or a lesser period in cases where sampling did not extend over that full calendar period). Green line = median, box limits are 25<sup>th</sup> and 75<sup>th</sup> percentiles of the samples, and distance between is the interquartile range. Whisker lines extend to  $1.5 \times$  interquartile range and correspond to approximately  $\pm 2.7$  sigma and 99.3% coverage if the data are normally distributed.

## HWQ 70

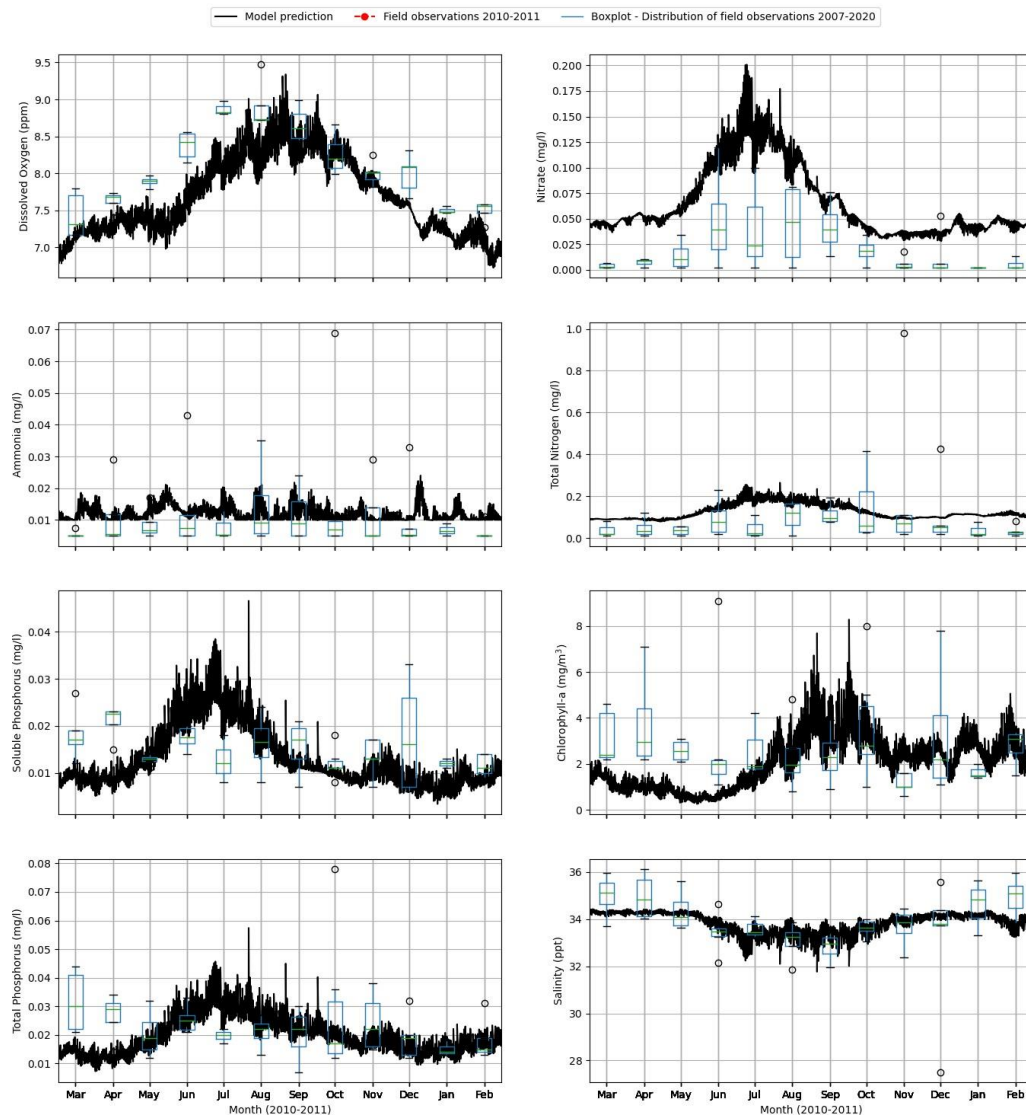


**Figure A-8: Measured and modelled data from HWQ 70. The boxplots show all the measured data.** Black line is the ebb-tide model prediction. Red symbols denote the monthly HEMP data for the 2010–2011 year (where available). Boxplots illustrate the spread of monthly HEMP data for the 2004–2019 period (or a lesser period in cases where sampling did not extend over that full calendar period). Green line = median, box limits are 25<sup>th</sup> and 75<sup>th</sup> percentiles of the samples, and distance between is the interquartile range. Whisker lines extend to  $1.5 \times$  interquartile range and correspond to approximately  $\pm 2.7$  sigma and 99.3% coverage if the data are normally distributed.

## HWQ 60

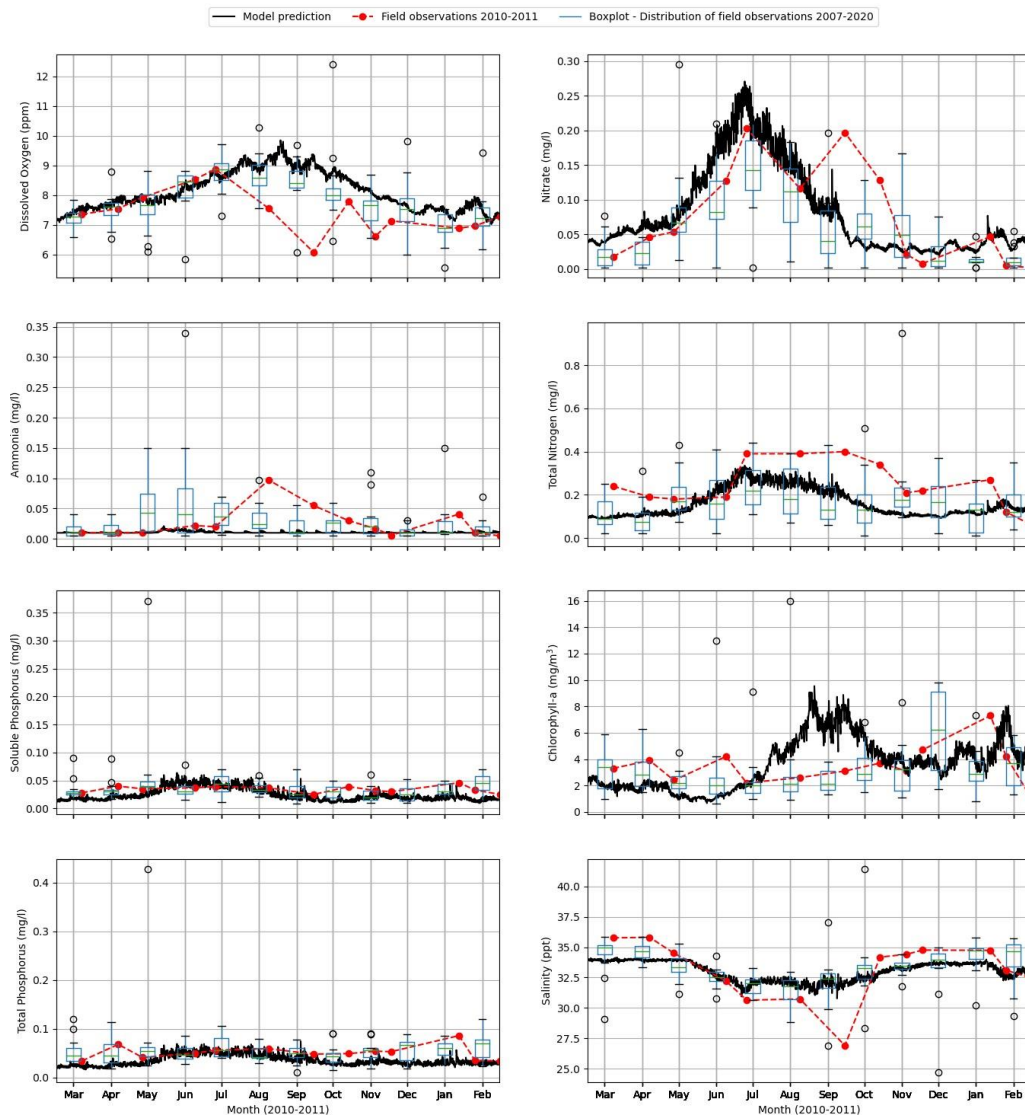


**Figure A-9: Measured and modelled data from HWQ 60. The boxplots show all the measured data. Black line is the ebb-tide model prediction. Red symbols denote the monthly HEMP data for the 2010–2011 year (where available). Boxplots illustrate the spread of monthly HEMP data for the 2004–2019 period (or a lesser period in cases where sampling did not extend over that full calendar period). Green line = median, box limits are 25<sup>th</sup> and 75<sup>th</sup> percentiles of the samples, and distance between is the interquartile range. Whisker lines extend to  $1.5 \times$  interquartile range and correspond to approximately  $\pm 2.7$  sigma and 99.3% coverage if the data are normally distributed.**

## HWQ 40

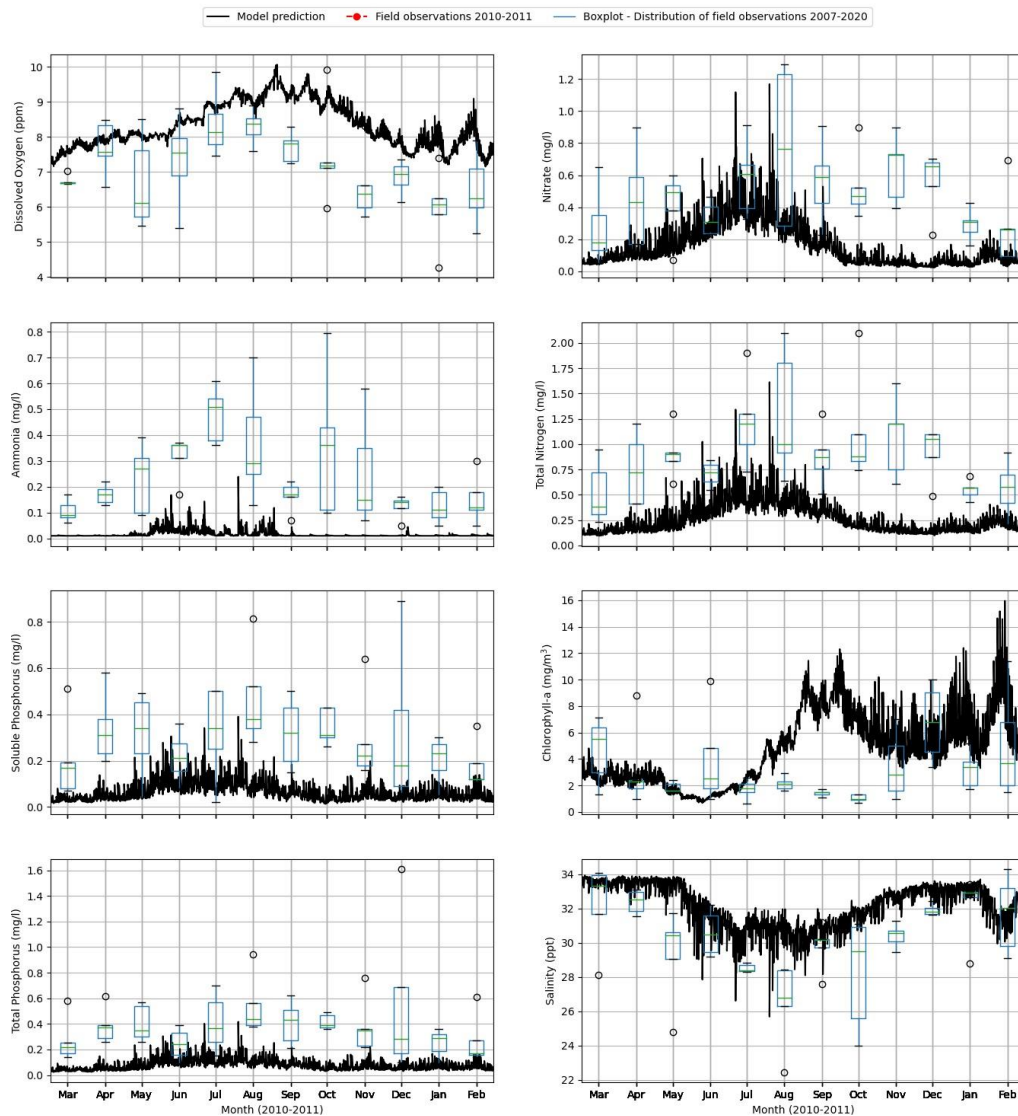


**Figure A-10: Measured and modelled data from HWQ 40. The boxplots show all the measured data.** Black line is the ebb-tide model prediction. Red symbols denote the monthly HEMP data for the 2010–2011 year (where available). Boxplots illustrate the spread of monthly HEMP data for the 2004–2019 period (or a lesser period in cases where sampling did not extend over that full calendar period). Green line = median, box limits are 25<sup>th</sup> and 75<sup>th</sup> percentiles of the samples, and distance between is the interquartile range. Whisker lines extend to 1.5 × interquartile range and correspond to approximately ± 2.7 sigma and 99.3% coverage if the data are normally distributed.

## HWQ 30

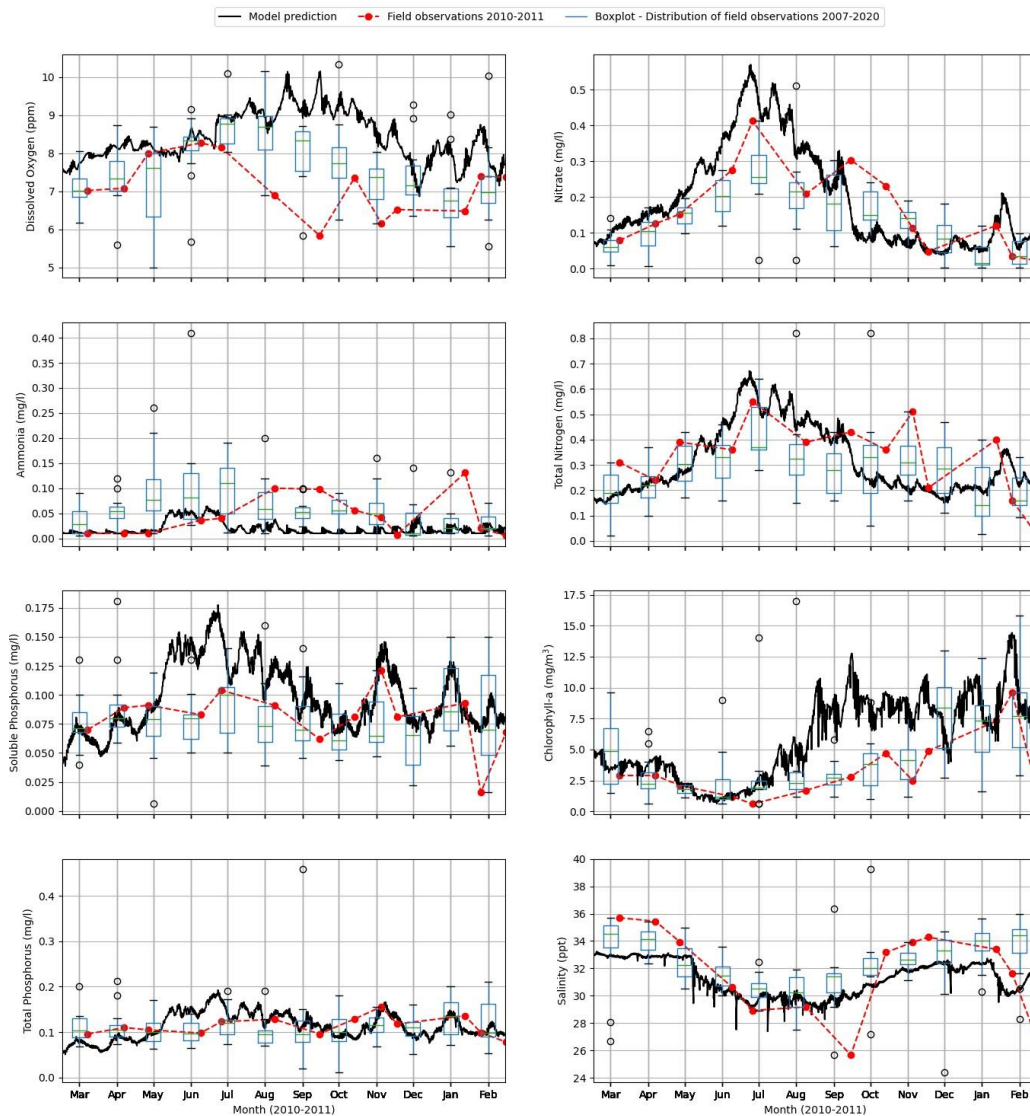


**Figure A-11: Measured and modelled data from HWQ 30.** The boxplots show all the measured data. Black line is the ebb-tide model prediction. Red symbols denote the monthly HEMP data for the 2010–2011 year (where available). Boxplots illustrate the spread of monthly HEMP data for the 2004–2019 period (or a lesser period in cases where sampling did not extend over that full calendar period). Green line = median, box limits are 25<sup>th</sup> and 75<sup>th</sup> percentiles of the samples, and distance between is the interquartile range. Whisker lines extend to  $1.5 \times$  interquartile range and correspond to approximately  $\pm 2.7$  sigma and 99.3% coverage if the data are normally distributed.



## HWQ 10

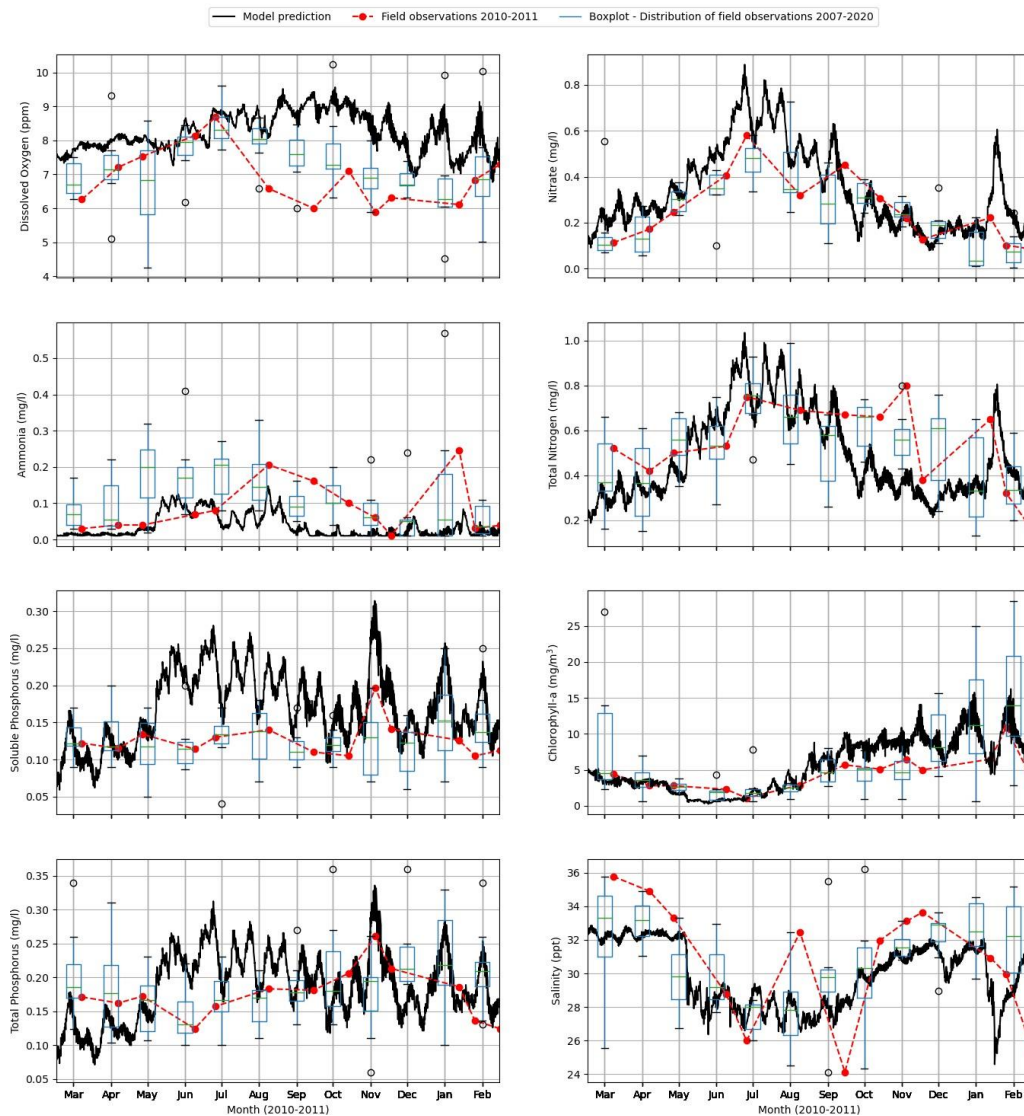


**Figure A-12: Measured and modelled data from HWQ 10.** The boxplots show all the measured data. Black line is the ebb-tide model prediction. Red symbols denote the monthly HEMP data for the 2010–2011 year (where available). Boxplots illustrate the spread of monthly HEMP data for the 2004–2019 period (or a lesser period in cases where sampling did not extend over that full calendar period). Green line = median, box limits are 25<sup>th</sup> and 75<sup>th</sup> percentiles of the samples, and distance between is the interquartile range. Whisker lines extend to  $1.5 \times$  interquartile range and correspond to approximately  $\pm 2.7$  sigma and 99.3% coverage if the data are normally distributed.

## Harbour Mouth

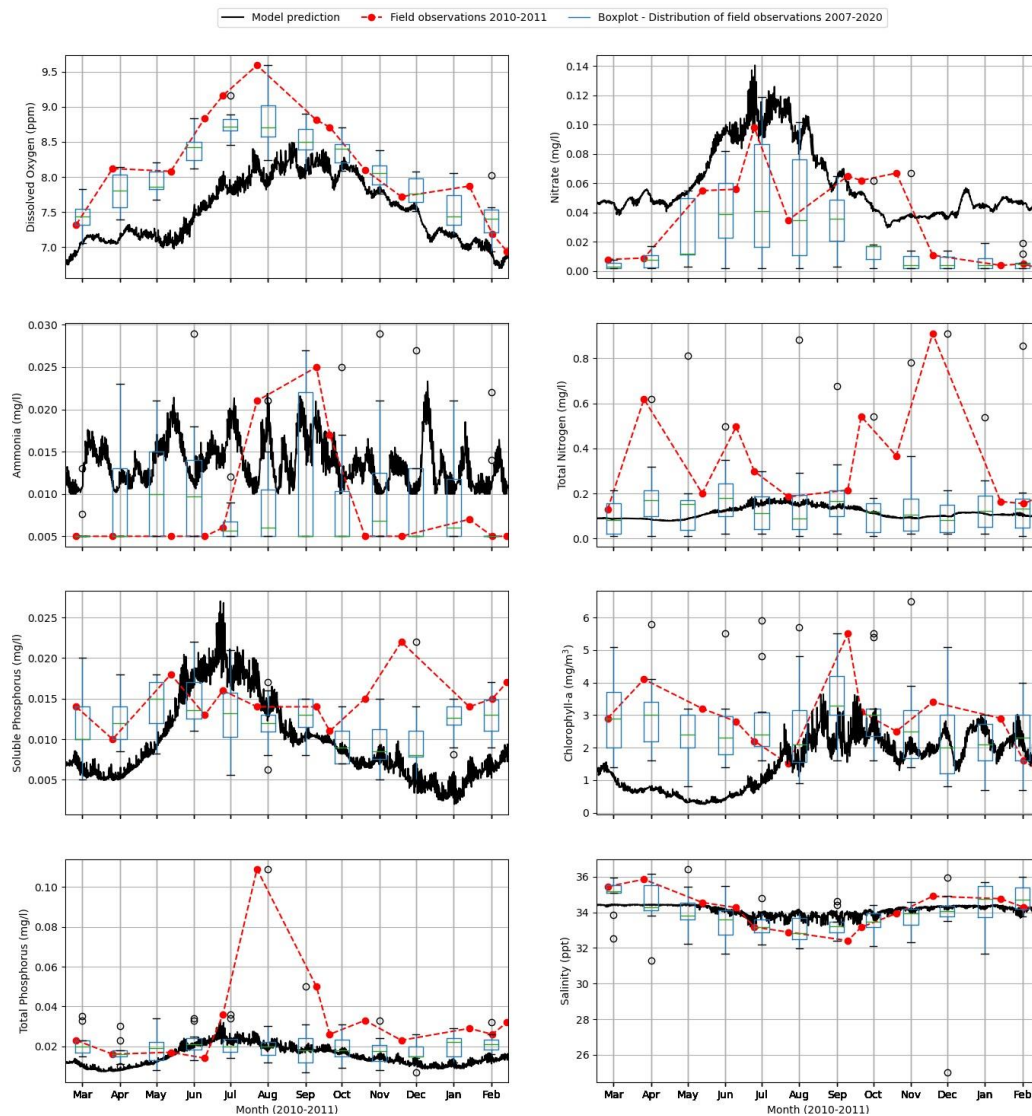


**Figure A-13: Measured and modelled data from Harbour Mouth.** The boxplots show all the measured data. Black line is the ebb-tide model prediction. Red symbols denote the monthly HEMP data for the 2010–2011 year (where available). Boxplots illustrate the spread of monthly HEMP data for the 2004–2019 period (or a lesser period in cases where sampling did not extend over that full calendar period). Green line = median, box limits are 25<sup>th</sup> and 75<sup>th</sup> percentiles of the samples, and distance between is the interquartile range. Whisker lines extend to  $1.5 \times$  interquartile range and correspond to approximately  $\pm 2.7$  sigma and 99.3% coverage if the data are normally distributed.

## Grahams

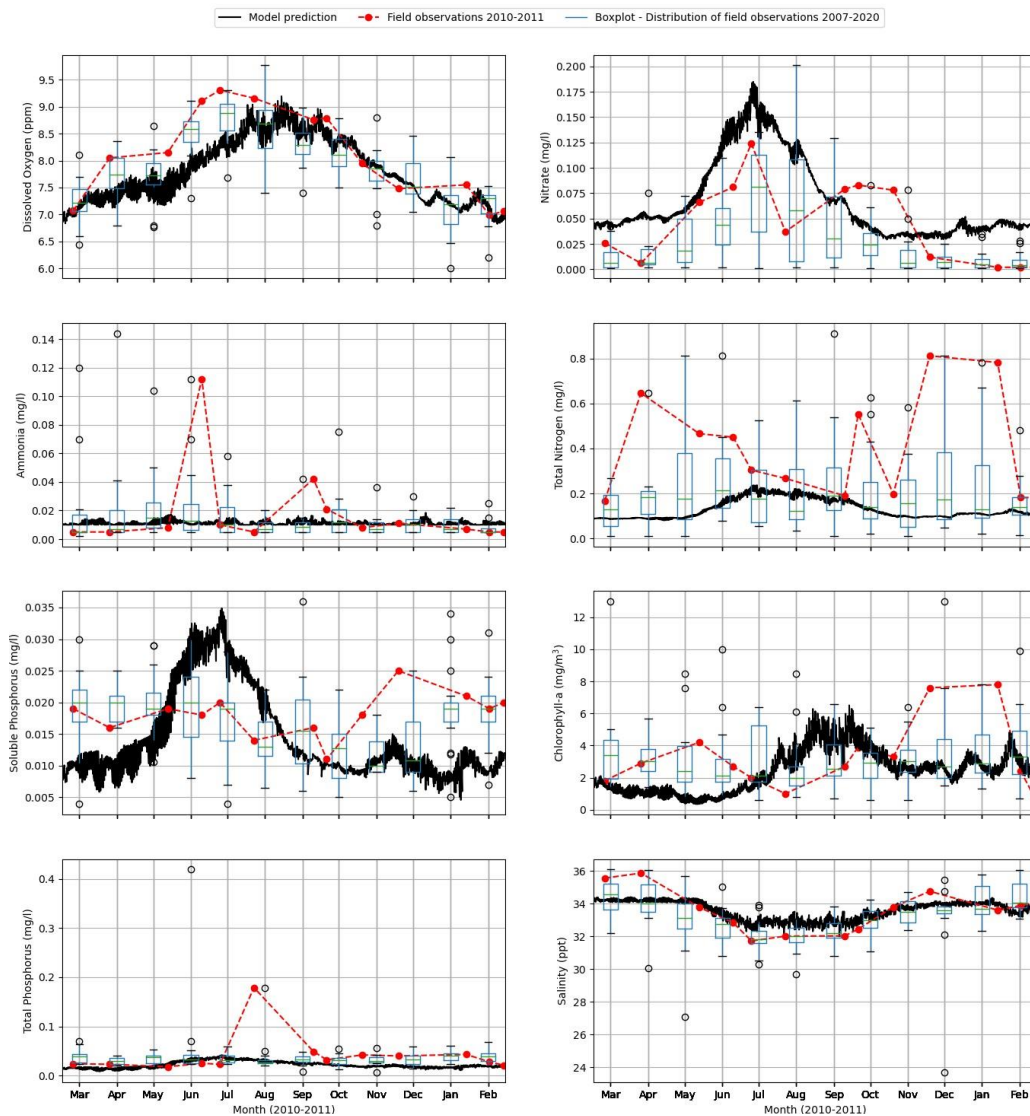


**Figure A-14: Measured and modelled data from Grahams.** The boxplots show all the measured data. Black line is the ebb-tide model prediction. Red symbols denote the monthly HEMP data for the 2010–2011 year (where available). Boxplots illustrate the spread of monthly HEMP data for the 2004–2019 period (or a lesser period in cases where sampling did not extend over that full calendar period). Green line = median, box limits are 25<sup>th</sup> and 75<sup>th</sup> percentiles of the samples, and distance between is the interquartile range. Whisker lines extend to  $1.5 \times$  interquartile range and correspond to approximately  $\pm 2.7$  sigma and 99.3% coverage if the data are normally distributed.



## Clarks

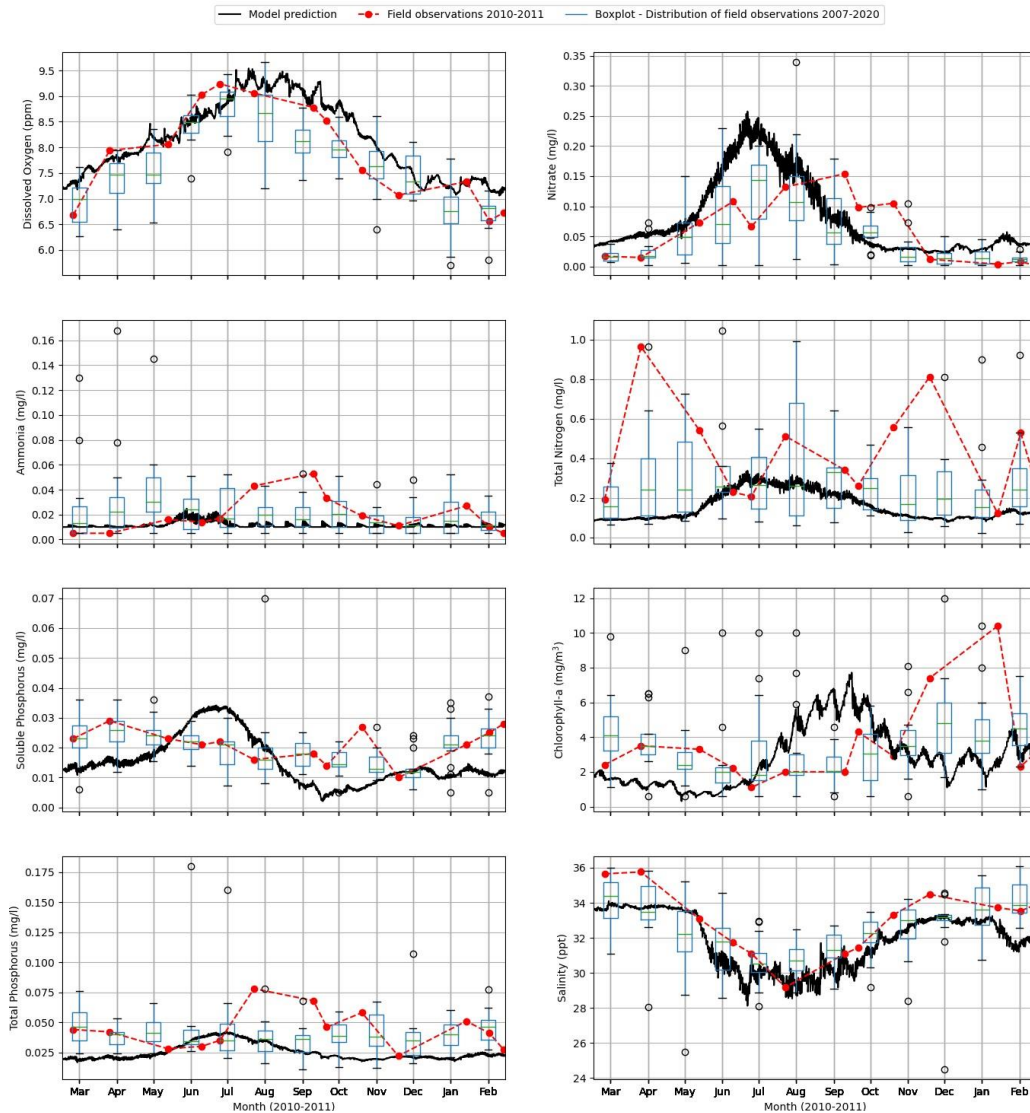


**Figure A-15: Measured and modelled data from Weymouth. The boxplots show all the measured data.** Black line is the ebb-tide model prediction. Red symbols denote the monthly HEMP data for the 2010–2011 year (where available). Boxplots illustrate the spread of monthly HEMP data for the 2004–2019 period (or a lesser period in cases where sampling did not extend over that full calendar period). Green line = median, box limits are 25<sup>th</sup> and 75<sup>th</sup> percentiles of the samples, and distance between is the interquartile range. Whisker lines extend to  $1.5 \times$  interquartile range and correspond to approximately  $\pm 2.7$  sigma and 99.3% coverage if the data are normally distributed.

## Appendix B Target Diagrams

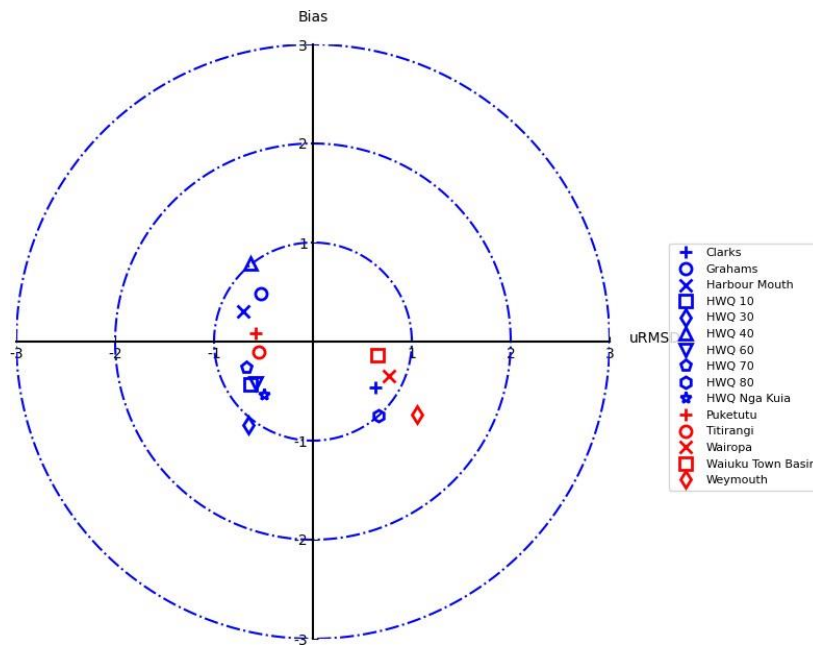


**Figure B-1: Target diagram for salinity at all the sample sites.** Where: y-axis is normalised bias ( $B^*$ ) and x-axis is normalised RMSD ( $uRMSD = RMSD^*$ ).

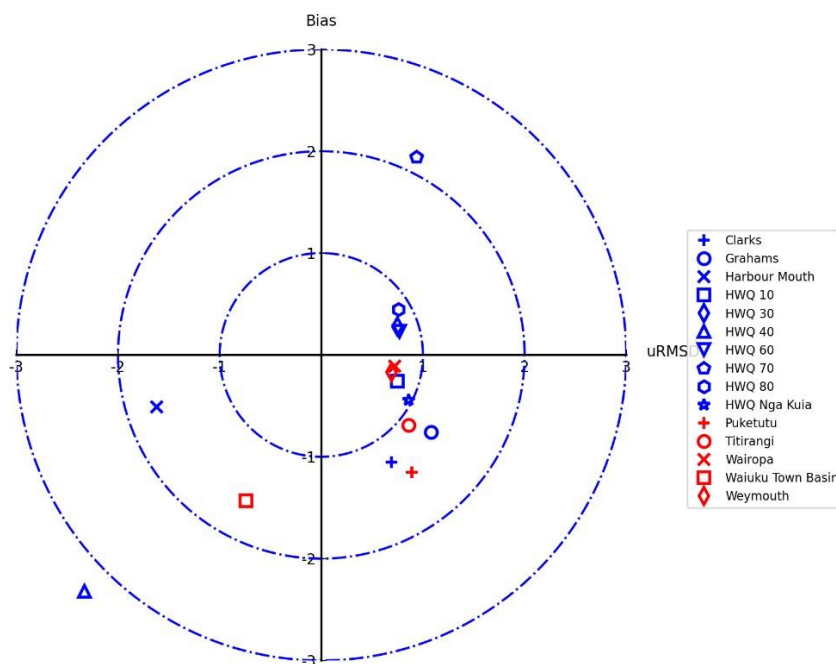


**Figure B-2: Target diagram for total nitrogen at all the sample sites.** Where: y-axis is normalised bias ( $B^*$ ) and x-axis is normalised RMSD ( $uRMSD = RMSD^*$ ).

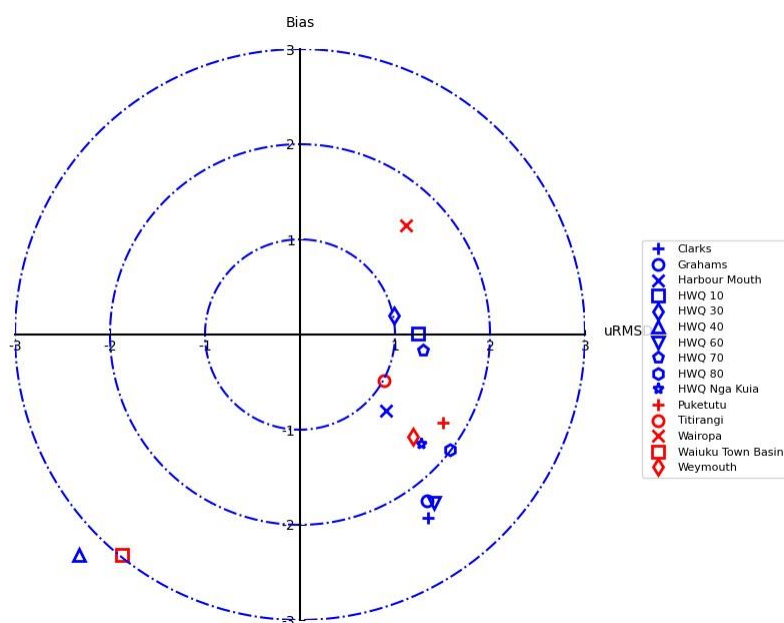


**Figure B-3: Target diagram for total phosphorus at all the sample sites.** Where: y-axis is normalised bias ( $B^*$ ) and x-axis is normalised RMSD ( $uRMSD = RMSD^*$ ).

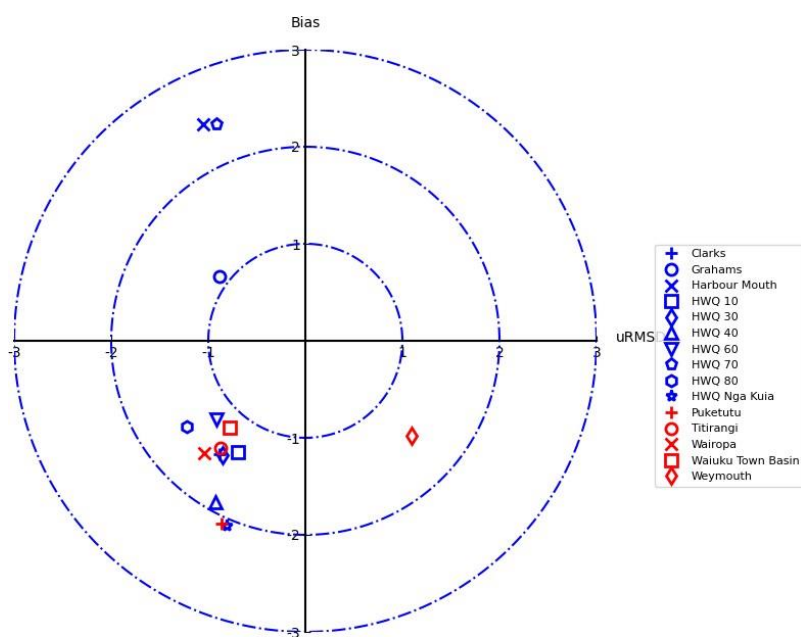


**Figure B-4: Target diagram for ammonia at all the sample sites.** Where: y-axis is normalised bias ( $B^*$ ) and x-axis is normalised RMSD ( $uRMSD = RMSD^*$ ).

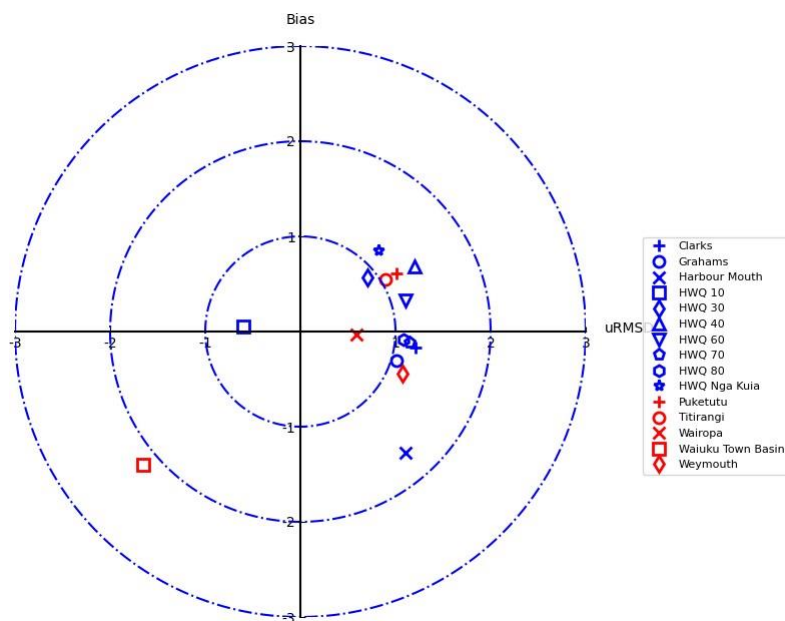


**Figure B-5: Target diagram for chlorophyll-a at all the sample sites.** Where: y-axis is normalised bias ( $B^*$ ) and x-axis is normalised RMSD ( $uRMSD = RMSD^*$ ).

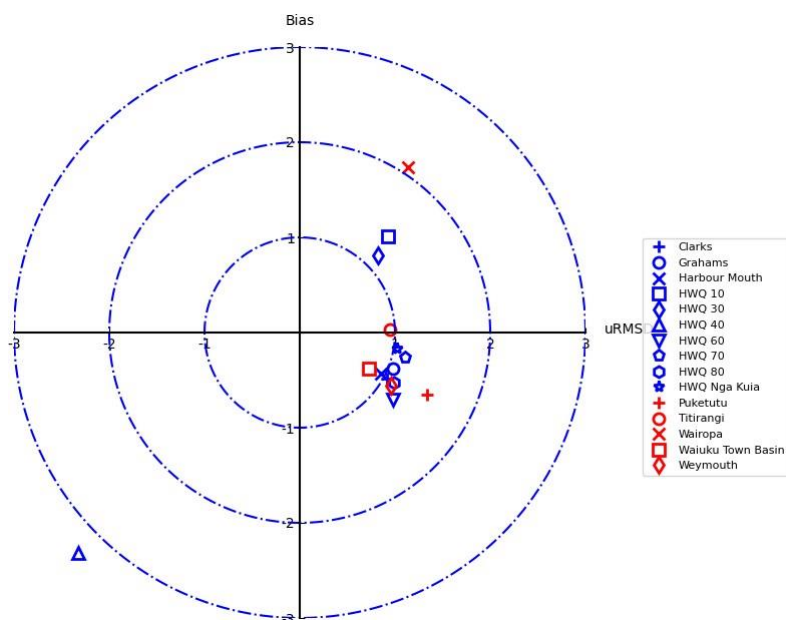


**Figure B-6: Target diagram for soluble phosphorus at all the sample sites.** Where: y-axis is normalised bias ( $B^*$ ) and x-axis is normalised RMSD ( $uRMSD = RMSD^*$ ).

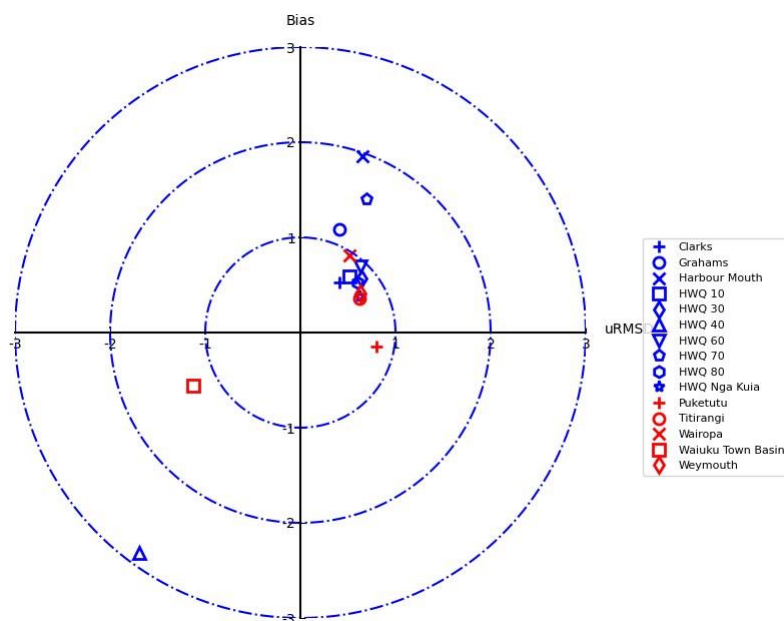


**Figure B-7: Target diagram for nitrate at all the sample sites.** Where: y-axis is normalised bias ( $B^*$ ) and x-axis is normalised RMSD ( $uRMSD = RMSD^*$ ).

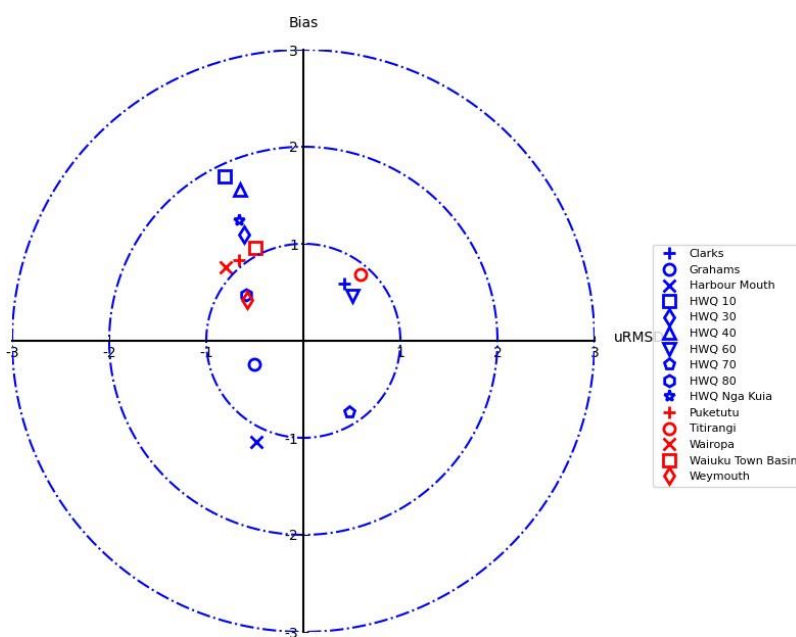
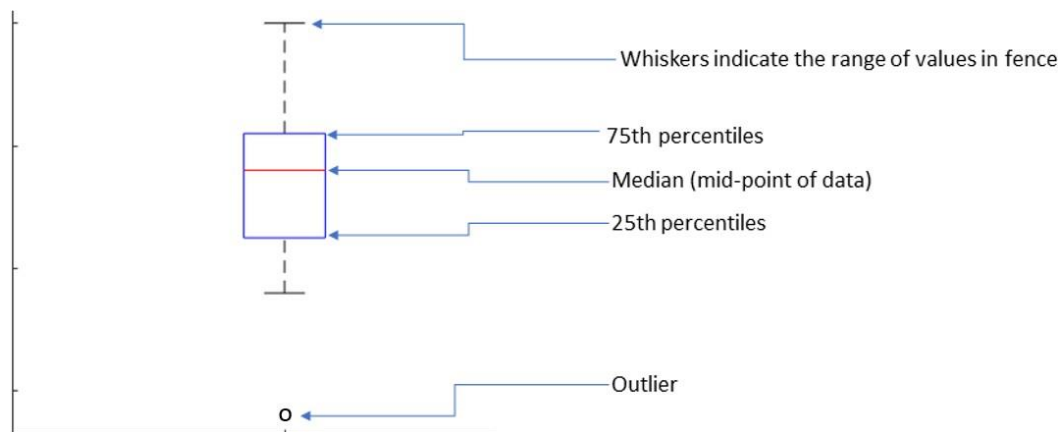


**Figure B-8: Target diagram for oxygen at all the sample sites.** Where: y-axis is normalised bias ( $B^*$ ) and x-axis is normalised RMSD ( $uRMSD = RMSD^*$ ).

## Appendix C Box and whisker plot description

Boxplots provide a visualisation of summary statistics for sample data and contain the following features.



The top of each box and bottom of each box are the 25th and 75th percentiles of the samples, respectively. The distance between the top and bottom is the interquartile range.

The red line in the middle of each box is the sample median. If the red line is not in the centre of the box, it shows sample skewness.

The whiskers are the lines extending above and below each box. Whiskers are drawn from the ends of the interquartile ranges to the furthest observations within the whisker length (the *adjacent values*).

Observations beyond the whisker length are marked as outliers. Outliers are displayed with a black circle (o). An outlier is a value that is more than 1.5 times the interquartile range away from the top or bottom of the box.

## Appendix D DYNAMO best-fit parameters

Table lists the parameters used in the best-fit Manukau Harbour model.

Parameter Definition	Units	DeIWAQ Parameter	Parameter Values
Chlorophyll- <i>a</i> :C ratio in Diatoms	(mg Chlfa/g C)	Ditochl	50
Chlorophyll- <i>a</i> :C ratio in Greens	(mg Chlfa/g C)	Grtochl	50
Total radiation growth saturation Diatoms	(W/m <sup>2</sup> )	RadSatDiat	15
Total radiation growth saturation Greens	(W/m <sup>2</sup> )	RadSatGree	20
Half-saturation value N Diatoms	(gN/m <sup>3</sup> )	KMDINDiat	0.005
Half-saturation value P Diatoms	(gP/m <sup>3</sup> )	KMPdiat	0.001
Half-saturation value Si Diatoms	(gSi/m <sup>3</sup> )	KMSidiat	0.027
Half-saturation value N Greens	(gN/m <sup>3</sup> )	KMDINGreen	0.005
Half-saturation value P Greens	(gP/m <sup>3</sup> )	KMPgreen	0.001
Half-saturation value Si Greens	(gSi/m <sup>3</sup> )	KMSigreen	NA
N:C ratio Greens	(gN/gC)	NCRatGreen	0.16
N:C ratio Diatoms	(gN/gC)	NCRatDiat	0.16
P:C ratio Greens	(gP/gC)	PCRatGreen	0.02
P:C ratio Diatoms	(gP/gC)	PCRatDiat	0.02
Si:C ratio Greens	(gSi/gC)	SCRatGreen	0
Si:C ratio Diatoms	(gSi/gC)	SCRatDiat	0.49
Maximum production rate Diatoms	(1/d)	PPMaxDiat	2.3
Maximum production rate Greens	(1/d)	PPMaxGreen	1.8
Maintenance respiration Diatoms st.temp	(-)	MRespDiat	0.036
Growth respiration factor Diatoms	(-)	GRespDiat	0.11
Maintenance respiration Greens st.temp	(-)	MRespGreen	0.045
Growth respiration factor Greens	(-)	GRespGreen	0.15
Mortality rate constant Diatoms	(1/d)	Mort0Diat	0.25
Mortality rate Diatoms at high salinity	(1/d)	MortSDiat	0.25
Daylength limitation function for Diatoms	(-)	LimDLdiat	1
Nutrient limitation function Diatoms	(-)	LimNutDiat	1
Radiation limitation function Diatoms	(-)	LimRadDiat	1
Temperature function growth Diatoms	(-)	TFGroDiat	1
Temperature function mortality Diatoms	(-)	TFMrtDiat	1
Mortality rate constant Greens	(1/d)	Mort0Green	0.35
Mortality rate Greens at high salinity	(1/d)	MortSGreen	0.35
Visual light specific extinction coefficient Greens	(m <sup>2</sup> /gC)	ExtVIGreen	0.15
Visual light specific extinction coefficient Diatoms	(m <sup>2</sup> /gC)	ExtVIDiat	0.15
Visual light specific extinction coefficient Detritus	(m <sup>2</sup> /gC)	ExtVLPOC1	0.1
Daylength for growth saturation Diatoms	(d)	OptDLDiat	0.5

Parameter Definition	Units	DelWAQ Parameter	Parameter Values
Daylength for growth saturation Greens	(d)	OptDLGreen	0.58
Sedimentation velocity Diatoms	(m/d)	VSedDiat	3
Sedimentation velocity Greens	(m/d)	VSedGreen	0
Input concentration of zooplankton-grazer1	(gC/m <sup>3</sup> )	Zooplank	NA
Chlorophyll- <i>a</i> :C ratio in MPB epipellic	(mg Chlfa/g C)	MPB1ToChl	50
Chlorophyll- <i>a</i> :C ratio in MPB epipsammic	(mg Chlfa/g C)	MPB2ToChl	50
Half-saturation value NO3 epipellic	(gN/m <sup>3</sup> )	MPB1Kni	0.005
Half-saturation value NH4 epipellic	(gN/m <sup>3</sup> )	MPB1Kam	0.005
Half-saturation value SiO epipellic	(gSi/m <sup>3</sup> )	MPB1Ksi	0.027
Half-saturation value PO4 epipellic	(gP/m <sup>3</sup> )	MPB1Kpho	0.001
Half-saturation value NO3 epipsammic	(gN/m <sup>3</sup> )	MPB2Kni	0.005
Half-saturation value NH4 epipsammic	(gN/m <sup>3</sup> )	MPB2Kam	0.005
Half-saturation value SiO epipsammic	(gSi/m <sup>3</sup> )	MPB2Ksi	0.027
Half-saturation value PO4 epipsammic	(gP/m <sup>3</sup> )	MPB2Kpho	0.001
Critical oxygen concentration for growth and respiration	(g/m <sup>3</sup> )	MPBOXYCRIT	0.1
Carrying capacity MPB1 epipellic	(gC/m <sup>3</sup> )	MPB1Ccap	100
Carrying capacity MPB2 epipsammic	(gC/m <sup>3</sup> )	MPB2Ccap	100
N:C ratio MPB epipellic	(gN/gC)	MPB1NCrat	0.16
N:C ratio MPB epipsammic	(gN/gC)	MPB2NCrat	0.16
P:C ratio MPB epipellic	gP/gC	MPB1PCrat	0.02
P:C ratio MPB epipsammic	gP/gC	MPB2PCrat	0.02
Si:C ratio MPB epipellic	(gSi/gC)	MPB1SiCrat	0.49
Si:C ratio MPB epipsammic	(gSi/gC)	MPB2SiCrat	0.49
Visual light specific extinction coefficient MPB epipellic	(m <sup>2</sup> /gC)	ExtVIMPB1	0.15
Visual light specific extinction coefficient MPB epipsammic	(m <sup>2</sup> /gC)	ExtVIMPB2	0.15
Temperature coefficient gross production MPB epipellic	(-)	MPB1ktgp	1
Temperature coefficient gross production MPB epipsammic	(-)	MPB2ktgp	1
Maximum gross prim prod 20°C MPB epipellic	(1/d)	MPB1Pmax20	2.3
Maximum gross prim prod 20°C MPB epipsammic	(1/d)	MPB2Pmax20	2.3
Mortality at 20°C under oxygen depletion MPB epipellic	(1/d)	MPB1mO_20	0.2
Mortality at 20°C under oxygen depletion MPB epipsammic	(1/d)	MPB2mO_20	0.2
Growth respiration fraction MPB epipellic	(-)	MPB1r_pr	0.11
Growth respiration fraction MPB epipsammic	(-)	MPB2r_pr	0.11
Maintenance resp. rate 20°C MPB epipellic	(1/d)	MPB1r_mt20	0.036



Parameter Definition	Units	DelWAQ Parameter	Parameter Values
Maintenance resp. rate 20°C MPB epipsammic	(1/d)	MPB2r_mt20	0.036
Temperature coefficient mortality MPB epipellic	(-)	MPB1rt	1.072
Temperature coefficient mortality MPB epipsammic	(-)	MPB2rt	1.072
MPB1peli maximum excretion fraction	(-)	MPB1b_ex	0.3
MPB2psam maximum excretion fraction	(-)	MPB2b_ex	0.3
MPB1peli first order mortality at 20°C	(1/d)	MPB1m1_20	0.2
MPB2psam first order mortality at 20°C	(1/d)	MPB2m1_20	0.2
MPB1peli second order mortality at 20°C	(m <sup>3</sup> /d/gC)	MPB1m2_20	0
MPB2psam second order mortality at 20°C	(m <sup>3</sup> /d/gC)	MPB2m2_20	0
MPB1peli temperature coefficient mortality	(-)	MPB1mt	1
MPB2psam temperature coefficient mortality	(-)	MPB2mt	1
MPB1peli temperature function S1	(-)	MPB1ftmpS1	1
MPB2psam temperature function S1	(-)	MPB2ftmpS1	1
Biomass threshold value MPB epipellic	(gC/m <sup>3</sup> )	MPB1Tresh	0.000999
Biomass threshold value MPB epipsammic	(gC/m <sup>3</sup> )	MPB2Tresh	0.000999
Initial slope PI MPB1 epipellic	(m <sup>2</sup> /d/w)	MPB1alpha	0.07666
Initial slope PI MPB2 epipsammic	(m <sup>2</sup> /d/w)	MPB2alpha	0.07666
Sedimentation velocity MPB1 epipellic	(m/d)	VSedMPB1	100
Sedimentation velocity MPB2 epipsammic	(m/d)	VSedMPB2	100
Minimum water depth for sedimentation/resuspension	(m)	MinDepth	0.1
daynumber of reference day simulation	(d)	RefDay	0
Atmospheric deposition flux PO4	(gP/m <sup>2</sup> /d)	fAtmDepPO4	0.00009
Atmospheric deposition flux NH4	(gN/m <sup>2</sup> /d)	fAtmDepNH4	0.0008
Atmospheric deposition flux NO3	(gN/m <sup>2</sup> /d)	fAtmDepNO3	0.0008
Extinction of visible-light (370-680nm) IM1	(m <sup>2</sup> /gDM)	ExtVLIIM1	0.01
Background extinction of visible-light (370-680nm)	(1/m)	ExtVIBak	0.08
Reaeration transfer coefficient	(m/d)	KLRear	1
Angle of incidence solar radiation	(degrees)	UitZangle	30
Salinity:Chloride ratio in sea water	(L/kg)	GtCl	1.805
Salinity at zero chloride concentration	(g/kg)	Sal0	0.03
pH	(-)	pH	8.1
Pseudo first-order rate PO4 sorption	(1/d)	RCadsPgern	1
Latitude of study area	(degrees)	Latitude	-36.7
Depth of microphytobenthos layer	(m)	Zsed	0.0015
Depth of microphytobenthos layer	(m)	Nutlen	0.02
Upper limit mineralization rate fast detr-C	(1/d)	ku_dFdcC20	0.18
Lower limit mineralization rate fast detr-C	(1/d)	kl_dFdcC20	0.12
Upper limit mineralization rate fast detr-N	(1/d)	ku_dFdcN20	0.18

Parameter Definition	Units	DelWAQ Parameter	Parameter Values
Lower limit mineralization rate fast detr-N	(1/d)	kl_dFdcN20	0.12
Upper limit mineralization rate fast detr-P	(1/d)	ku_dFdcP20	0.18
Lower limit mineralization rate fast detr-P	(1/d)	kl_dFdcP20	0.12
Sedimentation velocity POC	(m/d)	VSedPOC1	0.5
Sedimentation velocity Silica (Opal)	(m/d)	VSedOpal	0.5
Optimum oxygen concentration for denitrification	(gO2/m <sup>3</sup> )	OOXDEN	1
Optimum oxygen concentration for nitrification	(gO2/m <sup>3</sup> )	OOXNIT	5
Critical oxygen concentration for denitrification	(g/m <sup>3</sup> )	COXDEN	3
Critical oxygen concentration for nitrification	(g/m <sup>3</sup> )	COXNIT	1
Oxygen function level for oxygen below COXNIT	(-)	CFLNIT	0
Curvature of DO function for nitrification	(-)	CurvNit	0
First-order nitrification rate	(1/d)	RcNit	0.1
Critical shear stress for resuspension DM layer S1	(N/m <sup>2</sup> )	TaucRS1DM	0.2
Critical shear stress for resuspension POC layer S1	(N/m <sup>2</sup> )	TaucSPOC1	0.2
Critical shear stress for resuspension IM layer S1	(N/m <sup>2</sup> )	TaucSIM1	0.1
First order resuspension velocity DM	(1/d)	VResDM	0
zeroth-order resuspension flux	(gDM/m <sup>2</sup> /d)	ZResDM	0
Critical NH4 concentration	(gN/m <sup>3</sup> )	NH4KRIT	0.01
Adsorption rate PO4 --> AAP	(1/d)	RcAdPO4AAP	1
Distrib. coeff. (-) or ads. eq. const.	(m <sup>3</sup> /gP)	KdPO4AAP	0.1
Adsorption capacity TIM for PO4	(gP/gFe)	MaxPO4AAP	0.15
First-order AAP desorption rate in layer S1	(1/d)	RcAAPS1	0.01
First-order denitrification rate in water column	(1/d)	RcDenWat	0.1
First-order mineralisation rate DetC in layer S1	(1/d)	RcDetCS1	0.03
First-order mineralisation rate DetN in layer S1	(1/d)	RcDetNS1	0.03
First-order mineralisation rate DetP in layer S1	(1/d)	RcDetPS1	0.03
2nd order dissolution rate SiO2 at 20 oC	(m <sup>3</sup> /gSi/d)	RcDisSi20	0.0001
first-order denitrification rate in the sediment	(m/d)	RcDenSed	0.1
first-order mineralisation rate DetSi in layer S1	(1/d)	RcDetSiS1	0.015
Sedimentation velocity IM1	(m/d)	VSedIM1	0.3
Switch for Michaelis-Menten kinetics Nitrification model	(-)	SWVnNit	0
switch PO4 adsorption <0=Kd  1=Langmuir  2=pHdep>	(-)	SWAdsP	1
switch for oxygen reaeration formulation (1-13)	(-)	SWRear	1
switch <1=Tamminga  2=Swart  3=Soulsby>	(-)	SWTau	1
Switch Tauveloc (1=calculate  2=TauFlow)	(-)	SWTauVeloc	1

## Appendix E      Phytoplankton dynamics – BLOOM, DYNAMO and MICROPHYT

Despite intensive efforts, we were unable to achieve a reasonable calibration of DelWAQ with the BLOOM phytoplankton dynamics module. We attribute this to the unusual way BLOOM seeks to approximate the consequences of time-varying cell-specific physiological/behavioural state.

Growth rates of individual algal cells can vary through time as a function of their historical experiences of light intensity, nutrient concentrations and water temperature. Like many phytoplankton models, BLOOM explicitly represents several different algal taxa, and seeks to approximate their time-varying growth.

BLOOM explicitly acknowledges that the member phytoplankton population may be in one of several physiological states. At each BLOOM time-step (which is an integer multiple of the time-step used to solve the spatial advection–dispersion equations), BLOOM determines which physiological sub-population would grow most rapidly given the prevailing environmental conditions. Having made that determination, the entire taxon-specific population is instantaneously re-allocated to ('transferred into') that fastest growing physiological sub-population.

In many situations, the **transfer** of materials between differing biogeochemical forms (e.g., incorporation of inorganic nutrient into living algal biomass) and between different phytoplankton sub-populations is slow relative to the **transport** of those materials across space by advective and dispersive hydrodynamic processes. The calculation of biogeochemical transfers can be computationally expensive relative to the costs of calculating spatial transport; to achieve computational savings, BLOOM transfers material only intermittently relative to the frequency at which transport is calculated.

Deltares indicates that the BLOOM transfer coefficients have been calibrated on the assumption that the BLOOM time-step is set to 24 hours, and they have suggested to us that the BLOOM time-step cannot be set to less than six hours without raising the possibility of unrealistic changes in emergent algal physiological state.

This constraint on time-step implies that BLOOM is not well suited for application to Manukau Harbour because phytoplankton can change rapidly in response to episodic wastewater discharges and periodic tidally-driven changes in water depth as it affects light regime and exposure to nutrients emanating from the seabed. Depending upon the phase of the BLOOM-updates relative to tidal height and the timing of wastewater discharges, the simulated phytoplankton sometimes behaves as if the tide has never covered the intertidal flats over the course of a BLOOM time-step. At other times, the simulated phytoplankton behaves as though the intertidal flats remain submerged throughout the BLOOM time-step. Also, on some occasions, phytoplankton will respond to wastewater discharges as soon as they enter the harbour but on other occasions wastewater will not be 'perceived by' the phytoplankton for several hours, by which time the wastewater will have been transferred large distances by the tide.

Because of these kinds of issues, BLOOM tended to generate untrustworthy results, including a 'strobe' effect in chlorophyll-*a* concentration, particularly in the Purakau and Puketutu arms of the harbour (Figure E-1).

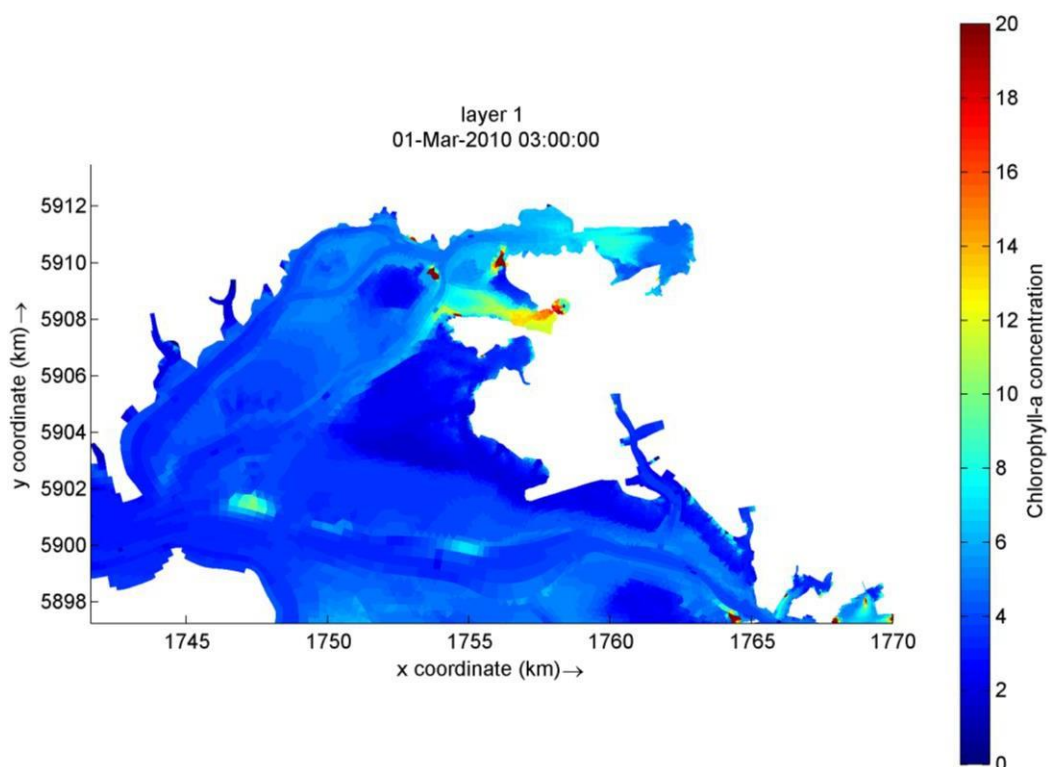


**Figure E-1: Example of a “strobe effect” in surface chlorophyll concentrations in northern Manukau Harbour as predicted by the BLOOM model.** Colourmap represents chlorophyll-*a* concentrations in mg Chl-*a* m<sup>-3</sup>. The “strobe-effect” is evident as brief, spatially discrete bursts of unrealistically high Chl-*a* concentrations that arise periodically (each time the “BLOOM biogeochemical processes” are given a chance to operate). The geographic locations of the bursts were somewhat irregular (reflecting the combination of tidally phased WWTP discharge, BLOOM time-steps which are integer fractions of 24 hours and the fact that the tidal cycle is not an integer fraction of 24 hours).

Having identified that BLOOM was unsuitable for application to Manukau Harbour, we consulted with Deltares and we jointly agreed that the DYNAMO phytoplankton module would be better suited for our application.

DYNAMO distinguishes between two types of algae – green algae and diatoms – but makes no attempt to represent changing physiological/behavioural state within each of those two taxa.

DYNAMO takes a more conventional approach than BLOOM by solving its constituent equations on the same time-step used by the coupled hydrodynamic model; in our case, 5 minutes. In contrast to BLOOM, matching of model time-steps facilitates better resolution of the effects on phytoplankton growth of periodic wastewater discharges and episodic changes in tidal currents and water depth.

DelWAQ offers separate groups of state-variables to represent phytoplankton populations and benthic micro-algal populations; the user has the option to include neither, one, or both groups. In a system with extensive intertidal flats, benthic micro-algae are likely to play an important role in nutrient-cycling. Nonetheless, our initial trials (with both DYNAMO and BLOOM) did not include any benthic algae.

In the initial trials, the DYNAMO model would typically reproduce observed nutrient and phytoplankton dynamics moderately well (order-of-magnitude accuracy) but, over the course of a few months, the phytoplankton populations (more specifically, the diatoms) would climb to unrealistically high concentrations and then crash to unrealistically low levels after exhausting the supplies of inorganic nutrient (N, P and Si).

We thought that the absence of benthic micro-algae in BLOOM was a likely cause for the boom-and-bust. To investigate the matter further, we turned on the **default benthic micro-algal module** that shipped with DelWAQ at the time (before late 2021), but that did not fix problem. The reasons are complicated, as follows.

In the default benthic micro-algal module, the benthic algae have pre-emptive access to the nutrient efflux out of the bed and, like phytoplankton, they also have access to nutrients in the overlying water-column. The efflux of nutrients from the seabed is insufficient to meet the demands of the benthic algae. Thus, no remineralised nutrient re-enters the water column from the seabed. In the meantime, living phytoplankton and detritus continue to settle to the bed, scavenging nutrient out of the water column and into a benthic-detritus/benthic-algae cycle. Because the benthic algae have pre-emptive access to nutrient that is regenerated from organic material that settles to the seabed, they slowly strip the water column of nutrient with the result that phytoplankton become unable to grow (Figure E-2). Because new nutrient is continually being delivered to the harbour (from the ocean, catchment and WWTPs), the benthic algae populations are able to continue to accrue, even when water-column nutrient concentrations are low enough to prevent phytoplankton growth, and too low – without efflux of nutrient from the decaying benthic detritus – to permit the benthic algae to grow.

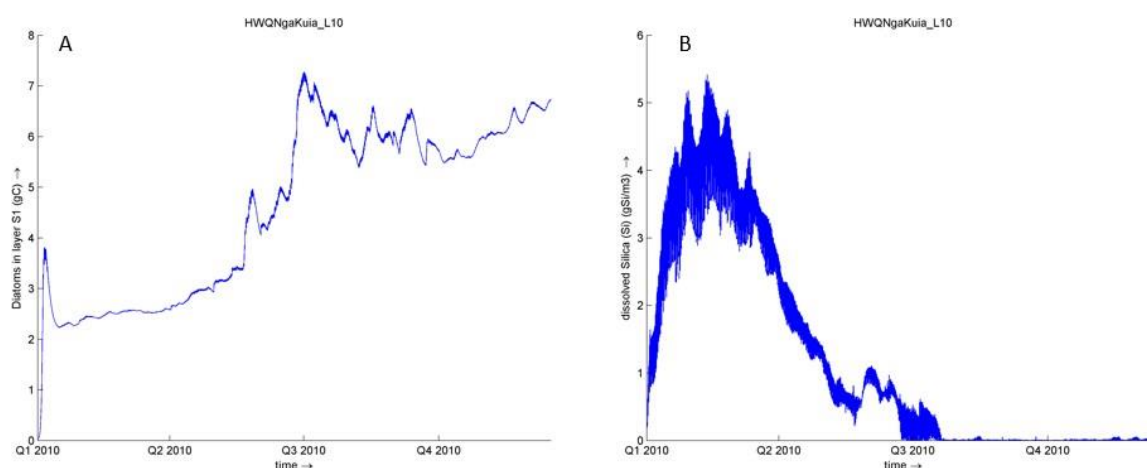


**Figure E-2: Panel A. Predicted DYNAMO benthic diatoms ( $\text{g C m}^{-2}$ ) on the bed at Nga Kuia HEMP monitoring station. Panel B. Dissolved silica ( $\text{g m}^{-3}$ ) in the water column.** Note: as benthic diatom biomass increases there is a draw down in the available silica in the water column to the point where silica is exhausted. Diatom concentration of  $6 \text{ g C m}^{-2}$  is approximately  $120 \text{ mg m}^{-2}$  Chla.

Inspection of the model equations governing the growth of benthic algae revealed that, whilst growth is influenced by nutrient concentrations in the overlying water, fluxes of nutrient regenerated at the seabed, temperature, and light intensity impinging upon the top of the benthic algal mat, it is not influenced by the density of the benthic algal population (thickness of the algal mat).

In reality, as benthic algae grow, those growing at the bottom of the mat will become increasingly shaded (from light) by those at the top, and those in the middle of the mat will become increasingly isolated from nutrients emerging from the seabed or circulating in the overlying water. Such density-dependent/self-regulatory influences were not represented in the original benthic micro-algae module.

Consequently, each additional quantum of nutrient delivered from the catchment or ocean would eventually become incorporated into the tight cycling between benthic algae and benthic detritus.

We discussed this issue with Deltares and commissioned them to develop and incorporate into DelWAQ an 'enhanced benthic algal module' (one which they had previously developed and coded, but not yet incorporated).

This enhanced module (dubbed 'MICROPHYT'), includes a phenomenological/empirical representation of self-limitation. It does this by assuming that the maximum weight-specific growth rate (when light, nutrients and temperature are optimal) declines linearly as the density of benthic algae ( $\text{mg benthic algal carbon m}^{-2}$ ) increases. In short, the new MICROPHYT module incorporates a so-called logistic growth term.

The maximum weight-specific growth rate falls to zero at the carrying capacity ( $\text{g C m}^{-2}$ ), which the user is able to specify.

Using the enhanced benthic algal module (MICROPHYT) together with DYNAMO in DelWAQ, a satisfactory calibration was achieved.

## Appendix F Numerical integration of model governing equations

There is a vast literature concerning the numerical solution of coupled (partial-) differential equations. Loosely speaking, the numerical solution is generated by:

- evaluating the coupled differential equations at a ‘present’ (modelled) time  $t$  to yield an estimate of each state-variable’s instantaneous rate of change, and
- projecting a (near-term) future value for each state-variable from its present state (at time  $t$ ), and its associated instantaneous rate of change at that time. The projection is made across a small but non-zero time interval  $\Delta t$ .

The size of the projection interval  $\Delta t$  and the choice of numerical integration scheme both influence the likely accuracy of the eventual numerical solution.

Accuracy tends to increase as  $\Delta t$  decreases. This is because the extent to which the system can change between  $t$  and  $t+\Delta t$  declines as  $\Delta t$  shrinks. As a result, the *instantaneous* rates of change calculated at time  $t$  tend to become better approximations to the true-but-unknowable time-step average rates of change across the interval  $\Delta t$ . The choice of numerical integration scheme influences solution accuracy because different schemes use differing methods to try to ‘correct’ for any possible evolution of the (true) instantaneous rates of change across the interval  $\Delta t$ .

The DelWAQ user-manual (Deltares 2011) provides brief descriptions of the various numerical integration schemes that can be implemented. Each of the schemes implies a different trade-off between runtime, stability, accuracy and memory requirements.

The integration methods which are less computationally demanding (consume less runtime and less memory) tend to generate results which are poorer approximations to the true (but unknowable) solutions of the set of coupled differential equations. In some instances, the inaccuracy can manifest itself as numerical instability (abrupt, catastrophic loss of accuracy/abrupt transition to entirely implausible dynamics or extreme sensitivity to initial conditions). Such instability is usually easy to spot (indeed, the simulation often ‘crashes’ before it can run to completion). In other cases, however, the loss of accuracy is less easy to detect – because the solutions continue to appear plausible.

Since no solution will be 100% accurate, it becomes a matter of choice (by the model user) to determine ‘whether the solutions at hand are sufficiently accurate in the context of the questions that are being asked of the model’. Clearly, this requires that the user identify the natures and magnitudes of ‘tolerable errors’ *a priori*. Thereafter, the model user is strongly advised to make simulations using a variety of integration methods and a range of integration step-sizes ( $\Delta t$ ) to explore the extents to which model solutions are sensitive to the choice of time-step and integration scheme.

As noted above, the numerical solutions will usually tend to converge towards the true-but-unknowable solution as  $\Delta t$  is reduced. The rates of convergence will tend to differ by numerical integration scheme, but solutions from all numerical methods should converge towards the same (one hopes, true) solution. Ultimately, the model user should aim to adopt a time-step and numerical scheme which offer an adequate compromise between runtime and accuracy. Note however, that both run-time and accuracy can change if model inputs (coefficients, boundary conditions, or forcing data) are changed.

Thus, it is often wise to adopt a ‘better safe than sorry’ approach by selecting a time-step that is smaller than is thought to be strictly required and by adopting a numerical scheme that is accurate across the full spectrum of anticipated inputs, even if that is more computationally demanding.

As a part of our investigations towards selecting a favoured numerical scheme, we sought to minimise loss of continuity (non-conservation of mass or volume) through investigations with a passive tracer model.

The tracer model assumes that the influx loads at all model sources and boundary conditions have a tracer concentration value of one ( $\text{m}^{-3}$ ). The initial tracer concentration in the harbour and ocean water of the model’s domain was also set to  $1 \text{ m}^{-3}$ . With these initial conditions and boundary conditions, the simulated concentrations within each control-volume of the model domain should remain exactly<sup>22</sup>  $1.0 \text{ m}^{-3}$ ). Output from the DeltaFM hydrodynamic model was written to archive (to be picked up by the subsequent DelWAQ model run) with a resolution of two simulated minutes (smaller than 1 minute resulted in excessively large files). At this temporal resolution, the difference between water-column specific sea-surface height simulated by the DeltaFM hydrodynamic model and inferred from integration of the archived water-velocities and sea-surface heights at the start of each DelWAQ projection interval never exceeded 1% even in inter-tidal areas that undergo wetting and drying. Furthermore, the sea-surface height discrepancies oscillated about zero with the tides rather than exhibiting longer-term trend. That is, volume (and mass) conservation was good.

The DelWAQ tracer model was run, increasing the DelWAQ model transport time-step in each sequential simulation, until the tracer concentration in any control-volume of the model grid fell below  $0.95 \text{ m}^{-3}$  or climbed above  $1.05 \text{ m}^{-3}$  (95%). The best overall transport time-step proved to be a little more than five minutes.

With Deltares, we tested numerical integration schemes 12 (explicit horizontal and implicit vertical upwind discretisation) and 21 (switching between a local explicit and implicit solution method), using this method. Both of these schemes resulted in poor performance and instabilities. The DelWAQ integration scheme 15 (implicit both in vertical and horizontal) with a time-step of 5 min was ultimately selected as it was numerically stable and achieved the best continuity result.

---

<sup>22</sup> give-or-take rounding errors of the order approx.  $10^{-14} \text{ m}^{-3}$  arising from the fact that computers cannot represent real numbers to infinite precision.